



University of
Stavanger

FACULTY OF SCIENCE AND TECHNOLOGY

MASTER'S THESIS

Study program/Specialization: MSc. Petroleum Engineering / Natural Gas Engineering	Spring semester, 2018 Open access
Author: Mirza Hassan Baig (signature of author)
Supervisors: Anders Nermoen, Pål Østebø Andersen, Paul Henry Nadeau, Ivar Austvoll	
Title of master's thesis: Digital Image Analysis for Petrophysical Evaluation	
Credits (ECTS): 30	
Key words: Digital image analysis, thin sections, optical microscopy, porosity, permeability, core, petrophysics, log, irreducible water saturation, electron microscopy, Barents Sea	Number of pages: 47 + Appendices: 37 pages Stavanger, June 15/ 2018

ABSTRACT

Economic feasibility of any field development largely depends upon its reservoir storage and flow capacity. Porosity, saturation and permeability are important parameters to determine the type and volume of hydrocarbons in place and to estimate recoverable reserves. They are also key parameters in planning, modelling and development of a reservoir.

The porosity and saturation of the reservoir can be determined with reasonable certainty through interpretation of petrophysical logs or through analysis of physical core samples. Permeability evaluation is challenging, because the definition and the scale of this measurement varies across its sources. Well logs provide an empirically derived absolute value, cores provide both scalar (K_{air}) and vector (K_v , K_h , vertical and horizontal) permeabilities, while the reservoir volume investigated by a well test is quite large as compared to logs or cores. Hence, porosity, saturation and permeability are often compared between its sources, and calibrated as needed. While logs based interpretation is a fast interpretation technique, getting core results can take significant time. Also, not all wells are cored, or sometimes core samples are too small to carry out the analysis, leading to a missing link between core-log integration. To improve some of the inaccuracies and limitations, 'digital image analysis' on core or on drill cuttings 'thin sections' can be a useful technique in estimating reservoir properties. Digital image analysis can provide porosity, pore size distribution, flow path tortuosity (permeability), irreducible water saturation and mineralogy of the samples. Pore space area and perimeter is also determined and can be used in studying chemical reactions in the pore wall area for improved oil recovery.

This research work aims to develop novel automated digital image analysis methods for Petrophysical Evaluation, and thus overcomes some of the limitations with regards to objectivity and repeatability of traditional manual techniques. To analyze porosity of thin section images, a threshold value on pixels intensity histogram is required to separate pores response from the matrix. A set of rules have been developed to remove human subjectivity in selecting this threshold value. Correlations have been applied for permeability and tortuosity evaluation to understand reservoir flow potential.

Petrographic thin section samples of reservoir rocks from 7128/6-1 well in the Barents Sea are studied. The thin section images are digitalized and analyzed using MatLab functions. Petrophysical properties, namely porosity, permeability and irreducible water saturation are quantified. In addition, some features of the pore space are quantified, including area, perimeter, major & minor axis of the pore area and orientation of the pores. The results from digital image analysis are compared against results from conventional core analysis to establish validity and limitations of thin section image interpretation technique.

ACKNOWLEDGEMENT

I would like to express my highest gratitude to my supervisors, Mr. Anders Nerموen, Mr. Pål Østebø Andersen, Mr. Paul Henry Nadeau and Mr. Ivar Austvoll. Without their guidance, supervision and discussions this work would not have been possible. There had been several occasions when I lost hope that I will not be able to make it, but it was so amazing that they showed great patience, provided support and encouragement that kept me going. To my every delay, they responded promptly so I can deliver milestones in due time.

I am thankful for their time, as we had scheduled weekly meeting. Specially to Mr. Pål for scheduling and hosting project meetings in a dedicated meeting room, and for his positive critics to improve work quality. To Mr. Anders for hours of discussion and showing patience to guide me through MatLab basics in the beginning of thesis work. To Mr. Ivar for his expert opinions on digital image processing. And to Mr. Paul who based on his years of experience added technical depth to this work.

I am simply impressed with the professionalism and attitude of my supervisors towards their students. They know how to pave way for their students to complete their studies successfully and with best possible grades.

Last but not least, I am thankful to my family and friends. Whenever I told them I am delayed, they only said, no worries you can do it.

Table of Contents

1 INTRODUCTION.....	1
1.1 Background.....	2
1.2 Objectives	2
2 THEORY.....	3
2.1 The thin section sample	3
2.2 A digital image.....	4
2.3 Porosity	5
2.3.1 Porosity from well logs.....	5
2.3.2 Porosity from cores	7
2.3.3 Porosity from digital image analysis.....	8
2.4 Porosity partitioning.....	9
2.4.1 Porosity partitioning in context of image analysis.....	10
2.5 Permeability	12
2.5.1 Permeability from logs.....	13
2.5.2 Permeability from cores	14
2.5.3 Permeability from digital image analysis	15
2.6 Saturation and irreducible water saturation	18
2.6.1 Irreducible water saturation from NMR logs.....	18
2.6.2 Irreducible water saturation from cores	19
2.6.3 Irreducible water saturation from digital image analysis.....	19
3 METHODOLOGY.....	20
3.1 Digital image analysis.....	20
3.1.1 Main script	20
3.1.2 Slide color test.....	21
3.1.3 Thin section test Rc.....	21
3.1.4 Thin section test Rc auto.....	25
3.1.5 ImClusters Kmean	25
3.1.6 ImAnalysis	28
4 RESULTS.....	29
4.1 Porosity from image analysis.....	29

4.1.1	Manual threshold method	30
4.1.2	Auto threshold method.....	31
4.1.3	K-means clustering method	33
4.1.4	Clusters predicted threshold method.....	34
4.2	Permeability from image analysis.....	37
4.3	Irreducible water saturation	38
5	DISCUSSION	39
5.1	Porosity	39
5.2	Permeability	41
6	CONCLUSION.....	43
7	WAY FORWARD	44
	REFERENCES.....	46
	APPENDICES	48
	Appendix-A: Conferences representation	48
	Appendix-B: MatLab scripts	50
	Appendix-C: Optical microscopy scans of thin section samples	62
	Appendix-D: Core analysis report (7128/6-1 well).....	69

1 INTRODUCTION

Petrophysical properties like porosity, saturation and permeability characterizes success of an exploration well. These properties are either evaluated through formation evaluation logs or through laboratory measurements on core samples. Porosity and saturation are important inputs to evaluate hydrocarbon-in-place while permeability defines if these hydrocarbon reserves will be able to flow. Significance of these properties can also be judged from the fact that operators continue to acquire formation evaluation data in development wells to reduce uncertainties in geological and reservoir models.

Formation evaluation logs like neutron, density, sonic and nuclear-magnetic-resonance logs are used to evaluate formation porosity. Saturation is derived from resistivity log and interpreted porosity data. Logs based formation evaluation results are generally validated and calibrated against laboratory core measurements. This is especially true for permeability, where a porosity-permeability relation is derived from core measurements and applied on porosity log to get permeability profile. However, core data is usually acquired for exploration and appraisal wells only which represent a small number as compared to number of development wells. Formation evaluation of development wells highly relies on petrophysical logs and on core-log models established in early phase of field life.

A general industry practice is to regard core measurements as ground truth. However, there can be uncertainties associated with core measurements especially when laboratory conditions are ignored under which core measurements were made. For example, if logs based total porosity consistently read higher than core porosity, then there is a possibility of core samples not dried enough at given temperature, and measured porosity is effective instead of total porosity [Crain's handbook]. Similarly, porosity from logs is derived based on mathematical models needing analyst input of formation properties e.g. sandstone matrix density of 2.65g/cc and oil density of 0.8g/cc may not be true to estimate porosity from a density log in an oil bearing sandstone reservoir. For logs based formation evaluation, porosity is an input to saturation and permeability equations. Uncertainty in porosity analysis will result uncertainty in estimates of saturation and permeability as well.

There are certain factors that control above mentioned petrophysical properties of a reservoir; pore and grain size distribution, mineralogy, sorting, diagenesis, irreducible saturation, relative permeability and asphaltene deposition etc. Characterizing these controlling factors require advanced logging and special analysis on core data (SCAL), yet some of these properties require alternate interpretation techniques. 'Digital image analysis of thin sections' is presented as this alternate technique. Diagenesis is usually studied on core thin section samples to identify features like chlorite coating on quartz grains that tend to preserve porosity, or quartz overgrowth that reduces porosity [Guojun, 2011; Saadi, 2017]. Asphaltene deposition can be characterized through thin sections which severely impedes reservoir permeability [Mishra, 2012]. Porosity, mineralogy, pore size distribution, sorting and permeability can also be analyzed through digital image analysis of thin sections [Lawrence, 2017; Varfolomeev, 2016].

Thin section samples can either be prepared from cores or from drill cuttings, where later is available for all drilled wells. Estimate of petrophysical properties from thin section can be studied together with core and log data to reduce uncertainties. Especially for the wells where core data is not available, thin section analysis can improve logs based interpretation.

The focus of current year research work is to estimate petrophysical properties (porosity, permeability and saturation) from thin section samples. Digital images used were obtained from 'optical microscopy' scanning with pixel resolution of approx. 25 μm which is significantly lower than e.g. SEM images (scanning electron microscopy).

1.1 Background

Zerabruk (2017) and Fens, T. W. (2000) studied digital images of thin section samples obtained from optical microscopy scanning. Their work primarily focused on estimating porosity from these samples and used Kozeny-Carman capillary model to estimate permeability. Both researchers used similar methodology where digital image was segmented into its red, green and blue components, and a threshold (cutoff) was applied on red component of the image to extract pore space from matrix. Porosity and permeability from thin sections was compared against core data.

Fens, T. W. (2000) did not achieve one-to-one correlation between thin section and core porosity and had to regress data for best fit. The limitation of his work was that good fit was achieved with regression and by knowing the ground truth from core data. Same set of regression may not be applicable for other samples.

Zerabruk (2017) in his work relied on visual analysis and manual shifting of thresholds to extract porosity, which showed a good correlation with core porosity. Limitation of their work was tedious adjustment of thresholds and the subjectivity to pick threshold values. Permeability correlation from porosity was poorly established.

1.2 Objectives

Main objectives of the current study are;

- Overcome limitations of previous work i.e. improve predictive power of thin section image analysis as an independent interpretation for petrophysical properties
- Develop and improve digital image analysis tool at University of Stavanger (UiS)
- Automate process of selecting threshold values
- Study an alternate technique to determine porosity from thin section samples
- Improve permeability correlation
- Suggest future development

2 THEORY

Porosity, permeability and saturation are important reservoir rock properties that are used in determination of hydrocarbon volume in place and recoverable reserves. There are different means to measure these properties, some are direct methods while others are indirect and uses correlations and model based calculations.

Core measurements such as Helium porosity, Dean-Stark saturation tests and Gas permeability (K_{air} or K_{gas}) are examples of direct measurement techniques, while interpretation based on petrophysical well log data determine these properties indirectly. Usually properties from well logs and core tests are calibrated or validated against each other, and any differences are analyzed to understand uncertainties associated with each measurement.

To reduce some of these differences, an additional source of petrophysical properties can be ‘digital image analysis’ on ‘core thin sections’. From literature review and methods developed in current study, digital image analysis can estimate total porosity, effective porosity, absolute permeability, irreducible water saturation, mineralogy and pore size distribution [Varfolomeev, 2016; Fens, 2000, Heilbronner, 2014]. The potential of this technique, when properly trained from empirical tools, is to derive capillary pressure and relative permeability profiles [Brooks, 1964; Ramakrishnan, 1994; Glorioso, 2003].

In the current study, we have focused on determining porosity (total & effective), absolute permeability and irreducible water saturation. Historical thin section image analysis techniques have determined porosity from manual thresholding [Fens, 2000; Zerabruk, 2017], which was somewhat subjective, so automated thresholding and clustering techniques are introduced in current study. Absolute permeability was estimated with Kozeny-Carman correlation [Carman, 1937; Dvorkin 2009], and Timur-Coates [Coates, 1973] correlation is newly introduced. Irreducible water saturation is simply derived from total and effective porosity. Hence, determination of these properties from digital image analysis of thin section can be termed as an indirect method.

We first define thin section sample and digital image before looking into definitions of petrophysical properties; porosity, permeability and saturation, and how they are traditionally determined from logs and cores, and with image analysis.

2.1 The thin section sample

A thin section sample is a thin slice of rock mounted onto a glass surface. The dimensions of the samples are approximately 1 inch in diameter and 30 μm (micron) thick. The rock sample is first cleaned to remove residue of drilling fluids and mounted onto a glass slide, it is then grinded and polished to the desired thickness. Prior to grinding and polishing procedures, sample is filled with blue color epoxy so the grains remain intact. The benefit of using blue epoxy is that it usually does not occur in rocks and occupies the pore space within the grains, hence, detection of blue color allows analysis of sample porosity. The technique, however, is limited by the grain size, as grains smaller than 30 μm in diameter will be trapped in thin section, and a pixel resolving this grain will consist of blue color epoxy and the grain itself.

A thin section sample is a physical sample and need to be digitized so an appropriate software can be used to study digital images. Samples used in the current study are taken from [Zerabruk, 2017] work and are the digitized images from 7128/6-1 well in Barents Sea. Canon 9000F Mark-II scanner was used to scan the samples. The scanned image has resolution of about 25 μm /pixel. This procedure of scanning and

digitizing the image is called ‘optical microscopy’ and is of lower resolution as compared to digital images obtained from ‘scanning electron microscopy’. The advantage of the former is that it is a fast technique to obtain digital images and a disadvantage that pore sizes less than 25 μm cannot be quantitatively resolved with optical microscopy.

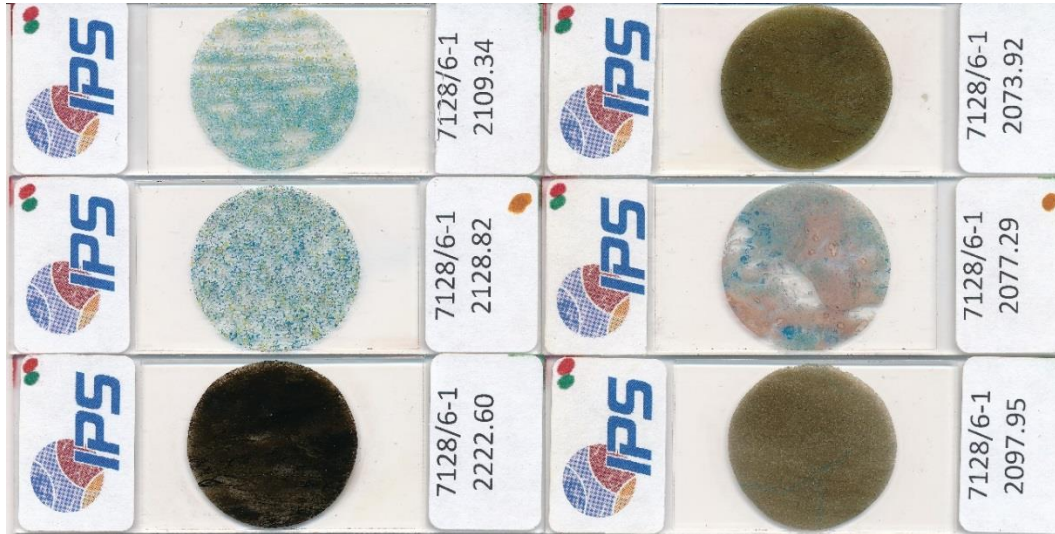


Figure 2.1: Scanned digital image of six thin section samples for the well 7128/6-1 with depth reference. Diameter of each sample is 1 inch

2.2 A digital image

Digital images are made of elements called pixels, which are the building blocks of an image. The size of an image is determined by the dimensions of pixel array, organized as array. The image width is the number of columns (M), and the image height is the number of rows (N) in the array. Thus, the pixel array is a matrix of M columns x N rows [*excerpt modified from ImageJ webpage*].

Image size specifically describes the number of pixels within a digital image. The real-world representation of a digital image requires one additional factor called resolution, which is the spatial scale of the image pixels. For example, an image of 2200x1600 pixels with a resolution of 200 pixels per inch (ppi) would be a real-world image size of 11"x8".

Having defined the number of pixels, MxN, only provides a rectangular shape to an image. One more parameter, intensity, is needed to truly define an image. Each pixel has its own intensity value, or brightness. If all the pixels have the same value, the image will be a uniform shade; all black, white, gray, or some other shade. Black and white images only have intensity from the darkest gray (black) to lightest gray (white). Color images, on the other hand, have intensity from the darkest and lightest of three different colors, Red, Green, and Blue. The various mixtures of these color intensities produce a color image. Thus, the two most basic types of digital images, B&W and Color, are known as grayscale and RGB images.

In addition to the intensity type of each pixel, the range of intensity values also varies. Intensity values in digital images are defined by bits. A bit is binary and only has two possible values, 0 or 1. An 8-bit intensity range has 256 possible values ($2^{\# \text{ of bits}}$), 0 to 255. For a 1-bit, or binary image, $2^1 = 2$ possible

values and for an 8-bit image, $2^8 = 256$ possible values. Thin section digital images used in current study are 8-bit images hence, have pixel intensity range of 0 to 255.

2.3 Porosity

The volume fraction of void spaces, i.e. non-rock space, divided by the total volume of sample is defined as porosity. Consider a solid rock sample filled with liquid, liquid can only occupy the empty (pore) space within that sample. The volume occupied by fluid over total (bulk) volume is equivalent to total porosity of the sample.

$$\text{Porosity } (\Phi) = \frac{\text{Pore volume}}{\text{Bulk volume}} = \frac{V_p}{V_b} \quad (2-1)$$

From equation (2-1), unit of porosity is in fraction or in percentage. In Figure 2.2, the term solid grains is interchangeably used with rock matrix.

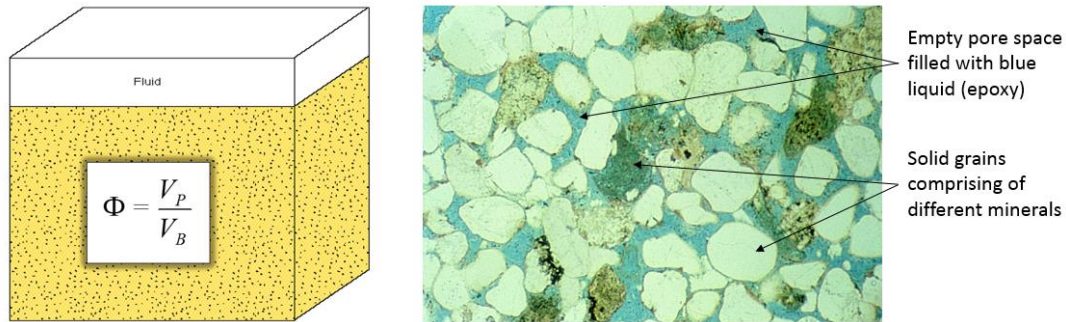


Figure 2.2: Rock sample illustrating definition of porosity, where empty pore space within the solid grains (matrix) is filled with blue colored liquid [Schlumberger technical course]

2.3.1 Porosity from well logs

There are four log measurements that determine porosity namely, density log, neutron porosity log, sonic log and nuclear magnetic resonance (NMR) log. Density, neutron and sonic logs are bulk measurements with matrix effect in it which shall be determined from external means or assumed to get porosity from these logs. While NMR is a matrix independent porosity log.

Bulk density log (ρ_b) measurement is discussed, while neutron and sonic logs use similar equations to determine porosity. The density log works by Compton scattering and photoelectric effects that occur when gamma-rays from the source interact with the electrons of the elements present in the formation. By measuring returning number of gamma rays and their energy levels at a given distance from the source, the electron density of the formation is predicted. Bulk density of the formation is determined from electron density.

Equation (2-2), shows the components of a bulk density log, where a bulk rock sample of unit volume is investigated by a density log, then the term $(1 - \Phi_{total})$ is volume fraction occupied by matrix and (Φ) is

volume fraction occupied by fluids. (ρ_{matrix}) is density of solid grains (also known as matrix density) and (ρ_{fluid}) is fluid density occupying the pore space.

$$\rho_b = (1 - \Phi_{total}) \rho_{matrix} + \Phi_{total} \rho_{fluid} \quad (2-2)$$

Equation (2-2), can be re-arranged for porosity;

$$\Phi_{total} = \frac{\rho_{matrix} - \rho_b}{\rho_{matrix} - \rho_{fluid}} \quad (2-3)$$

Consider a clean sandstone rock sample comprising of quartz grains only ($\rho_{quartz} = 2.65 \text{ g/cc}$) filled with water (of $\rho_{water} = 1.0 \text{ g/cc}$), the total porosity of this sample can be determined by using equation (2-2) given the bulk density (ρ_b) measurement.

However, rocks seldom consist of single mineral and an analyst need to calculate or assume matrix density from other means to get ρ_{matrix} . Same for ρ_{fluid} , where fluid filling the pore space may be a mix of oil and water, or gas. Oil density typically varies from 0.6-0.9 g/cc depending upon its composition, pressure and temperature, while the water density is a function of the amount of salts dissolved in it. The gas density is special in a sense that equation (2-3) requires an apparent gas density response instead of actual gas density. All these unknowns add uncertainty to determination of total porosity from simply a bulk density log.

For neutron porosity, formation is bombarded with high energy neutrons. These neutrons collide with the atomic nuclei of the elements present in the formation. The incident neutrons through in-elastic and elastic scattering loose energy, some get absorbed into the formation while others make their way back to two neutron detectors (a near detector and a far detector provided on neutron tool). Transforms are used to convert near-to-far ratio of receiving neutrons into a neutron porosity log.

$$Neu_{log} = (1 - \Phi_{total}) * Neu_{matrix} + \Phi_{total} * Neu_{fluid} \quad (2-4)$$

Where Neu_{log} , Neu_{matrix} and Neu_{fluid} are neutron log porosity, matrix response of neutron and fluid neutron response respectively.

Further on, the sonic compressional slowness porosity is estimated via;

$$\Delta T_{compressional} = (1 - \Phi_{total}) * \Delta T_{matrix} + \Phi_{total} * \Delta T_{fluid} \quad (2-5)$$

Where ΔT is transit time in $\mu\text{s}/\text{ft}$ or in any other units of slowness (1/velocity). ΔT_{matrix} and ΔT_{fluid} are matrix and fluid transit times.

Usually final total porosity from well logs in an oil and water bearing reservoirs is an average of density and neutron porosity. In case of gas reservoirs, it can be estimated as $2/3^{\text{rd}}$ of density porosity and $1/3^{\text{rd}}$ of neutron porosity.

2.3.2 Porosity from cores

Porosity from cores may be determined on whole core sample, on full diameter or on core plugs. The volume investigated to determine porosity on each sample is different (Figure 2.3). For example, dimension of whole core can be 2 feet in length and diameter of 1.75 – 5.25 inch, full diameter sample is of shorter length about 6 inches, and core plug has dimension of 1 – 1.5 inch in diameter and 1 – 2 inch in length. Usually core plugs porosity is referenced and compared against petrophysical logs as they capture about the same level of sample heterogeneity as well logs. Whole core analysis is used for low porosity reservoirs.

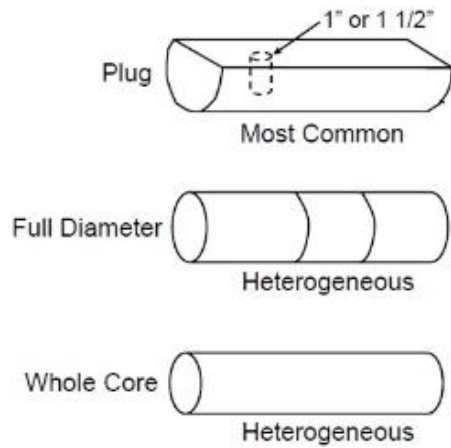


Figure 2.3: Core samples description for porosity analysis

As discussed in previous section, bulk volume of a reservoir rock (V_b) is sum of pore volume (V_p) and grain volume (V_g).

$$V_b = V_g + V_p \quad (2-6)$$

There are different laboratory methods that solve equation (2-6) to get V_p (i.e. porosity) in a semi-direct way. We will only discuss helium porosity (Boyle's law method) as this was the core porosity data available in current study.

The sample is placed in a rubber sleeve holder that has no void space around the periphery of the core and on the ends. Such a holder is called the Hassler holder, or a hydrostatic load cell. Helium or one of its substitutes is injected into the core plug through the end stem.

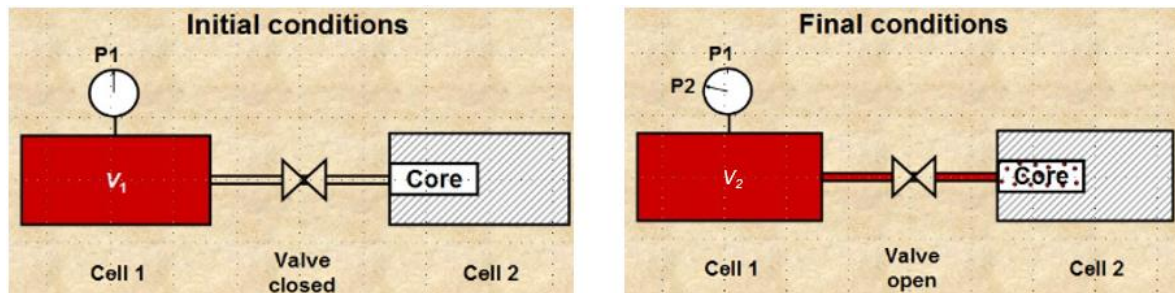


Figure 2.4: Boyle's law apparatus for determining porosity [Crain's handbook]

Pore volume (V_p) or porosity is determined through the set of equations as given below;

$$V_2 = \frac{P_1 V_1}{P_2} \quad (2-7)$$

$$V_2 = V_1 + V_p \quad (2-8)$$

$$V_p = V_2 - V_1 \quad (2-9)$$

Where P_1, V_1 is pressure, volume of cell-1 at initial condition, P_2, V_2 is pressure, volume of cell-2 after opening the valve, and V_p is pore volume of core plug i.e. porosity.

Porosity from core will be total porosity if the core sample used is full dried with no residues of original fluid. If core has not been fully dried (humidity dried only), then V_p will be less than total porosity by an amount equivalent to native residues left in the sample.

2.3.3 Porosity from digital image analysis

A digital image comprises of pixels, which are the building blocks of an image. Hence, a pixel can be defined as the smallest unit of a digital image. Core thin section scanned images used in current study were typical cropped at 800x800 pixels (MxN pixel array, section 2.2) and for some small size images at 780x780 pixels, hence total number of pixels in a sample ranged from 608,400 to 640,000 pixels.

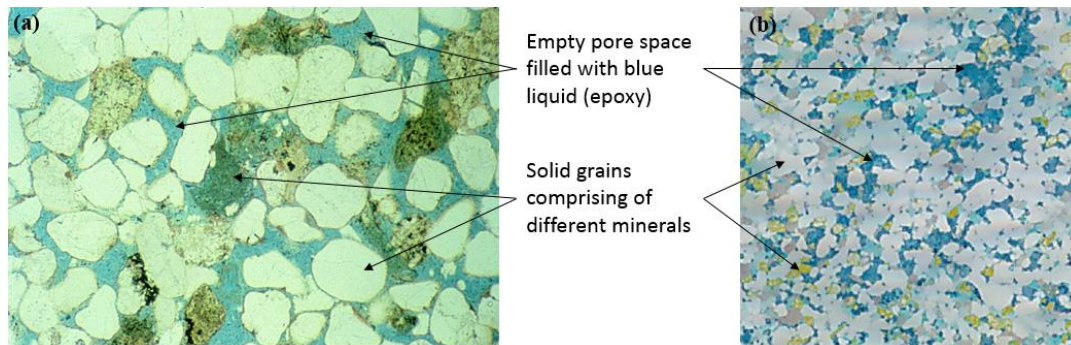


Figure 2.5: Core thin section samples (a) a generic image taken from literature [Schlumberger technical course] (b) an example of thin section image used in current study

Through image segmentation techniques that will be discussed in detail under section 3, it is possible to extract regions associated with blue epoxy only, i.e. pore space. Number of pixels residing in pore space are cumulated and divided by total number of pixels to get image porosity. The definition of porosity from image analysis is somewhat similar to equation (2-1) but written in pixels term.

$$\Phi_{image} = \frac{\sum \text{pixels in pore space}}{\text{Total number of pixels}} \quad (2-10)$$

From Figure 2.5, sample (b) was scanned with optical microscopy technique while sample (a) was scanned with electron microscopy. The accuracy of porosity from image analysis is dependent upon its pixels resolution. Samples analyzed in current study have pixel resolution of about 25 μm , which means pore sizes

greater than 25 μm are accurately quantified with this technique and a different interpretation technique was used to quantify porosity associated with pore sizes less than 25 μm .

2.4 Porosity partitioning

Porosity has several terminologies with each having different meaning. Porosity may be defined as primary or secondary porosity, total or effective porosity, micro-meso-macro porosity, or isolated porosity etc. Such differences shall be kept in mind while documenting porosity results.

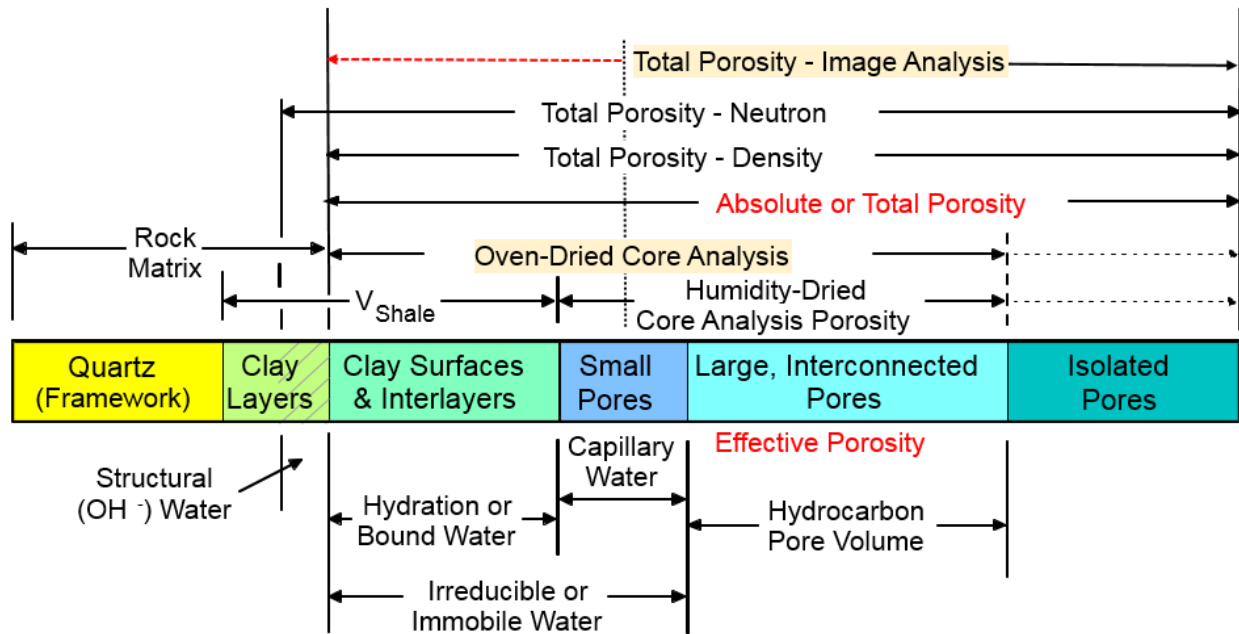


Figure 2.6: Components of total porosity, and sensitivity of each measurement to different components of porosity (modified from Eslinger, 1988)

In this study, core helium porosity and image analysis porosity are being compared. For core data, the drying conditions were not mentioned [appendix-D]. It is therefore assumed that the porosity estimated by image analysis has to be compared to what is inferred to be total porosity.

From Figure 2.6, total pore volume is sum of constituent pores of different sizes, with clay bound pore system being the smallest in size.

$$\Phi_{total} = \Phi_{clay\ bound} + \Phi_{capillary\ bound} + \Phi_{large\ connected\ pores} + \Phi_{isolated\ pores} \quad (2-11)$$

In Petrophysics terminology, effective porosity is non-clay porosity;

$$\Phi_{effective,petrophysics} = \Phi_{capillary\ bound} + \Phi_{large\ connected\ pores} + \Phi_{isolated\ pores} \quad (2-12)$$

While a Reservoir engineer may define only the inter-connected porosity as effective porosity. Clay bound and capillary bound pore system is usually considered as non-connected pores, they do not contribute to formation permeability. In Petrophysics term such porosity is equivalent to free fluid porosity.

$$\Phi_{effective,reservoir} = \Phi_{large\ connected\ pores} = \Phi_{free\ fluid\ porosity} \quad (2-13)$$

Isolated porosity if connected will significantly contribute to reservoir permeability, and can be added to equation (2-13). Isolated porosity sometimes also referred as secondary porosity and is usually observed in carbonate reservoirs as vugs and fractures. Sandstones are also known to contain fractured porosity but not the vuggy porosity.

Porosity can also be defined in terms of pore sizes as micro, meso and macro pores.

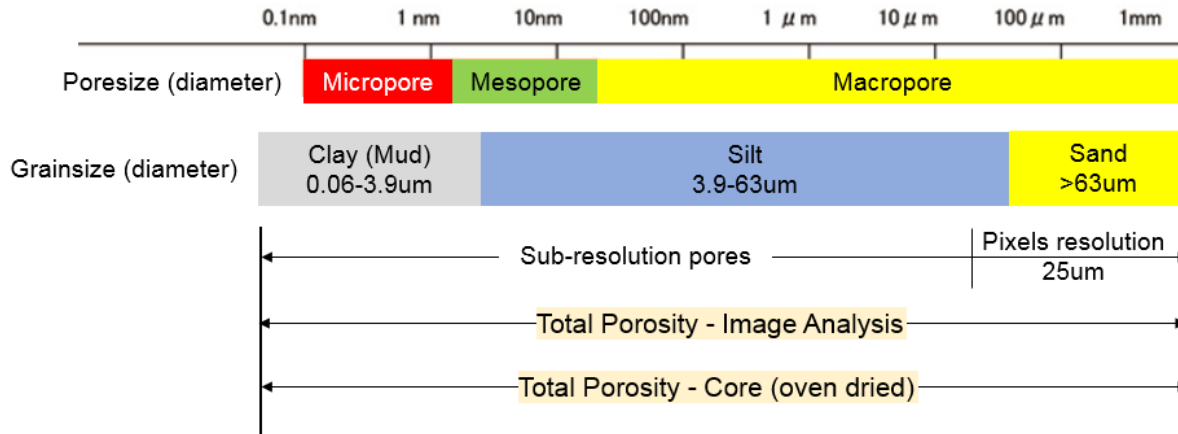


Figure 2.7: Pore size and grain size definitions (modified from Wentworth, 1922). Optical microscopy pixel resolution sensitivity to pore size

Core thin section samples used in current study were scanned with optical microscopy having pixel resolution of 25 μm. From Figure 2.7, for clastic reservoirs it can be inferred that digital image analysis can quantify intergranular porosity of medium-sized silt grains (~16 μm) to coarse grained sands. However, substantial porosity may be residing in pore sizes less than 25 μm, i.e. sub-resolution pores. Such sub-resolution pores were visually observe-able on thin section images but with a mixed response of clay-silt matrix and porosity. A subjective adjustment factor was used to extract matrix effect from sub-resolution pores, details are discussed in section 2.4.1.

2.4.1 Porosity partitioning in context of image analysis

In current study, sub-resolution pores are defined as ‘Micro Pores’ and pore sizes greater than 25 μm are defined as ‘Macro Pores’. Hence, terminology of micro and macro pores porosity in context of image analysis (scanned with optical microscopy) is used differently than their actual geological definitions.

$$\Phi_{image} = A * \Phi_{micro} + \Phi_{macro} = \Phi_{total} \quad (2-14)$$

Where ‘A’ in equation (2-14) stands for adjustment factor (between 0 and 1) to remove matrix effect from sub-resolution pores, as a pixel representing pore size of less than 25 μm may consist of *both* a grain and a pore. Φ_{micro} is micro pores porosity, and Φ_{macro} is macro pores porosity.

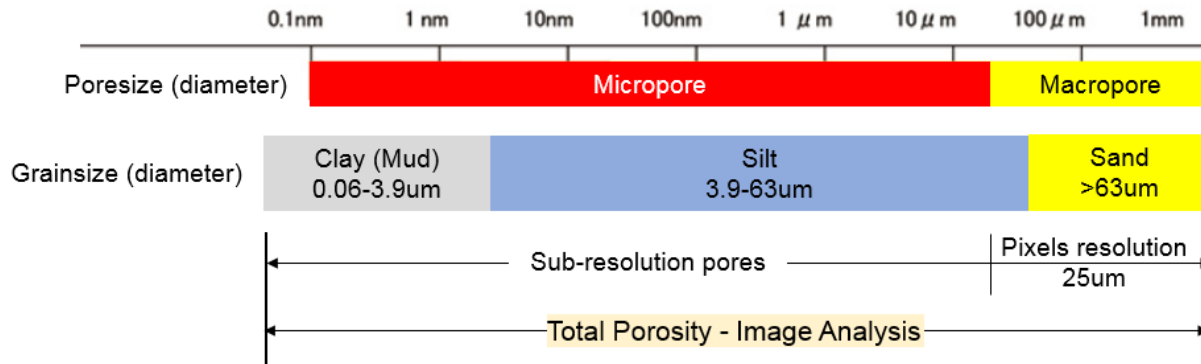


Figure 2.8: Modified definitions of Micro and Macro porosity in context of image analysis

Micro pores: pore sizes below the pixel resolution of optical scanning microscopy, hence contain matrix effect in it. An adjustment factor (A) must be used to remove this effect i.e. micro porosity shall be reduced by some fraction. Pore size less than $25 \mu\text{m}$.

Macro pores: these are the pores that are fully resolved at resolution of optical microscopy. No adjustment factor is required. Pore size greater than $25 \mu\text{m}$.

The following two equations define the micro porosity (Φ_{micro}) and macro porosity (Φ_{macro}) from image analysis presented in the current study;

$$\Phi_{micro} = \frac{\sum \text{pixels in micro pores}}{\text{total number of pixels}} \quad (2-15)$$

$$\Phi_{macro} = \frac{\sum \text{pixels in macro pores}}{\text{total number of pixels}} \quad (2-16)$$

The blue color epoxy used to fill the pore space, physically is one homogeneous color. But due to pixel resolution limitation of optical microscopy, pores ($> 25 \mu\text{m}$) appear bluer as compared to pore sizes $< 25 \mu\text{m}$, and defines color based definition of macro and micro pores respectively as shown in Figure 2.9.

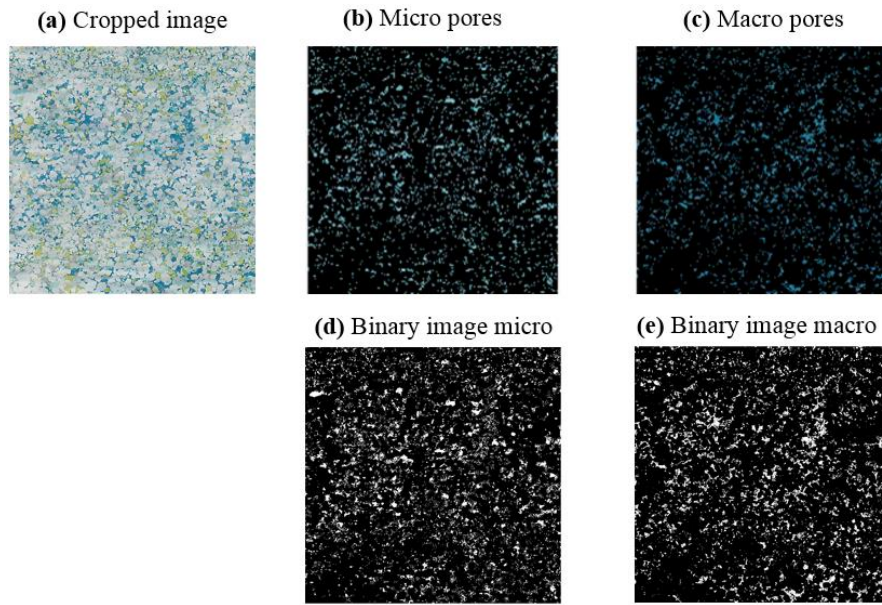


Figure 2.9: (a) original cropped image is segmented into micro pores (b, light blue) and macro pores (c, dark blue), (d&e) represents binarized images of micro and macro pores respectively. These binary images are used to calculate porosity from respective micro and macro pores

2.5 Permeability

Permeability is the dynamic property of reservoir rock and measures ease at which a fluid can flow through a rock. Darcy law (Darcy, 1856) states that flow rate of a single-phase fluid through a porous media is proportional to permeability of the rock and effective pressure gradient, and is inversely proportional to fluid viscosity. Permeability has units of milli-Darcy (mD).

Permeability is function of connectivity of pores, pore throats and grain size. For clastic reservoir, a general assumption is; bigger the pore size \rightarrow bigger the grains and pore throats. This assumption may not be true for carbonate reservoirs as their matrix framework is usually not granular.

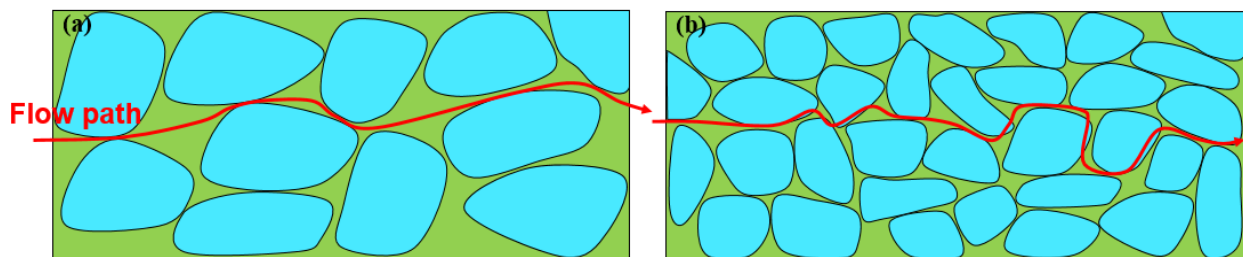


Figure 2.10: Schematic illustration of flow path (a) high porosity with big grain sizes providing less tortuous path to flow (b) less porosity with smaller grains providing more tortuous path to flow. Permeability of sample (a) will be better than sample (b)

A reservoir may contain significant quantity of hydrocarbons, but if pores are not connected with each other, hydrocarbons will not flow. Permeability is an important reservoir property influencing recoverable reserves.

Permeability is classified into absolute permeability (K_{abs}), effective permeability (K_{eff}) and as relative permeability (K_{ro} , K_{rg} , K_{rw}), where;

Absolute permeability: is a physical property of reservoir rock when it is saturated with only one fluid.

Effective permeability: ability of a fluid to follow in the presence of another fluid. For example, oil flowing in presence of water. Effective permeability is less than absolute permeability.

Relative permeability: ratio of effective permeability of a specific fluid to absolute permeability. Relative permeability profiles of two fluids is expressed as function of saturation. Since, relative permeability is a ratio, it is unitless.

2.5.1 Permeability from logs

Petrophysical logs are generally permeability indicators, because permeability is a dynamic property while well logs are static data. Except for sonic Stoneley mobility [Ahmed, 1991] where sonic Stoneley waves does move near-wellbore fluids. Permeability from logs is usually a correlation based function of porosity. One common practice is to plot core porosity-permeability data from individual routine core analysis tests, and regress it to establish permeability as a function of porosity through the reservoir. Since, porosity is determined through logs, correlation is applied on this porosity to get ‘absolute permeability’ estimates from logs.

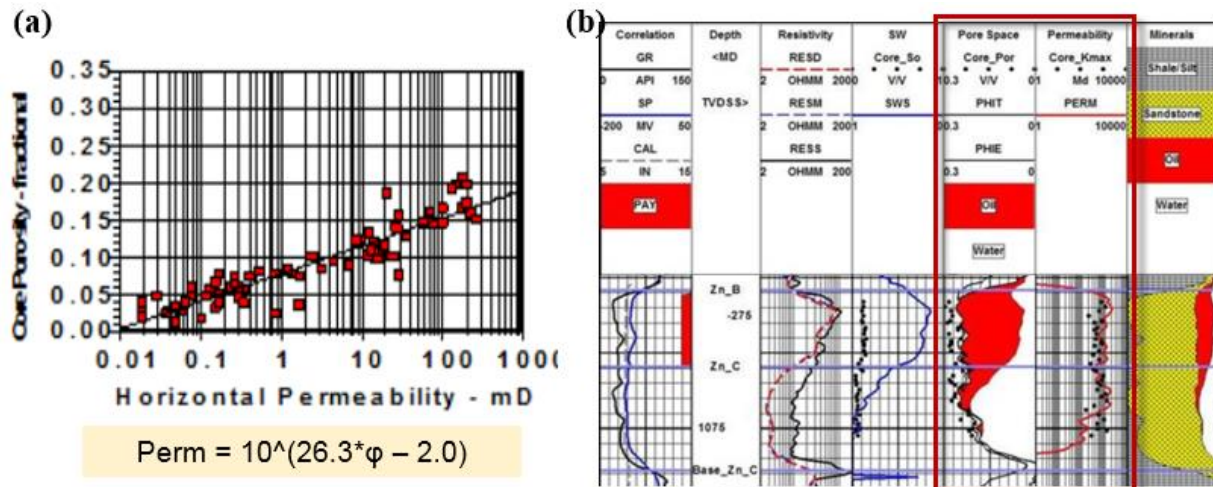


Figure 2.11: (a) developing permeability correlation as a function of porosity from core data (b) applying it on log porosity to get permeability curve [Crain's handbook]

Over the years, several correlations have been developed to determine permeability from logs and most of them are function of porosity e.g. Coates equation and Wyllie-Rose method. Some correlations are suited for clastic reservoirs, while others for carbonate reservoirs or for fracture permeability. One such correlation discussed here is geochemical algorithm [Herron, 1987] which is suitable for clastic reservoirs;

$$K_{air} = 10^{PermExp} \quad (2-17)$$

$$PermExp = 4.4 + 3\log_{10}(\Phi_{total}) - 2\log_{10}(1 - \Phi_{total}) + \sum_{i=1}^n ((PrmFac)(Mineral\ Weight))_i \quad (2-18)$$

Where $PrmFac$ is permeability factor that is a constant for each mineral and can be tuned to get better match of log based permeability with core gas or air permeability.

2.5.2 Permeability from cores

Dry gas (air, N₂ or He) permeability from cores is determined from Darcy Law;

$$Q = \frac{-KA\Delta P}{\mu L} \quad (2-19)$$

Where Q is flow rate, K is permeability, ΔP ($P_1 - P_2$) is pressure drop, L is path length and μ is dynamic viscosity.

A clean dried core plug is placed inside a sample holder, and dry gas is flowed through core plug at several flow rates. Inlet and outlet pressures are recorded. Fluid flow velocity (Q/A) is plotted vs $(\Delta P/L)$. At low flow rates, data exhibit a straight line with slope (K/μ) .

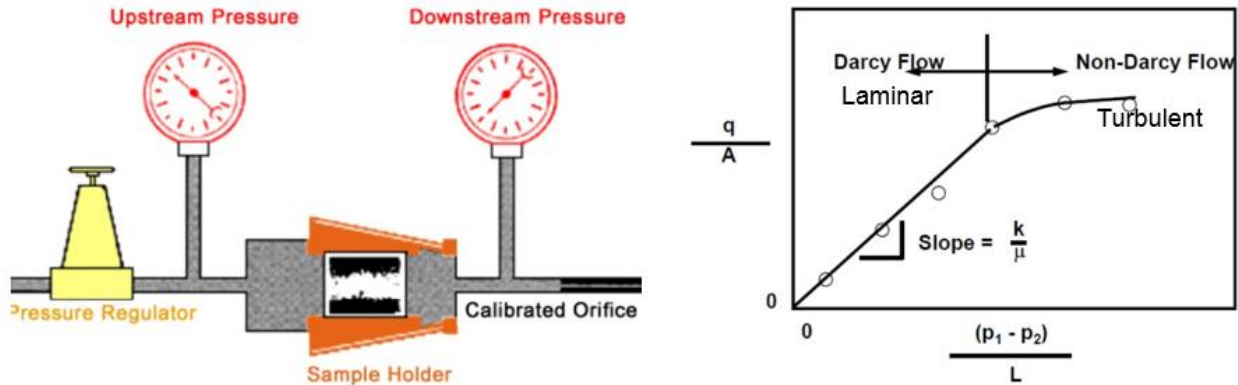


Figure 2.12: Schematic illustration of dry gas permeability from core plugs [Crain's handbook]

Core plugs gas permeability (K_{gas}) is 'absolute permeability' and is comparable for dry gas bearing reservoirs. For oil or water bearing reservoirs, Klinkenberg correction is applied to core gas permeability to correct for gas slippage effect. Klinkenberg correction provides equivalent liquid permeability (K_{el}), which is also an 'absolute permeability'. K_{el} is less than K_{gas} . Permeability from core plugs is measured in both horizontal (K_h) and vertical (K_v) directions.

2.5.3 Permeability from digital image analysis

Pore space in thin section image is filled with blue epoxy i.e. only one fluid is saturating the pore space. Hence, permeability from thin section is interpreted as ‘absolute permeability’. Permeability from thin section is derived in similar fashion as for the logs where correlations are used as a function of porosity. It is believed such correlations are suitable when porosity is granular, and the assumption that pore size distribution is proportional to grain size distribution Figure 2.8.

Two correlations are studied;

- 1- Kozeny-Carman permeability model
- 2- Timur-Coates permeability, adapted from NMR bound and free fluid porosity

2.5.3.1 Kozeny-Carman permeability

Josef Kozeny and Philip C. Carman [Carman, 1937; Dvorkin 2009] developed a correlation that express permeability as a function of porosity and specific surface area. The model is based on flow through capillary tubes, rock with connected pores is represented by a sample with cross-sectional area ‘A’ and length ‘L’ consisting of ‘n’ number of capillary tubes of microscopic length ‘l’ and radius ‘r’.

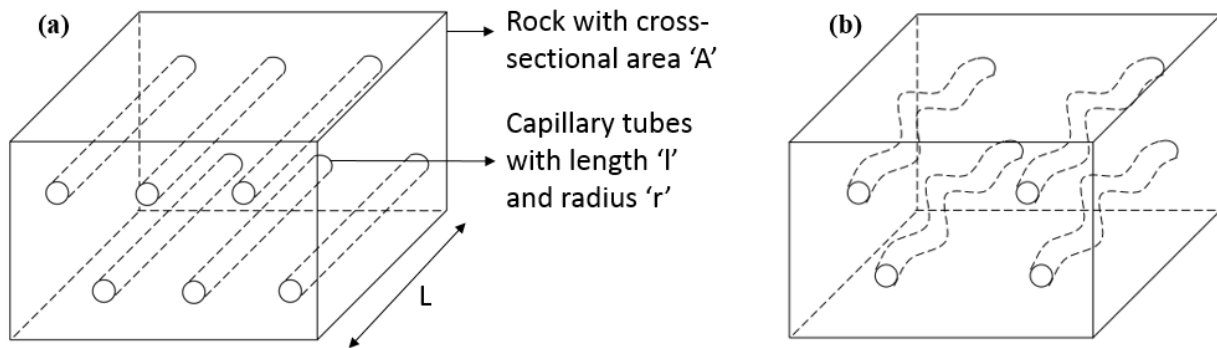


Figure 2.13: capillary bundle model, (a) straight tubes with $l = L$, (b) tubes with tortuous path $l > L$

When pressure difference ΔP is applied across the model, the fluid flow (Q) of viscosity (μ) through each individual capillary tube of length (l) is given by Poiseuille’s law [Dullien, 1979];

$$Q = \frac{\pi r^4 \Delta P}{8 \mu l} \quad (2-20)$$

Similarly, flow through a single capillary tube in a medium of cross-sectional area (A) is expressed by Darcy Law as;

$$Q = \frac{KA \Delta P}{\mu L} \quad (2-21)$$

Comparing equations (2-20) and (2-21), and re-arranging to solve for permeability (K);

$$K = \frac{\pi r^4 L}{8A l} \quad (2-22)$$

However, porous media does not represent straight flow path where $l > L$ as depicted in Figure 2.13 (b), a tortuosity factor ($\tau = l/L$) is defined which is the length of the flow path over the length of permeable medium.

$$K = \frac{\pi r^4 l}{8A \tau} \quad (2-23)$$

In context of thin sections, a more useful form of equation would be that can relate permeability to porosity and other properties like pore specific surface area [Srisuttiyakorn, 2015]. These are the properties we can determine from image analysis.

Porosity is written as;

$$\Phi = \frac{\pi r^2 l}{AL} = \frac{\pi r^2 \tau}{A} \quad (2-24)$$

Specific surface area (S) is the ratio of pore surface area per unit volume and is written as;

$$S = \frac{2\pi r l}{AL} = \frac{2\pi r \tau}{A} \quad (2-25)$$

Equation (2-25) is re-arranged;

$$S = \frac{2\pi r^2 \tau}{r A} = \frac{2\Phi}{r} \quad (2-26)$$

$$r = \frac{2\Phi}{S} \quad (2-27)$$

Substituting equations (2-24) and (2-27) in (2-23);

$$K = \frac{\pi r^2 \tau}{A} \frac{r^2}{8\tau^2} = \Phi \frac{(2\Phi)^2}{8\tau^2 S^2} = \frac{\Phi^3}{2\tau^2 S^2} \quad (2-28)$$

The general form of Kozeny-Carman equation to determine permeability from thin section images is given as;

$$K_{Kozeny-Carman} = \frac{(\Phi_{total})^3}{C_o * S^x} \quad (2-29)$$

Where C_o is Kozeny-Carman constant and is approximately 5 [Carman, 1937; Zerabruk, 2017], the specific surface area exponent 'x' as shown in above derivation is 2, but this value can be adjusted to achieve a better correlation between image based permeability and the 'ground truth' derived from direct measurements such as core permeability.

Modifications to above form of the equation (2-29) has been discussed in literature [Dvorkin, 2009; Srisuttiyakorn, 2015] but are not implemented in current thesis work.

Specific surface area or surface to volume ratio is approximated by the ratio of pore perimeter to pore area. Perimeter and area of each pore (i) are outputs of ‘ImAnalysis’ script [section 3.1.6].

$$S_i = \frac{\text{Pore Perimeter}}{\text{Pore Area}} \quad (2-30)$$

The specific area of the analyzed sample is approximated as the average specific area of all pores.

$$S = \frac{1}{N} \sum S_i \quad (2-31)$$

Unit of specific area is [1/pixel] and is converted into units of [1/m] by knowing that 1 pixel = 25 μm [section, 2.1].

Hence, dimension of permeability from equation (2-29) will be [m^2] and is converted to [mD] unit by using conversion factor of $1\text{m}^2 = 1.01 \times 10^{15}$ mDarcy.

2.5.3.2 Timur-Coates permeability

Timur-Coates permeability equation is correlation based and determined experimentally by comparing NMR (nuclear magnetic resonance) permeability estimate against core permeability. This correlation relates permeability to total porosity and to the ratio of pores that will contribute to permeability to the pores that will not contribute to permeability [Coates, 1973; Allen, 2000].

$$K_{Timur-Coates} = 10000 \left(a(\Phi_{total})^b * \left(\frac{\Phi_{free\ fluid\ porosity}}{\Phi_{bound\ fluid\ porosity}} \right)^c \right) \quad (2-32)$$

Where a , b and c are constants with default values of 1, 4 and 2 respectively.

Equation (2-32) can be used to estimate permeability from image analysis based on the assumption that free fluid porosity is related to macro pores and bound fluid porosity to micro pores. In context of image analysis, equation (2-32) is re-written as;

$$K_{Timur-Coates} = 10000 \left(a(\Phi_{total})^b * \left(\frac{\Phi_{macro}}{\Phi_{micro}} \right)^c \right) \quad (2-33)$$

The equation outputs permeability in units of mD.

2.6 Saturation and irreducible water saturation

Saturation is defined as pore volume occupied by a fluid. In case of an oil bearing water wet reservoir, there will be a portion of pore space occupied by water and the rest by oil. Water saturation (S_w) can be defined as;

$$S_w = \frac{\text{Pore volume occupied by water}}{\text{Pore volume}} = \frac{V_w}{\Phi} \quad (2-34)$$

If porosity term in the denominator is total porosity then saturation is total water saturation (S_{wt}), and if effective porosity is used then it will be effective water saturation (S_{we}). For water wet reservoirs, S_{we} is less than S_{wt} . Unit of saturation is either expressed in fraction or as percentage. Hence, oil saturation (S_o) will be $1 - S_w$.

Total and effective water saturation was not available for the studied data. However, it was possible to estimate irreducible water saturation (S_{wirr}) from digital image analysis. Hence, a brief description of methods that can estimate S_{wirr} is mentioned here.

Irreducible water saturation can be defined as critical saturation below which water will not flow.

2.6.1 Irreducible water saturation from NMR logs

Only nuclear magnetic resonance (NMR) log can estimate S_{wirr} . It assumes that bound fluid porosity will not contribute to flow. Based on experimental data and observations over datasets in several fields, NMR porosity in sandstone reservoirs can be partitioned into bound and free fluid porosity by using transverse time (T2) cutoff of 33 ms, and for carbonates it is about 120 ms. For a water wet reservoir, bound fluid porosity is pore volume occupied by water that will not flow and is equivalent to S_{wirr} .

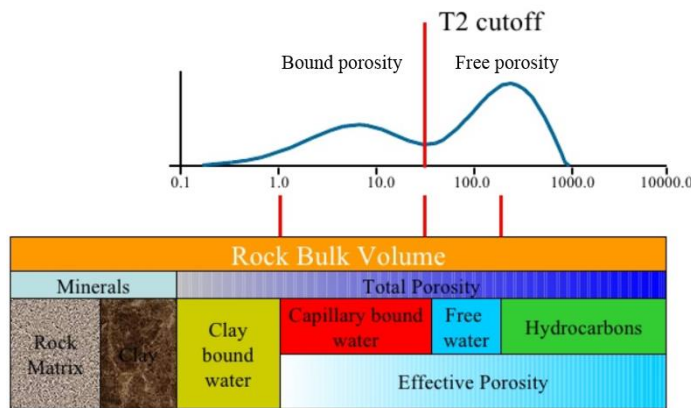


Figure 2.14: NMR definition of bound and free fluid porosity for irreducible water saturation

$$S_{wtirr,NMR} = \frac{\text{Bound fluid porosity}}{\text{Total porosity}} \quad (2-35)$$

Caution shall be taken as the term in the denominator shall be total porosity. NMR porosity is equivalent to total porosity in oil and water bearing reservoirs. But for gas and very light oil bearing reservoirs, NMR porosity needs correction for hydrogen index effect to give total porosity.

Correlations can also be developed based on core data or from logs as function of porosity and permeability [Herron, 1987] to estimate irreducible water saturation.

$$S_{wtirr,log} = 0.25(4.4\log_{10}(\Phi_{total}) - \log_{10}(K_{log}) + 6.7) \quad (2-36)$$

2.6.2 Irreducible water saturation from cores

For an oil bearing reservoir drilled with oil-based-mud (OBM) at irreducible water saturation. The volume of water collected with Dean-Stark experiment will be irreducible water volume.

S_{wirr} from core is determined with special-core-analysis (SCAL) experiments; centrifuge or mercury-injection capillary pressure and through relative permeability profiles.

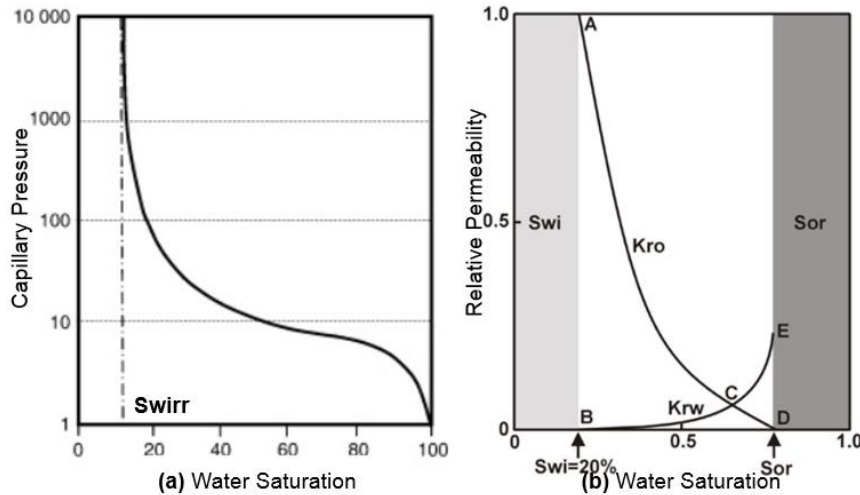


Figure 2.15: Special core analysis (a) irreducible water saturation from capillary pressure data (b) from relative permeability profile

2.6.3 Irreducible water saturation from digital image analysis

S_{wirr} from image analysis is derived the same way as in equation (2-35). From figures Figure 2.8 and Figure 2.14, micro porosity from image analysis is equivalent to NMR bound fluid porosity.

$$S_{wtirr,image} = \frac{\Phi_{micro}}{\Phi_{total}} \quad (2-37)$$

3 METHODOLOGY

3.1 Digital image analysis

Digital images were studied using Matlab R2017b software and six different codes were developed for image preparation, segmentation, petrophysical properties extraction and for morphological analysis of pore space. The purpose of each script is briefly mentioned below while the code details are included in appendix-B. The scripts focus on finding optimum technique(s) that can extract porosity from thin section image. A manual thresholding technique on pixel intensity histogram is discussed first, and due to subjective nature of picking these threshold values, automatic clustering technique is introduced.

1. Main script
2. Slide color test
3. Thin section test Rc
4. Thin section test Rc auto
5. ImClusters Kmean
6. ImAnalysis

3.1.1 Main script

The script crops the thin section digital image into 800x800 pixels dimension square array. It also calls out the scripts (2-to-6) mentioned above. While most of the samples were cropped at 800x800, but there were some scanned samples with trimmed dimensions and were cropped at reduced pixel dimensions e.g. 780x780.

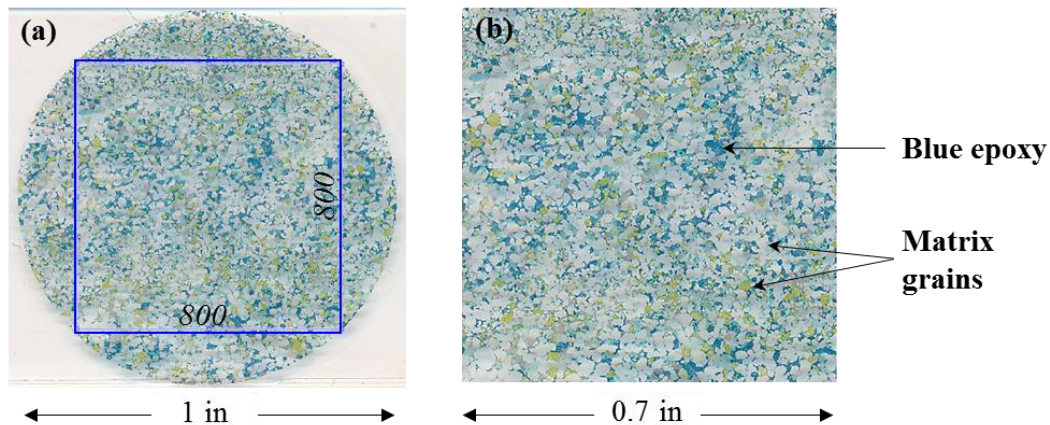


Figure 3.1: (a) represents the 1 inch diameter thin section digital image and 800x800 pixels dimension blue square that was used to crop the image (b) cropped image, dimension of the thin section image is reduced to 0.7 inch after cropping

3.1.2 Slide color test

Slide color test script is mainly an initial visual analysis of the cropped image, it segments the image into red-green-blue (RGB) space and luminosity-chromaticity (Lab) space. Any color image is basically a combination of three colors red, green and blue mixed in different proportions [Heilbronner, 2014]. Hence, by segmenting the image into these three basic colors and analyzing the pixel intensity histogram of each color component, different features residing in an image can be extracted. In Lab space, 'L' stands for luminosity and features the brightness or light emitted by an image, 'a' is chromaticity layer indicating where colors fall along the red-green axis, 'b' is also chromaticity layer indicating where colors fall along blue-yellow axis. All of the color information resides in 'a' and 'b' layers.

In Figure 3.2, it can be visualized that blue epoxy stands out on the red component of the segmented image. Inverted R component (R_c) in Figure 3.2 is inverse (complement) of red component and the bright features appearing on its image are associated with blue epoxy. The pixel intensity histogram (scale 0-255) of each image is also displayed and by thresholding (cut-off) the histogram, feature of desired interest can be extracted. It was observed from analysis of several samples that blue epoxy can be properly captured by thresholding the inverted red component of the segmented image, in our case the lack of red intensity (low number, i.e. high number when inverted) implies the presence of blue color, hence epoxy placed in pores. Matlab scripts where thresholds were used to capture sample porosity, only the inverted red component of the image was used.

3.1.3 Thin section test R_c

This script uses the pixel intensity histogram of red component complement (R_c) to extract blue epoxy feature residing in pore space. As can be seen from Figure 3.2, not all part of the pixel intensity histogram represents the pore space, instead histogram is representation of the entire image in its respective color space. Hence, a threshold (or cut-off) is needed on intensity histogram to extract the desired feature.

Figure 3.4 shows simplified workflow of the script, the analysis starts from the cropped original image, which is then segmented into RGB space and only the red component (inverted, R_c) was analyzed appropriate to capture pore space (b). A threshold was applied on pixel intensity histogram such that pixels representing the pore space resides between threshold value and scale maximum value of 255 pixels (c). To quality control the results of captured pores a red boundary is marked around the captured pores (e). A binary image (d) is also created which is used to quantify porosity from pixels count in white region of the binarized image.

The image has a pixel resolution of $25 \mu\text{m}/\text{pixel}$, hence pore sizes greater than $25 \mu\text{m}$ can be quantified with a single threshold. But there can be significant number of pores with size less than $25 \mu\text{m}$ contributing to porosity. It was analyzed that a second threshold was needed to capture these sub-resolution pores, and micro pores required a qualitative adjustment factor to separate matrix effect from these sub-resolution pores. An adjustment factor of 0.4 was used in Zerabruk et al. work. Details of the two thresholds and associated porosity definitions are discussed under sections 2.4.1 and 3.1.5.

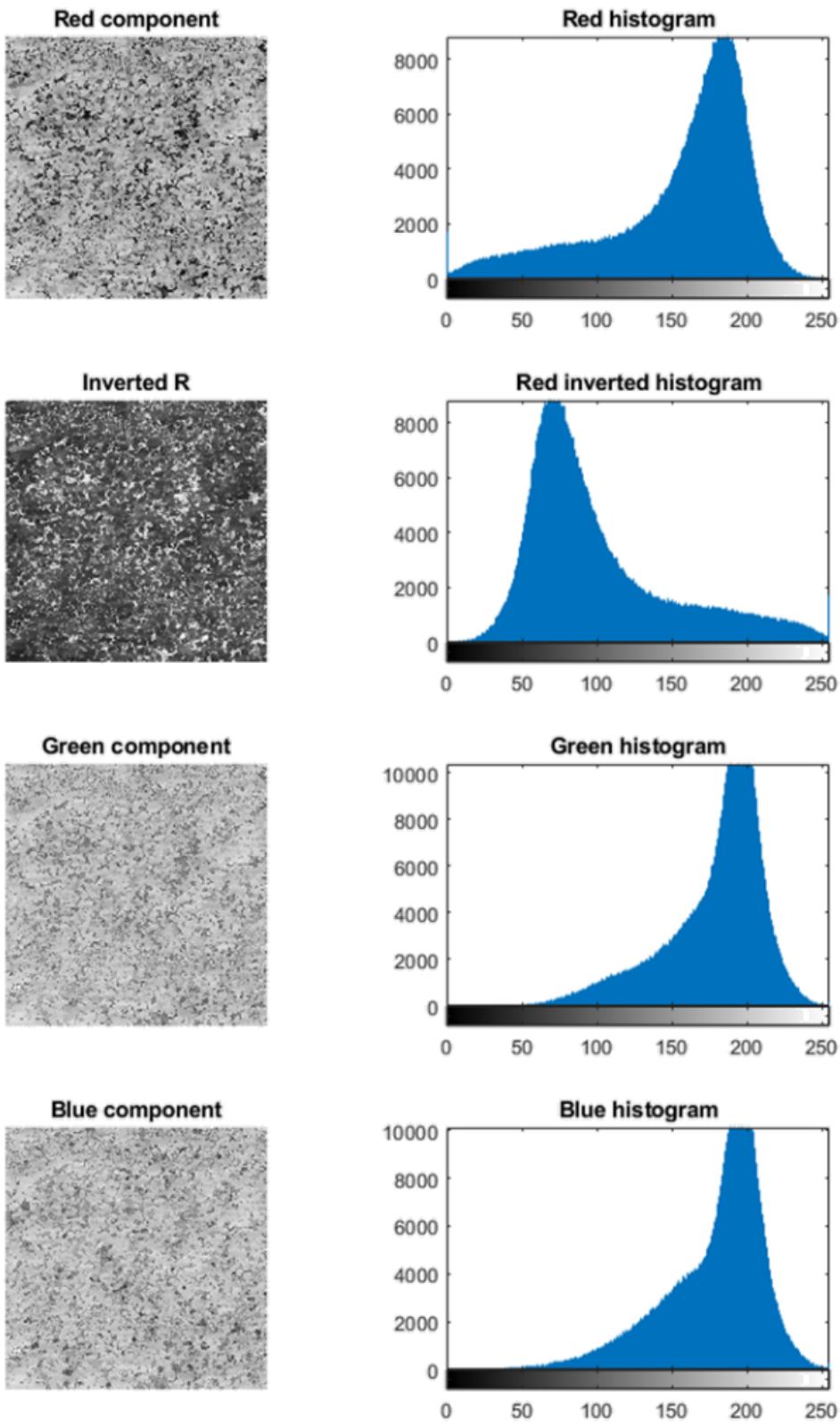


Figure 3.2: image segmentation into red-green-blue (RGB) space

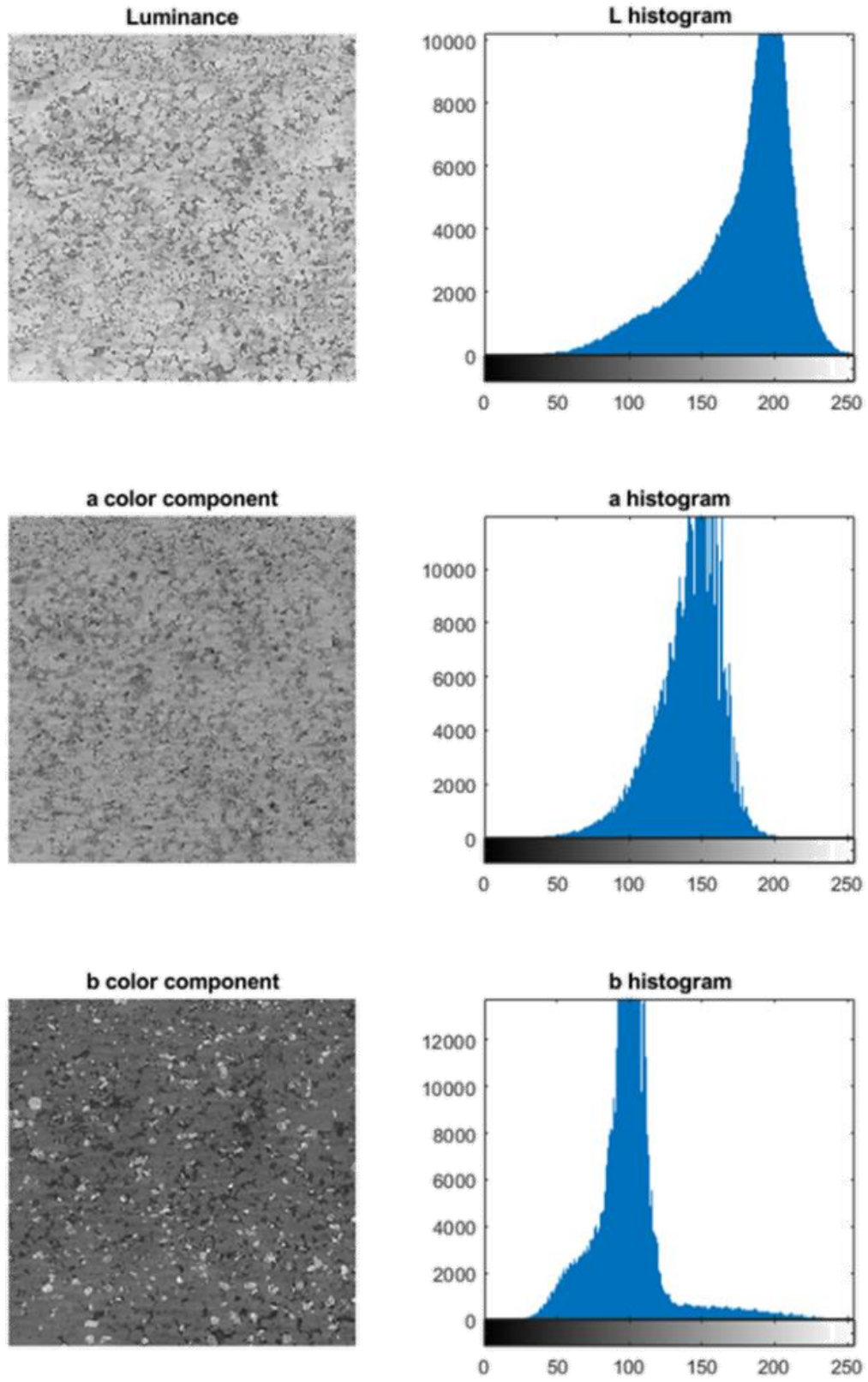


Figure 3.3: image segmentation into luminosity-chromaticity (Lab) space

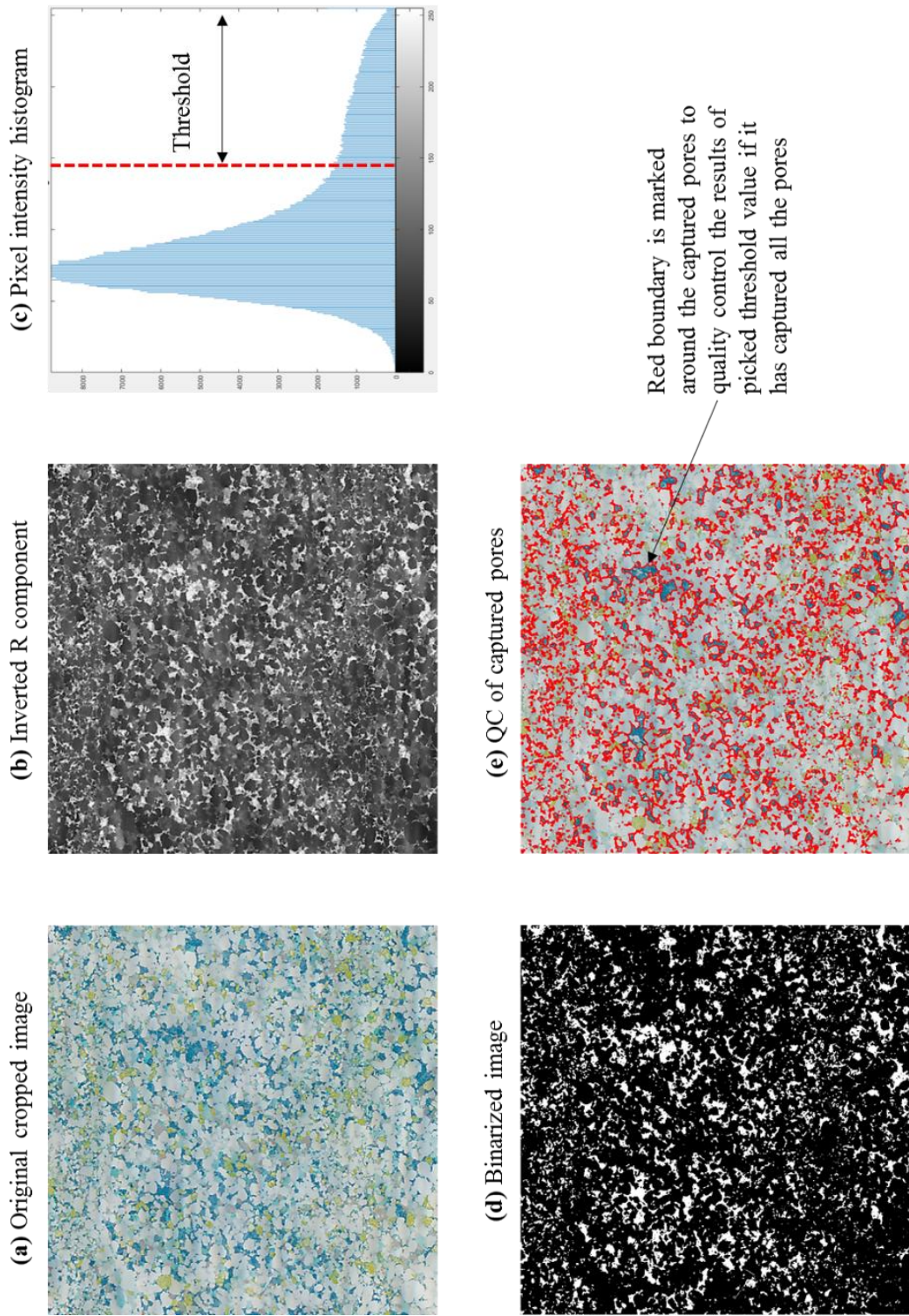


Figure 3.4: Thin section test Rc workflow to capture pore space by using inverted red component of thin section image

3.1.4 Thin section test Rc auto

Thresholding pixels histogram to capture pore space is a manual technique where threshold value is adjusted until analyst is visually satisfied that all pores have been captured correctly. The workflow is qualitative in a sense that resolution of optical microscopy is not sufficient to settle on one threshold value.

It was desired in this project to aim at removing subjectivity from picking the threshold values and automate the process. To automatically identify threshold values, a curve (Fourier order 3) was fit to pixel intensity histogram and its second order derivative was used to suggest threshold values.

Figure 3.5 (a) shows the 3rd order Fourier fit on pixel intensity histogram of inverted red component. Then 2nd order derivative of this fit was used to identify inflexion points (b) as potential threshold values to capture both visualize able and sub-resolution pores. This approach was applied on several samples and it was analyzed that suggested auto-threshold values did not capture all the pores which led to under estimation of porosity when compared against core helium porosity. The results and short comings of this approach are discussed under section 4.1.2.

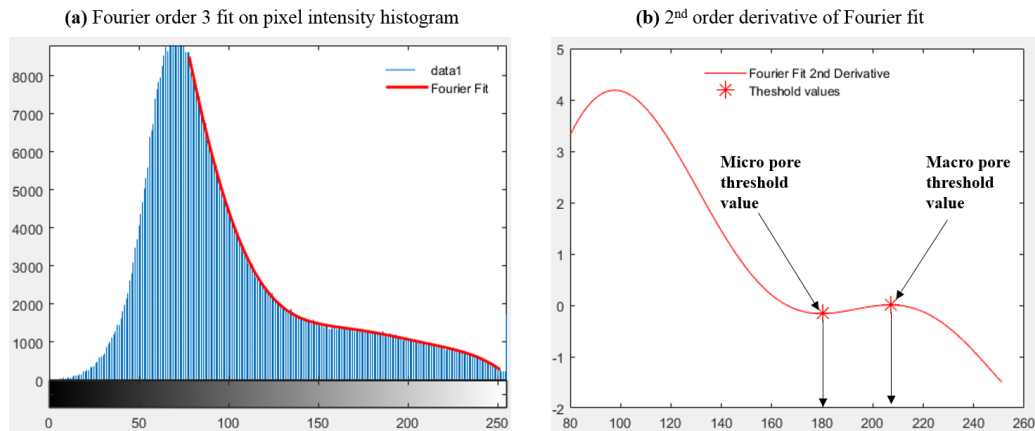


Figure 3.5: Fourier fit and its 2nd derivative analysis to suggest threshold values

3.1.5 ImClusters Kmean

One main objective of current year thesis work was to automate process of extracting pore space. After the short comings of auto-thresholding technique, data partitioning technique like k-means clustering was analyzed. In Figure 3.6, the function k-means partitions 'n' observations into 'k' number of mutually exclusive clusters and returns clusters indices assigned to each observation. It is an iterative process and partitioning is achieved in a way that data points within a cluster are as close to each other as possible and as distant from data points in other clusters. Each cluster is characterized by its centroid or center point. There are five different distance measuring techniques in Matlab; sqeuclidean, cityblock, cosine etc.

Number of clusters and centroids initialization need to be defined initially. After analyzing several samples and based on resolution limitation of optical microscopy it was concluded that three number of samples were sufficient to reliably extract blue feature of the image, Figure 3.7. Choosing number of clusters greater than 3 deteriorated cluster associated with blue color and under-estimated porosity. 'Kmeans++' algorithm [MathWorks documentation] was used for centroids initialization and 'Euclidean distance' was used for distance minimization to partition clusters. To avoid local minima, initialization was repeated three times.

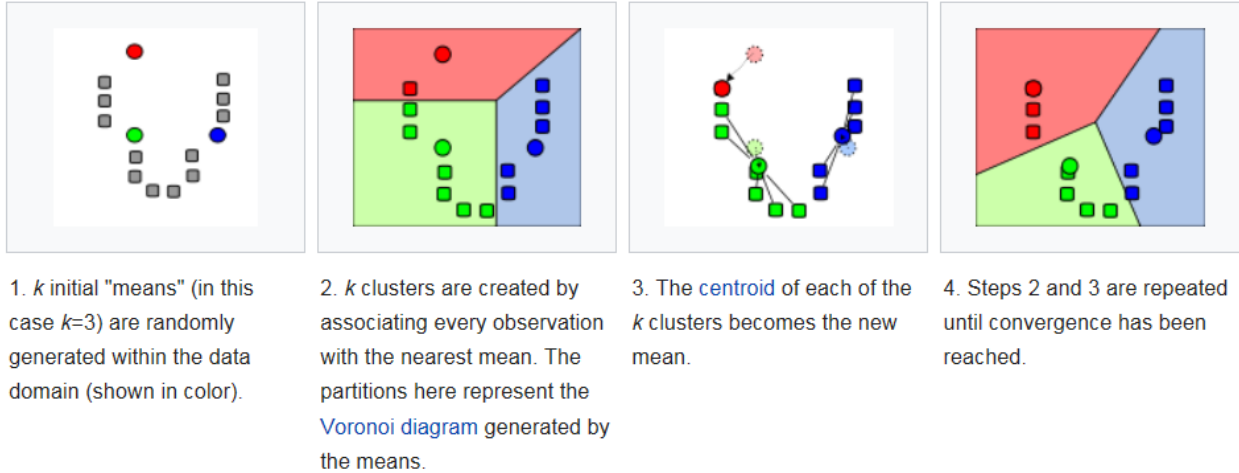


Figure 3.6: K-means logic to partition data points into clusters based on minimizing data points distance from cluster centroid

While clustering, analysis can be performed on any color space, RGB, Lab or HSV. It was analyzed for the studied thin section samples that Lab scale (Lab) clustering best resolved blue epoxy to capture pore space. In Lab scale, color information lies in 'a' and 'b' segments of the image, this color information was used to capture blue color epoxy associated with pore space, cluster#2 Figure 3.7. However, it can be observed from the captured cluster#2 image that intensity of blue color is not the same across all pores. Pore sizes greater than pixel resolution of the image (macro pores) appear bluer as compared to sub-resolution pores (micro pores) which includes matrix effect in it.

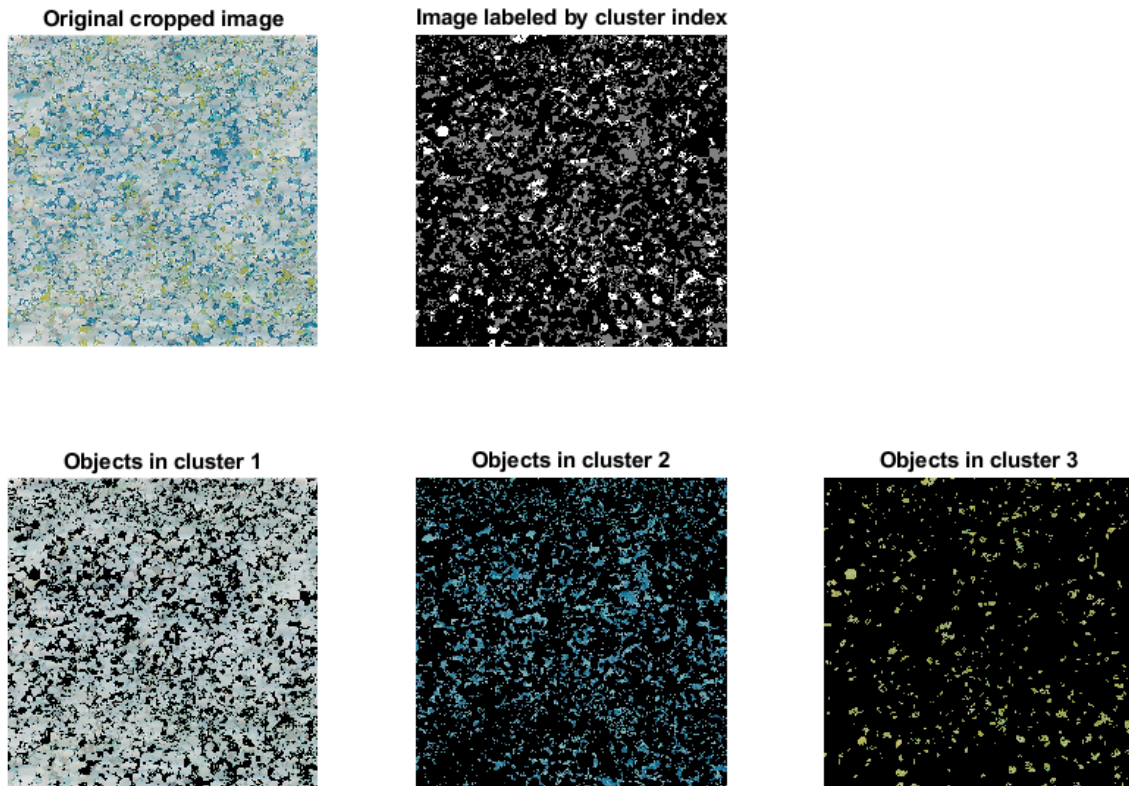


Figure 3.7: K-means clustering to partition cropped thin section image into three clusters

'L' luminosity was used to further segment blue color into dark blue easily visualize-able pores and light blue sub-resolution pores, Figure 3.8. Like manual thresholding technique, an adjustment factor was required to take out matrix effect from sub-resolution pores. After analyzing all the samples, an adjustment factor of 0.8 was found suitable to capture porosity of small pores [section 4.1.3].

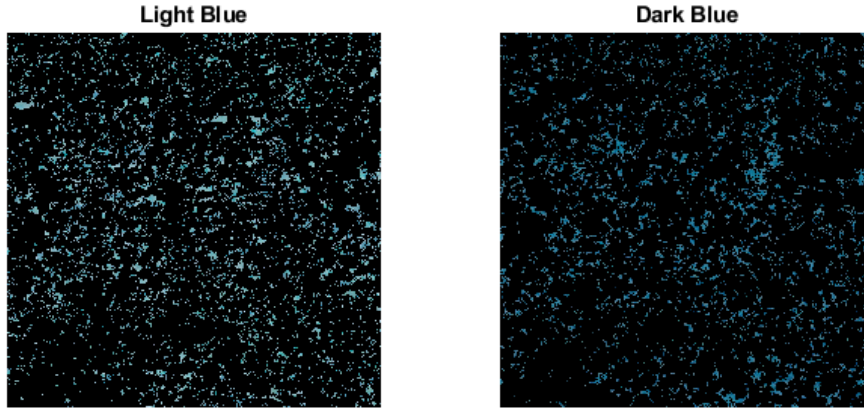


Figure 3.8: Using luminosity 'L' component to further partitioning the captured blue epoxy into dark and light blue

For comparison and quality control purpose, pixel intensity of captured pores from K-means clustering was plotted on inverted red component histogram. It served two purposes;

1. To predict threshold values if it is required to capture porosity by using the thresholding technique.
2. It highlights how pixel intensity associated with blue epoxy (pores) is distributed over the pixel intensity histogram of the entire image.

From Figure 3.9, it can be analyzed that it will be difficult to interpret sub-resolution pores by using manual thresholding technique which would capture significant portion of matrix and a very subjective adjustment factor will be required to remove matrix effect.

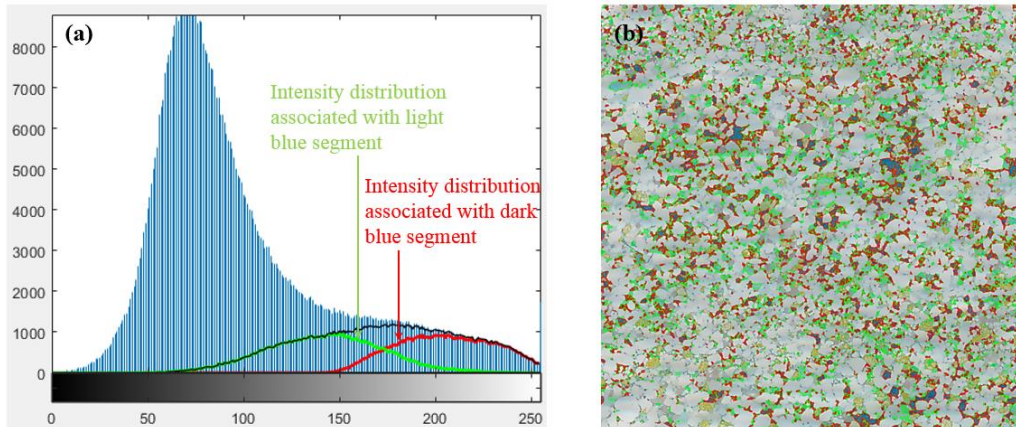


Figure 3.9: (a) pixel intensity distribution of cluster associated with blue color on inverted red component of the original cropped image. (b) quality control of captured pores using k-means clustering, where green boundary is used to capture sub-resolution pores and red boundary for visible pores

3.1.6 ImAnalysis

This script uses 'regionprops' built-in function of Matlab to identify physical features of each pore;

- 1- Pore area: actual number of pixels in the region
- 2- Center of pore space in x, y coordinate: center of mass of the region
- 3- Major and minor axis: major and minor axis of the ellipse, it is length in units of pixels
- 4- Perimeter of each pore: distance around the boundary of the region
- 5- Orientation: angle between the x-axis and the major axis of the ellipse
- 6- Eccentricity: is the ratio of the distance between the foci of the ellipse and its major axis length. An ellipse whose eccentricity is 0 is a circle, and value of 1 is a line segment

Pore area can be used to establish pore size distribution, sphericity of the pore can be estimated from specific surface area (equation (2-30)). Pore specific surface area is an input to Kozeny-Carman permeability equation (2-29). We did not explore other applications of these morphological properties in current study.

4 RESULTS

Thin section samples from NPD database for the well 7128/6-1 from Barents Sea that were drilled from 11.08.1991 to 08.11.1991 by Conoco Norway Inc. are analyzed. Oil shows were encountered in some formations penetrated by the well, but the field was not developed. More information about the well can be found on NPD website, facts page. These samples cover the range of rock types as carbonates, sandstone and fractured shales. The scanned images of all thin section samples are presented in appendix-C. Selected 26 samples were chosen for porosity and permeability analysis, as the physical quality of remaining samples was considered not good enough.

Sample ID	Sample Depth (m)	Groups	Formation	Lithology	
1	1630.10	Tempelfjorden	Røye	Carbonate	
2	1637.81			Carbonate	
3	1643.88			Carbonate	
4	1891.90	Gipsdalen	Ørn	Carbonate	
5	1896.70			Carbonate	
6	1902.72			Carbonate	
7	1904.75			Carbonate	
8	1913.49			Carbonate	
9	1916.15			Carbonate	
10	1930.44			Carbonate	
11	1945.28			Carbonate	
12	1947.94			Carbonate	
13	1952.04			Clastic	
14	1957.66			Carbonate	
15	1964.40			Carbonate	
16	1971.63			Carbonate	
17	1975.63			Carbonate	
18	2000.70			Carbonate	
19	2006.47			Carbonate	
20	2015.03			Carbonate	
21	2019.03			Carbonate	
22	2044.52			Carbonate	
23	2046.03			Carbonate	
24	2109.34			Falk	Clastic
25	2128.82				Clastic
26	2243.39			Billefjorden	Tettegras

Table 4-1: thin section samples lithostratigraphy and lithology

4.1 Porosity from image analysis

Porosity is analyzed by using methods discussed under [section 3];

- (1) Manual threshold method
- (2) Auto-threshold method

- (3) K-means clustering method
- (4) Clusters predicted threshold method

4.1.1 Manual threshold method

It is the same method as used in [Zerabruk, 2017] work where thresholds were used on pixel intensity histogram of the inverted red component (Rc). The threshold values were manually picked and adjusted until analyst is visually satisfied that all pores have been captured correctly. The results of this method are included as a reference, to compare validity and goodness of the results from newly developed techniques in current year’s thesis work.

Two thresholds were chosen, one to capture porosity of macro pores that are fully resolved at pixel resolution of optical microscopy and a second level threshold to capture sub-resolution micro pores. Total porosity is the sum of micro and macro porosity. Micro porosity in Zerabruk, 2017 work was adjusted by the factor ($A = 0.4$) to exclude matrix effect from micro pores.

$$\Phi_{total} = A * \Phi_{micro} + \Phi_{macro} \tag{4-1}$$

Conventional core analysis data used for comparison is included in [appendix-D].

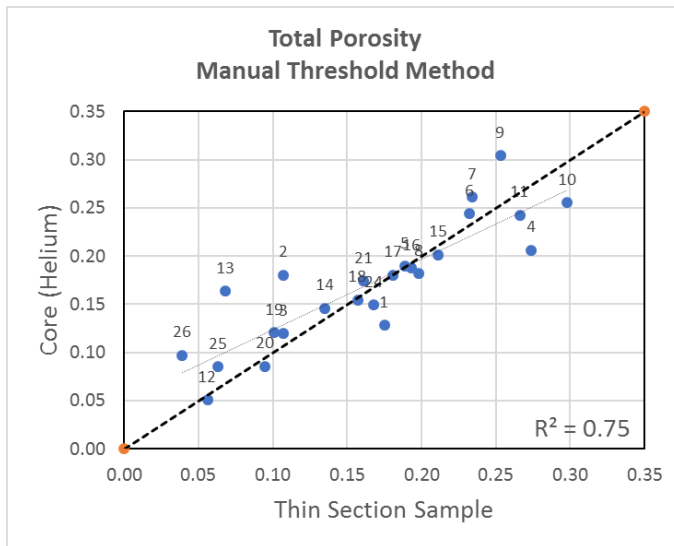


Figure 4.1: Comparison of image based total porosity using **manual threshold** with core helium porosity

Sample ID	Sample Depth (m)	Micro pores cut-off	Macro pores cut-off	Micro porosity (fraction)	Macro porosity (fraction)	Total porosity (fraction)
1	1630.10	90	105	0.043	0.132	0.175
2	1637.81	110	140	0.013	0.094	0.107
3	1643.88	140	170	0.045	0.062	0.107
4	1891.90	140	170	0.064	0.210	0.274
5	1896.70	140	170	0.084	0.105	0.189
6	1902.72	150	175	0.068	0.164	0.232
7	1904.75	160	175	0.092	0.142	0.234
8	1913.49	140	170	0.078	0.120	0.198
9	1916.15	200	210	0.039	0.214	0.253
10	1930.44	150	170	0.100	0.198	0.298
11	1945.28	150	180	0.088	0.178	0.266
12	1947.94	130	160	0.011	0.045	0.056
13	1952.04	190	210	0.011	0.057	0.068
14	1957.66	110	150	0.061	0.074	0.135
15	1964.40	160	200	0.025	0.186	0.211
16	1971.63	110	150	0.058	0.135	0.193
17	1975.63	130	175	0.049	0.132	0.181
18	2000.70	150	170	0.031	0.126	0.157
19	2006.47	130	160	0.050	0.051	0.101
20	2015.03	110	150	0.018	0.077	0.095
21	2019.03	150	175	0.053	0.108	0.161
22	2044.52	210	230	0.062	0.110	0.172
23	2046.03	220	230	0.072	0.137	0.209
24	2109.34	110	150	0.072	0.096	0.168
25	2128.82	190	210	0.014	0.049	0.063
26	2243.39	200	220	0.019	0.020	0.039

Table 4-2: Image porosity analysis by using two levels manual threshold method

4.1.2 Auto threshold method

Manual thresholding technique required back-and-forth threshold adjustment and workflow was analyzed as tedious and subjective. It can be difficult to judge where to stop macro and micro pores cut-off. Hence, it was desired to automate this process. The methodology used to predict auto threshold values for micro and macro process was discussed under [section 3.1.4].

For most of the samples, auto threshold method under estimated the total porosity. In Table 4-2, no adjustment factor was applied on micro pores, as use of such factor will further reduce total porosity. Auto threshold predictions were discarded for any further analysis, and it was required to consider alternate automatic method.

Sample ID	Sample Depth (m)	Micro pores cut-off	Macro pores cut-off	Micro porosity (fraction)	Macro porosity (fraction)	Total porosity (fraction)
1	1630.10	107	181	0.110	0.015	0.124
2	1637.81	107	209	0.115	0.044	0.159
3	1643.88	155	205	0.059	0.035	0.094
4	1891.90	166	222	0.151	0.076	0.227
5	1896.70	189	220	0.039	0.014	0.053
6	1902.72	185	232	0.099	0.026	0.125
7	1904.75	177	229	0.114	0.022	0.136
8	1913.49	157	205	0.027	0.058	0.085
9	1916.15	197	221	0.222	0.132	0.354
10	1930.44	166	230	0.219	0.016	0.234
11	1945.28	171	225	0.186	0.038	0.224
12	1947.94	129	215	0.054	0.018	0.073
13	1952.04	125	192	0.128	0.082	0.210
14	1957.66	166	223	0.039	0.014	0.053
15	1964.40	158	212	0.081	0.170	0.251
16	1971.63	148	207	0.064	0.094	0.158
17	1975.63	167	221	0.078	0.068	0.146
18	2000.70	147	189	0.135	0.086	0.221
19	2006.47	179	227	0.024	0.004	0.028
20	2015.03	146	217	0.035	0.045	0.080
21	2019.03	130	218	0.414	0.034	0.448
22	2044.52	197	236	0.320	0.073	0.393
23	2046.03	231	249	0.114	0.014	0.128
24	2109.34	142	224	0.114	0.007	0.121
25	2128.82	177	203	0.048	0.061	0.110
26	2243.39	146	212	0.221	0.062	0.283

Table 4-3: Image porosity analysis by using two levels *auto threshold* method

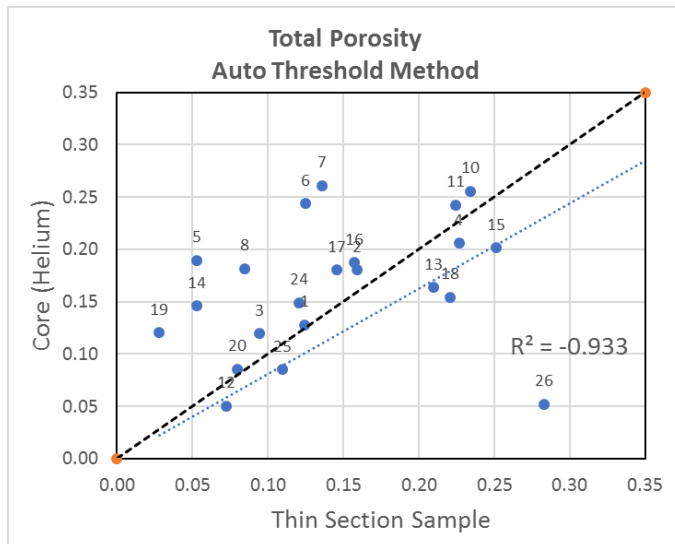


Figure 4.2: Comparison of image based total porosity using *auto threshold* with core helium porosity

4.1.3 K-means clustering method

The automatic method analyzed in current study to estimate porosity is K-means clustering. Three clusters were used and the cluster associated with blue color (epoxy) was further analyzed to estimate porosity. Micro and macro porosity was differentiated based on luminosity (L) of the blue color, where light blue represents micro pores and dark blue as macro pores.

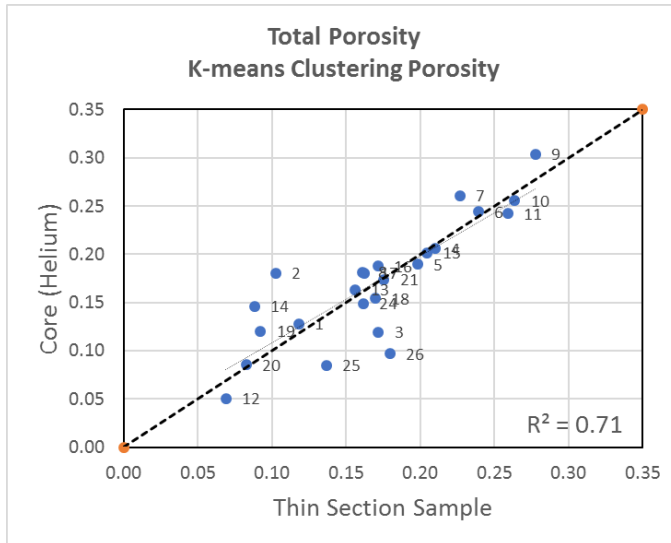


Figure 4.3: Comparison of image based total porosity using **K-means clustering** with core helium porosity

Like manual threshold method, an adjustment factor was required for micro porosity to remove matrix effect. For the analyzed samples, factor of 0.8 was required in equation (2-14) to achieve a good correlation between image derived porosity and core porosity. Samples 22 & 23 were discarded in Figure 4.3, as the color of the samples itself was blue, hence porosity was over-estimated with clustering technique. It points to the limitation of clustering technique, where blue color shall only be present in pore space.

Sample ID	Sample Depth (m)	Micro porosity (Adj. factor = 0.8)	Macro porosity	Total porosity
1	1630.10	0.077	0.041	0.118
2	1637.81	0.033	0.070	0.103
3	1643.88	0.108	0.064	0.172
4	1891.90	0.061	0.149	0.210
5	1896.70	0.096	0.102	0.198
6	1902.72	0.103	0.136	0.239
7	1904.75	0.107	0.120	0.227
8	1913.49	0.074	0.087	0.161
9	1916.15	0.107	0.171	0.278
10	1930.44	0.160	0.104	0.264
11	1945.28	0.118	0.141	0.259
12	1947.94	0.028	0.041	0.069

13	1952.04	0.050	0.106	0.156
14	1957.66	0.033	0.056	0.088
15	1964.40	0.080	0.124	0.205
16	1971.63	0.058	0.113	0.172
17	1975.63	0.049	0.114	0.162
18	2000.70	0.068	0.102	0.170
19	2006.47	0.050	0.042	0.092
20	2015.03	0.023	0.060	0.083
21	2019.03	0.084	0.092	0.176
22	2044.52	0.203	0.235	0.438
23	2046.03	0.129	0.254	0.383
24	2109.34	0.043	0.119	0.162
25	2128.82	0.029	0.108	0.137
26	2243.39	0.022	0.158	0.180

Table 4-4: Image porosity analysis by using K-means clustering method

4.1.4 Clusters predicted threshold method

As shown in Figure 4.4, pixels intensity associated with light and dark color clusters can be plotted over intensity histogram of inverted red component. Such plotting can be used to predict threshold values for micro and macro pores.

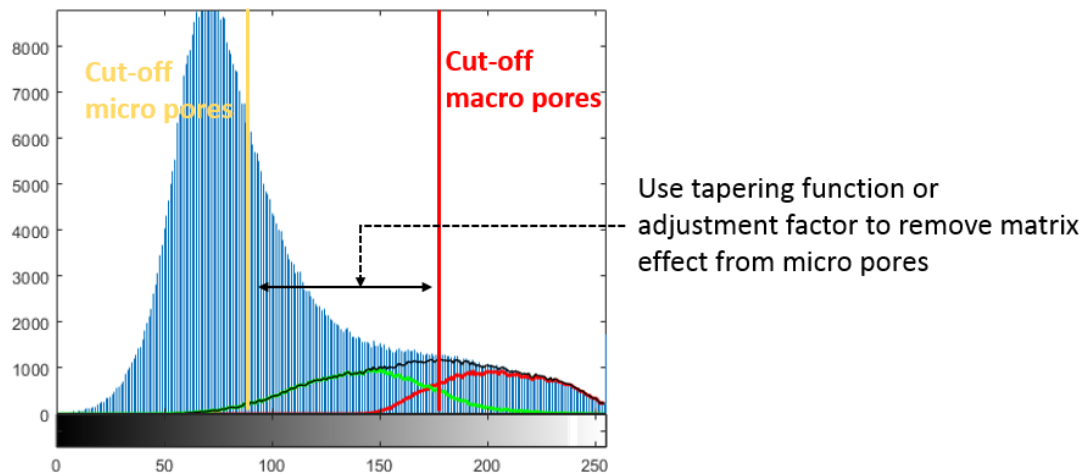


Figure 4.4: Thresholds prediction from K-means clustering method

Cut-off for macro pores is picked at the value where black color distribution starts to deviate from intensity histogram, and micro pore cut-off is picked on the left edge of the green distribution.

Sample ID	Sample Depth (m)	Micro pores cut-off	Macro pores cut-off	Micro porosity (fraction)	Macro porosity (fraction)	Total porosity (fraction)
1	1630.10	86	152	0.054	0.025	0.079
2	1637.81	112	156	0.021	0.078	0.099
3	1643.88	118	161	0.099	0.078	0.178
4	1891.90	141	200	0.071	0.131	0.201
5	1896.70	127	166	0.115	0.124	0.240
6	1902.72	139	178	0.099	0.152	0.251
7	1904.75	144	177	0.105	0.136	0.241
8	1913.49	142	175	0.055	0.110	0.165
9	1916.15	166	234	0.234	0.058	0.292
10	1930.44	146	174	0.118	0.170	0.288
11	1945.28	139	194	0.116	0.127	0.243
12	1947.94	116	140	0.011	0.060	0.071
13	1952.04	119	165	0.039	0.120	0.159
14	1957.66	121	161	0.028	0.059	0.086
15	1964.40	151	203	0.029	0.181	0.210
16	1971.63	116	166	0.036	0.132	0.168
17	1975.63	133	182	0.038	0.121	0.160
18	2000.70	136	175	0.057	0.114	0.171
19	2006.47	125	166	0.044	0.042	0.086
20	2015.03	126	150	0.008	0.075	0.082
21	2019.03	140	179	0.070	0.098	0.168
22	2044.52	144	245	0.318	0.031	0.348
23	2046.03	158	250	0.349	0.012	0.361
24	2109.34	110	156	0.063	0.082	0.145
25	2128.82	140	186	0.040	0.092	0.131
26	2243.39	160	235	0.078	0.013	0.091

Table 4-5: Image porosity analysis by using Clusters predicted threshold method, micro porosity with tapering function

Micro porosity in Table 4-5 between the two threshold values was determined using a tapering function instead of an adjustment factor. A tapering function was used to match pixel intensity profile (curvature) of micro pores from clustering technique, Figure 4.4. The tapering function used is given in equation (4-2), value of n used in current analysis is 1.5, but can be changed by the analyst in Matlab script provided in appendix-B.

$$\Phi_{\text{micro}} = \left(\frac{(\text{Pixel value} - \text{Micro pores threshold})}{(\text{Macro pores threshold} - \text{Micro pores threshold})} \right)^n \quad (4-2)$$

Adjustment factor approach was also analyzed with value of 0.3. Its results are presented in Table 4-6.

Sample ID	Sample Depth (m)	Micro pores cut-off	Macro pores cut-off	Micro porosity (fraction)	Macro porosity (fraction)	Total porosity (fraction)
1	1630.10	86	152	0.078	0.025	0.103
2	1637.81	112	156	0.020	0.078	0.098
3	1643.88	118	161	0.112	0.078	0.190
4	1891.90	141	200	0.071	0.131	0.201
5	1896.70	127	166	0.103	0.124	0.228
6	1902.72	139	178	0.090	0.152	0.242
7	1904.75	144	177	0.099	0.136	0.235
8	1913.49	142	175	0.057	0.110	0.167
9	1916.15	166	234	0.233	0.058	0.291
10	1930.44	146	174	0.106	0.170	0.277
11	1945.28	139	194	0.126	0.127	0.253
12	1947.94	116	140	0.009	0.060	0.069
13	1952.04	119	165	0.033	0.120	0.153
14	1957.66	121	161	0.028	0.059	0.087
15	1964.40	151	203	0.027	0.181	0.208
16	1971.63	116	166	0.040	0.132	0.172
17	1975.63	133	182	0.037	0.121	0.158
18	2000.70	136	175	0.055	0.114	0.168
19	2006.47	125	166	0.059	0.042	0.101
20	2015.03	126	150	0.006	0.075	0.081
21	2019.03	140	179	0.072	0.098	0.170
22	2044.52	144	245	0.256	0.031	0.287
23	2046.03	158	250	0.269	0.012	0.281
24	2109.34	110	156	0.058	0.082	0.140
25	2128.82	140	186	0.030	0.092	0.122
26	2243.39	160	235	0.067	0.013	0.079

Table 4-6: Image porosity analysis by using Clusters predicted threshold method, micro porosity with adjustment factor of 0.3

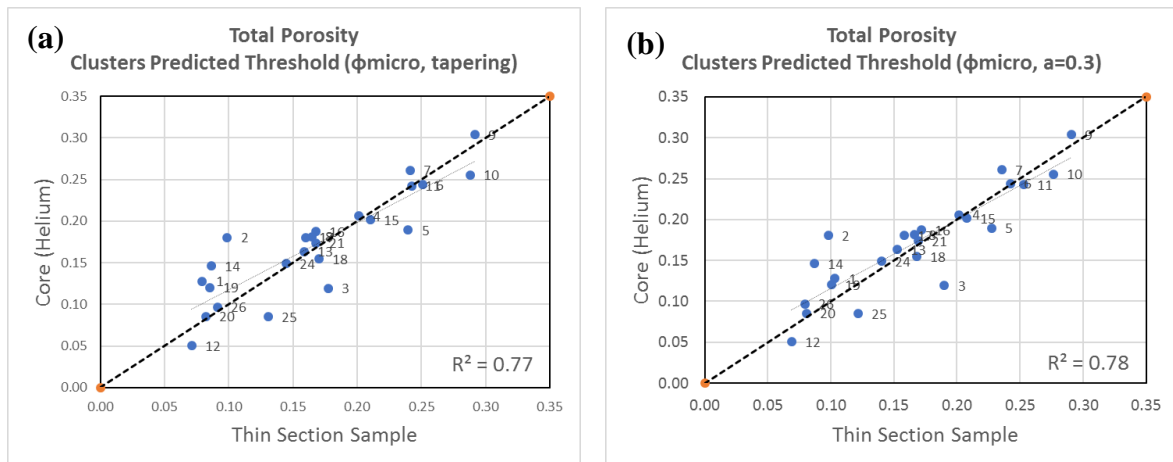


Figure 4.5: Comparison of image based total porosity using Clusters predicted thresholds method with core helium porosity, (a) matrix effect from micro porosity is removed by using tapering function, (b) matrix effect from micro pores is removed by using adjustment factor of 0.3

In sections 4.1.3 and 4.1.4, it has been demonstrated that process of porosity determination from thin section images can be automated. The results are as good if not better as manual threshold method, however the subjectivity of manually picking threshold values is removed.

4.2 Permeability from image analysis

Permeability (absolute) was analyzed with Kozeny-Carman and Timur-Coates permeability correlations as established under [section 2.5.3]. The correlations were applied on porosity results from K-means clustering method but can be applied on porosity data of other methods as well.

In Figure 4.6, permeability from image analysis is compared against core Klinkenberg permeability (Kel). Default values of constants and exponents in equations (2-29) and (2-33) were tuned to achieve better R^2 values. In Kozeny-Carman equation (2-29), constant C_o default value is 5, and exponent ‘ x ’ value for specific surface area is 2. Value of 2.34 was used for ‘ x ’ in crossplot below and is close to default value of 2. For Timur-Coates permeability equation (2-33), pre-multiplier ‘ a ’ value of 1.4 was used instead of 1, while exponents ‘ b ’ and ‘ c ’ were kept at their default values.

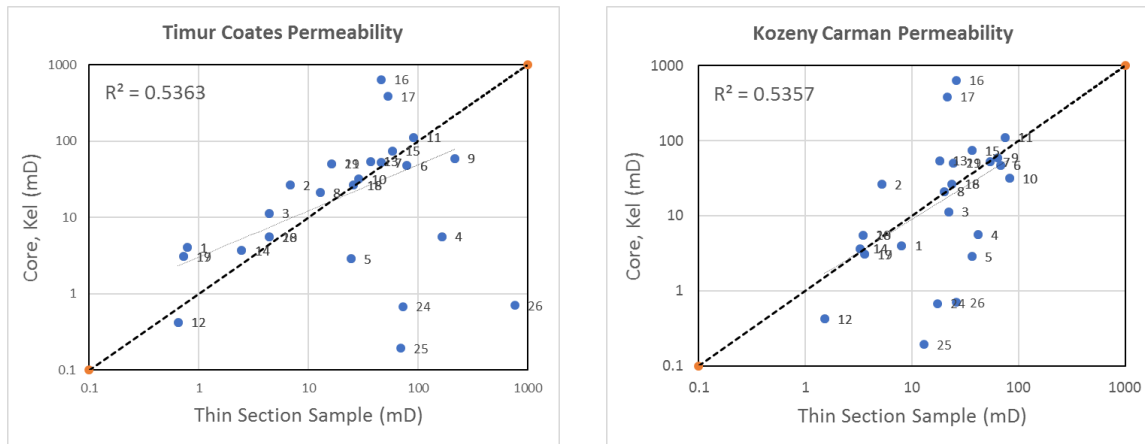


Figure 4.6: Absolute permeability estimate from thin section image analysis using Timur-Coates and Kozeny-Carman permeability correlations. Porosity data of K-means clustering method was used

ID	Depth	Porosity K-means	Core Horizontal Perm		Thin Section Samples			
					K _{Timur-Coates}	K _{Kozeny-Carman}		
	(m)	(fraction)	K _{gas} (mD)	K _{cl} (mD)		(mD)	S (1/pixel)	S (1/m)
1	1630.10	0.118	4.81	4.00	0.78	0.761	34575	8.00
2	1637.81	0.103	29.00	26.30	6.84	0.761	34588	5.22
3	1643.88	0.172	12.90	11.30	4.39	0.797	36225	22.07
4	1891.90	0.210	6.51	5.57	164.31	0.784	35646	41.82
5	1896.70	0.198	3.51	2.87	24.29	0.770	34992	36.60
6	1902.72	0.239	51.25	47.40	79.05	0.752	34185	68.03
7	1904.75	0.227	56.35	52.05	46.27	0.776	35270	53.83
8	1913.49	0.161	23.15	21.14	12.74	0.762	34622	20.12
9	1916.15	0.278	63.85	59.25	215.02	0.934	42469	64.13
10	1930.44	0.264	34.75	31.70	28.72	0.787	35782	82.00
11	1945.28	0.259	117.80	111.20	90.22	0.801	36389	74.66
12	1947.94	0.069	0.54	0.42	0.65	0.778	35350	1.51
13	1952.04	0.156	58.20	54.05	37.10	0.766	34831	18.16
14	1957.66	0.088	4.36	3.65	2.46	0.768	34913	3.25
15	1964.40	0.205	79.10	74.15	58.31	0.800	36378	36.78
16	1971.63	0.172	662.00	641.50	46.03	0.742	33713	25.99
17	1975.63	0.162	399.00	384.00	53.13	0.752	34171	21.27
18	2000.70	0.170	29.15	26.45	25.85	0.761	34581	23.63
19	2006.47	0.092	3.73	3.05	0.72	0.781	35484	3.60
20	2015.03	0.083	6.44	5.55	4.39	0.689	31300	3.47
21	2019.03	0.176	54.85	50.55	16.19	0.786	35739	24.25
24	2109.34	0.162	0.87	0.68	73.17	0.815	37061	17.34
25	2128.82	0.137	0.25	0.19	69.09	0.743	33792	13.05
26	2243.39	0.180	0.89	0.70	763.27	0.784	35627	26.26

Table 4-7: Absolute permeability estimates of thin section samples by using Kozeny-Carman and Timur-Coates permeability correlations

4.3 Irreducible water saturation

Comparison of irreducible water saturation between thin sections and core was not performed as this data was not available in core report.

Irreducible water saturation from thin section can be calculated from micro porosity and image total porosity numbers populated in tables 4-4 to 4-6 and using the equation (2-37).

5 DISCUSSION

5.1 Porosity

Porosity from image analysis was compared against core helium porosity to validate goodness of porosity prediction from image analysis. However, uncertainties associated with both measurements shall be considered as well.

- Porosity from image analysis is limited to pixels resolution of optical microscopy and represents a very small section of the rock sample. Core helium porosity is determined on 1-inch cylindrical plug while the dimensions of thin section sample is only 35 μm thick with diameter of 1-inch. The volume investigated is different.
- Depths where thin section samples were taken are not at the same depth as core plugs for helium porosity analysis.
- Core-plugs drying condition was not documented, hence there is uncertainty if core helium porosity is total porosity or effective porosity or in between. For example, drying at 60 °C can leave significant amount of clay bound water within core plug sample, and helium porosity will be closer to effective porosity.
- Most of the analyzed samples are carbonates, core helium porosity can miss porosity associated with isolated pores whereas such pores are captured in image analysis. For samples where image porosity is over-estimated as compared to core porosity may be the result of vugs porosity.
- Studied scanned samples with optical microscopy had pixel resolution of 25 μm . Pore sizes greater than 25 μm (macro pores) were correctly resolved but there was significant quantity of sub-resolution pores (micro pores) with mixed response of pore and matrix. A subjective adjustment factor was used to take out this matrix effect from micro-pores. This single value of adjustment factor was determined while comparing image porosity against core helium porosity for all samples. This factor has varied between 0.3 – 0.8 depending upon the chosen methodology. The suggested value(s) may have worked for the analyzed samples of current study and can differ in other environments.
- Thin section samples were globally cropped with a window of 800x800 pixels. However, as is always the case with geological material – heterogeneity can be seen at all scales. As exemplified in Figure 5.1 in which heterogeneity can be seen also within the 1 inch sample. This effect is analyzed by cropping the figure at 400x400 pixels, i.e. in four equal images, the image porosity results for each image will change. This technique can be used to estimate the accuracy of the porosity estimate.

Thin section samples and core plugs were not at the same depth, then it is not known to which core sample depth thin section porosity shall be compared with. Average core porosity was calculated based on plug depth one above and one below the thin section sample depth.

Sample-ID #3 in Table 5-1 shows that core helium porosity changed by 0.15 pu within depth interval of 0.3m only. This explains heterogenous nature of the reservoir rock, and porosity difference between core

and thin section image analysis can be the result of this heterogeneity. From Figure 5.1, it can be concluded that image analysis porosity for all samples is within the uncertainty band of core porosity.

ID	Sample type	Depth (m)	Helium porosity	Average Helium porosity	Image analysis porosity	Standard deviation Helium porosity
3	Core plug	1643.7	0.195			
	Thin section sample	1643.88		0.120	0.172	0.107
	Core plug	1644.0	0.044			
5	Core plug	1896.5	0.183			
	Thin section sample	1896.7		0.1895	0.189	0.009
	Core plug	1896.75	0.196			

Table 5-1: Examples demonstrating standard deviation on core helium porosity, image porosity is taken from K-means clustering method

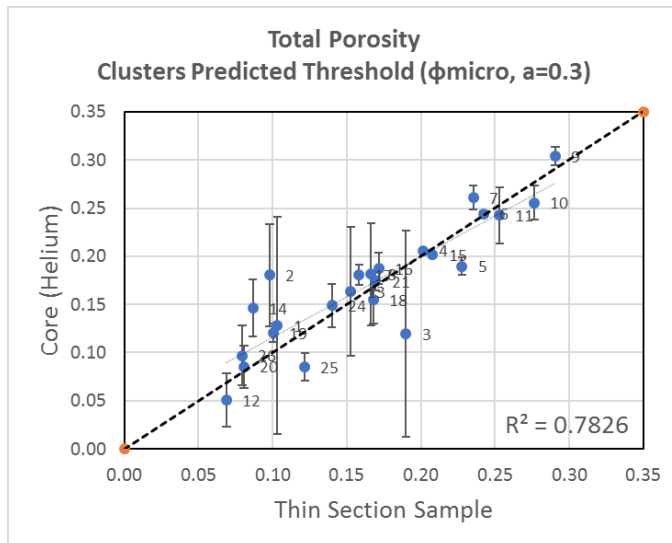


Figure 5.1: Uncertainty in porosity comparison when thin section samples depths and core plugs depths are different

Uncertainty can also be analyzed for porosity from thin section image analysis. Thin section scanned image was cropped at window size of 800x800 pixels as shown in Figure 5.2. But the same image can be locally cropped at any window size e.g. 400x400 pixels. Porosity of individual locally cropped regions can be compared against the porosity answer of globally cropped image.

The analysis of Figure 5.3 gives standard deviation of 0.074 pu on image derived porosity. It demonstrates that for heterogenous samples, porosity from image analysis or from core plugs are within the error range of each other. Uncertainty analysis on image derived porosity is demonstrated only for one sample (#3), Matlab code was not developed in current year’s work that can analyze standard deviation of image derived porosity for all samples.

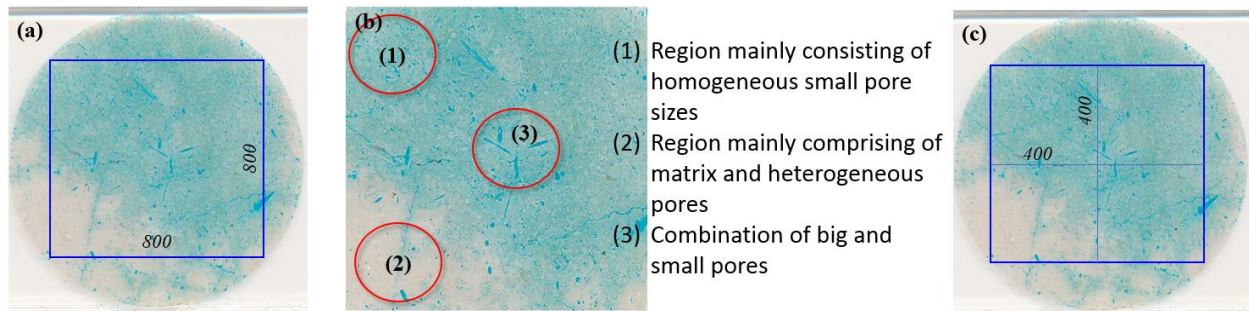


Figure 5.2: Sample ID 3; definitions of global and local cropping (a) is defined as global cropped region with window size of 800x800 pixels, (b) showing heterogeneity across thin section sample, (c) cropping windows can be defined as 400x400 or of any other size

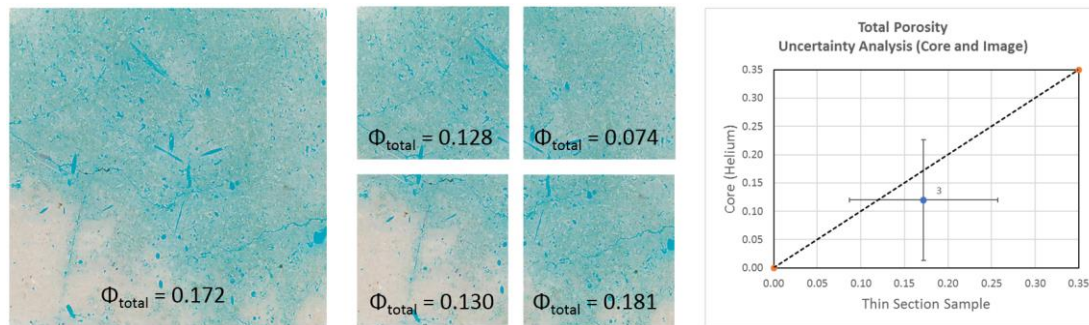


Figure 5.3: Sample ID 3; Effect of global and local cropping on image derived porosity (K-means clustering method)

5.2 Permeability

From Figure 4.6, samples 4, 5, 24, 25 and 26 are outliers, do not fall on $x=y$ line, and their permeability is over-estimated from both permeability correlations. The observed scatter and loose correlation (low R^2 value) can be due to the reasons;

- Thin section sample depths were not same as core plug depths, and average permeability value was used based on core depth one above and one below the thin section sample depth. It is already seen in porosity comparison cross-plot Figure 5.1, that there is an associated uncertainty when thin section and core sample depths are not same.
- Both correlations relate porosity to permeability and will conclude some permeability value if there is porosity, they cannot predict connectedness of the pores. There can be porosity in reservoir rock due to isolated pores (e.g. isolated vugs) with no permeability.
- Uncertainty in porosity will be transferred to permeability, as permeability correlations used are function of porosity.
- Data scatter was also observed when core porosity and permeability were plotted against each other, Figure 5.4. It indicates for some samples a different set of constants and exponents is required to achieve a better fit. But such practice will lose the predictive power of permeability estimate from

thin section samples as we will be imposing a match and will need to know ground truth permeability values.

- It is believed that estimate of permeability from porosity will show a better correlation if it is inter-granular porosity like in sandstone reservoirs. Samples studied in current work are mainly carbonate and heterogenous samples, which could explain to some extent scatter observed on permeability crossplots.

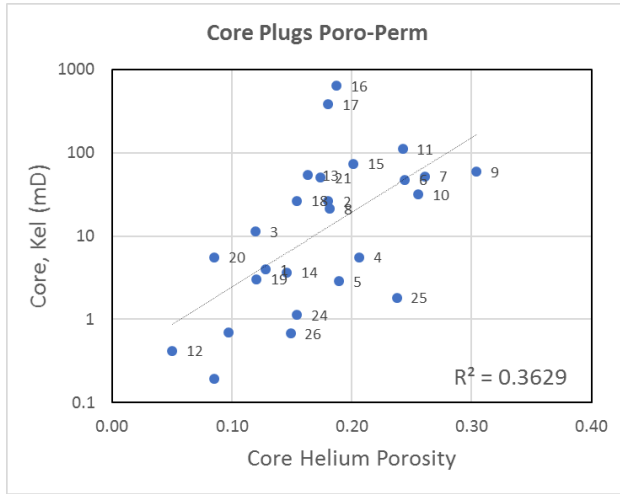


Figure 5.4: Core plugs porosity-permeability plot

Ideally, permeability correlations and tuning of constants and exponents used in respective equations shall be studied and concluded from samples taken from conventional reservoirs like simple / homogeneous sandstone and carbonate reservoirs, sandstone reservoirs with high feldspar content, chalk reservoirs, vuggy-carbonate reservoirs. Samples studied in current study are from Barents Sea with complex mineralogy, this information was not available to make firm conclusions about data scatter and outliers. However, poro-perm relationship from thin section image analysis showed an acceptable correlation when compared with [Ehrenberg, 2005] global database for sandstone and carbonate reservoirs, Figure 5.5.

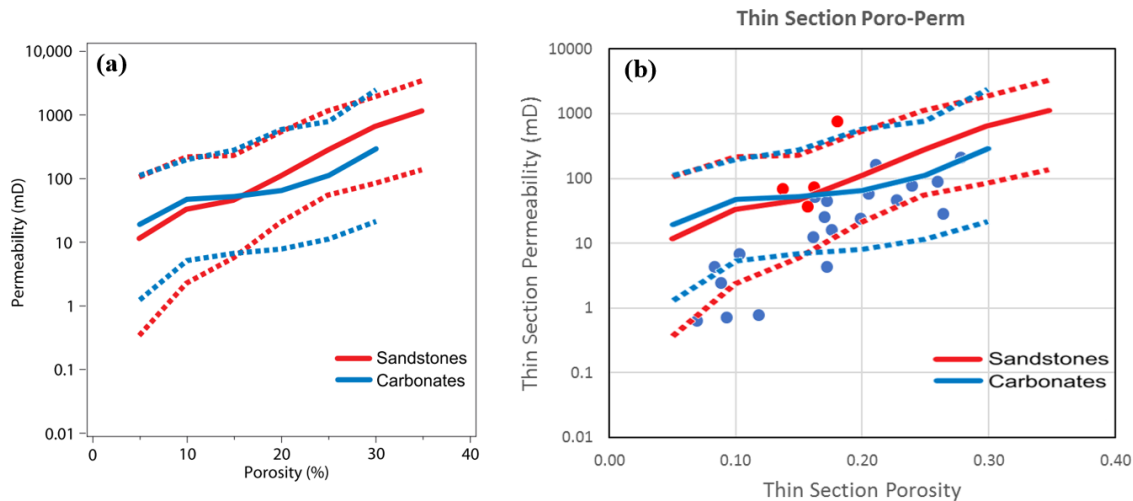


Figure 5.5: Thin section poro-perm results comparison with global sandstone & carbonate reservoirs poro-perm database [Ehrenberg, 2005]. x&y axis scales are exactly matched in the overlay

6 CONCLUSION

K-means clustering is presented as an alternate technique to evaluate porosity from thin section images. Previously established methods had element of subjectivity in it where threshold on pixel intensity histogram had to be manually adjusted till analyst is visually satisfied that pore space is properly captured. This visual analysis was challenging, as optically scanned images used in the current study had pixel resolution of $25\ \mu\text{m}/\text{pixel}$ and there were significant number of pores with size less than the pixel resolution. In another study, regression equations were used to achieve good correlation of petrophysical properties between image analysis and routine core analysis data. These adjustments and regression lost the predictive power of image analysis. Clustering is demonstrated as an automatic technique where analyst only need to define number of clusters. For optical scanned images used in the current study, three number of clusters were analyzed as optimum to extract pore space from the matrix.

Thin sections image porosity using clustering technique showed good match with core helium porosity, with the additional benefit that workflow is now automated. Moreover, clusters can predict threshold values if it is desired to do image interpretation with thresholding technique. Uncertainty analysis on heterogeneous samples showed that core and thin section porosities were within the standard deviation of each other.

In the current study, porosity is the main petrophysical property determined from thin section images. Permeability was estimated as a function of porosity, and it also showed acceptable match with core permeability. Some scatter on permeability correlation was observed which could be explained that permeability is a dynamic property and we tried to estimate it from 2D image. Nevertheless, the interpretation is useful to identify permeable layers.

The predictive power of clustering based thin section image analysis is encouraging, as it can be applied on vastly available drill cuttings as a secondary means of porosity and permeability data. And for the wells where conventional core data is not available or possible, petrophysical properties can be determined from thin section images for its integration with well logs interpretation to reduce uncertainties.

Some limitations to thin section image analysis were also observed. For optically scanned images, pore sizes less than $25\ \mu\text{m}$ had a mixed response of matrix and porosity. A subjective but a single adjustment factor was required to remove matrix effect from such pores for all analyzed samples. This is equally applicable for both clustering and manual thresholding techniques. Clustering, analyzes porosity from pore filling blue epoxy i.e. a blue cluster, it was observed that clustering over-estimates porosity if blue color is also present as a matrix color. Such a situation will be equally challenging for manual thresholding and hence, can be concluded as a general limitation of thin section image analysis.

7 WAY FORWARD

Certain petrophysical and geological properties like porosity, pore size distribution, grain size distribution, mineralogy, asphaltene deposition and diagenetic processes can be quantified or analyzed on thin section samples but other properties like permeability, capillary pressure and relative permeability profiles have to rely on empirical correlations. Some thoughts and ideas that were discussed but not implemented during the course of the current study are briefly mentioned here.

Pore size distribution

The image analysis script outputs morphological properties of captured pores. One such property is area of each pore size with units in pixel². Knowing the pixel resolution (e.g. 25 μm in this study), area is converted to μm² or mm², which can be plotted as pore area distribution or to derive pore size distribution.

Three samples are presented from current study, visually the samples look very different but the pore distribution (mm²) did not show contrasting differences. Pore size distribution may be correct and representative of the samples, but this property was not studied in detail. There was also a discussion if we shall use a variable bin size or same bin size for all samples. Probably micro pores and macro pores shall be plotted separate series. In Figure 7.1, pores were not corrected for matrix effect which may be the cause of suppressing the representative distribution profile.

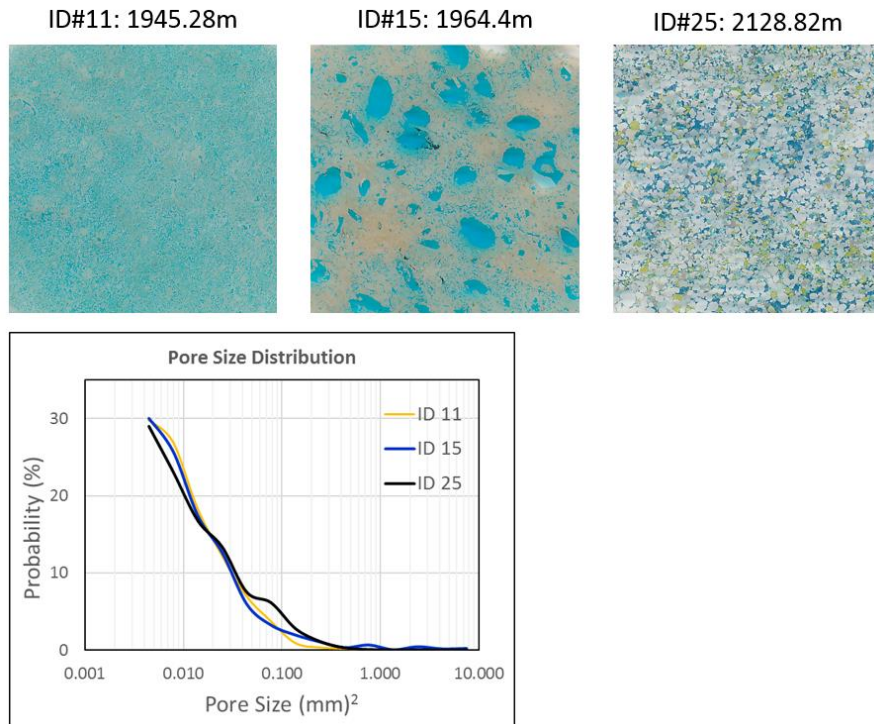


Figure 7.1: Pore distribution in mm² from thin section image analysis, logarithmically spaced equal sized bins

Capillary pressure

Capillary pressure profile can be derived from pore size distribution the same way as is done from NMR T2 distribution [Glorioso, 2003], Figure 7.2.

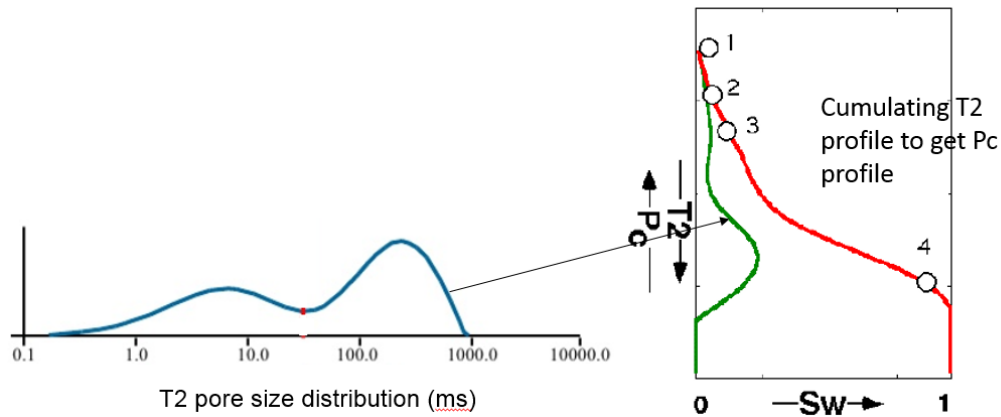


Figure 7.2: Deriving pseudo capillary pressure curve from NMR T2 distribution [Glorioso, 2003]

Image pre-processing

Image pre-processing techniques were not studied, which may help improve accuracy of porosity results and to even quantify mineralogy from optical microscopy scanned thin section images [Heilbronner, 2014].

Samples from conventional reservoirs

Thin section samples used in the current study were from Barent Sea well with complex / heterogenous mineralogy, only oil shows were reported, limited core data and with no well logs interpretation. It is suggested to study thin sections from prolific and conventional type reservoirs like relatively clean sandstone reservoirs, clastic reservoirs with high feldspar content, chalk, limestone and dolomite reservoirs. So, the constants used in empirical correlations and adjustment factors can be better calibrated and generalized specific to lithology types.

Wells with routine and special core analysis, and with advanced petrophysical logs like NMR and elemental capture spectroscopy will make it a better integrated study while comparing thin section petrophysical properties.

Equinor seems to have a specialized thin section department, may be a future study in coordination with industry. It will also allow access to more data and information.

REFERENCES

- [1] Heilbronner, R., Barrett, S., 2014, Image analysis in earth sciences, Springer, Ch 1, 2, 3 & 4
- [2] Crain's Petrophysical Handbook
- [3] Zerabruk, B.T., Nermoen, A., Nadeau, P.H., 2017, Digital image analysis for petrophysical characterization, Master's thesis, University of Stavanger
- [4] Fens, T.W., 2000, Petrophysical properties from small rock samples using image analysis techniques, PhD thesis, Delft University of Technology
- [5] Varfolomeev, I., Yakimchuk, I., Denisenko, A., Khasanov, I., Osinceva, N., Rahmattulina, A. 2016, Integrated study of thin sections: Optical petrography and electron microscopy, SPE 182071
- [6] Carman, P.C., 1937, Fluid flow through granular beds, Trans. Inst. Chemical engineering 15, page 150-166
- [7] Dvorkin, J., 2009, Kozeny-Carman equation revisited
- [8] Srisutthiyakorn, N., Mavko, G., 2015, An improved Kozeny-Carman for irregular pore geometries, SEG New Orleans Annual Meeting
- [9] Herron, M., 1987, Estimating the intrinsic permeability of clastic sediments from geochemical data, SPWLA 28th Annual Logging Symposium
- [10] Coates, G.R., Dumanoir, J.L., 1973, A new approach to improved log-derived permeability, SPWLA 14th Annual Logging Symposium
- [11] Lawrence, M., Jiang, Y., 2017, Bio-aggregates based building material: Porosity, pore size distribution and micro-structure, Springer, Ch 2
- [12] Ahmed, U., Crary, S.F., Coates, G.R., 1991, Permeability estimation: the various sources and their inter-relationships, SPE 19604
- [13] Allen, D., Flaum, C., Ramakrishnan, T.S., 2000, Trends in NMR logging, Schlumberger oilfield review
- [14] Ehrenberg, S.N., Nadeau, P.H., 2005, Sandstone vs. carbonate petroleum reservoirs: A global perspective on porosity-depth and porosity-permeability relationships, AAPG bulletin, V. 89, No. 4, Page 435-445
- [15] Dullien, F. A.L., 1979, Porous media, fluid transport and pore structure, 1st Edition, Academic Press, New York, USA
- [16] Ling, K., 2012, Correlation between rock permeability and formation resistivity factor: A rigorous and theoretical derivation, SPE 152724

- [17] Hidajat, I., Rastogi, A., 2002, Singh, M., Mohanty, K.K., Transport properties of porous media reconstructed from thin sections, SPE Journal
- [18] Doktor, T., Kytir, D., Valach, J., 2010, Assessment of pore size distribution using image analysis, 9th YSESM, Trieste, Italy
- [19] Wentworth, C.K., 1922, A scale of grade and class terms for clastic sediments, The journal of geology
- [20] Eslinger, E., Pevear, D., 1988, Clay minerals for petroleum geologists and engineers, Society of economic paleontologists and mineralogists, Tulsa
- [21] Guojun, C., Guichao, D., Gongcheng, Z., Qi, W., Chengfu, L., Ji, C., 2011, Chlorite cement and its effects on the reservoir quality of sandstones from the Panyu low-uplift, Pearl river Mouth Basin, Petroleum science journal, Springer open
- [22] Mishra, V.K., Skinner, C., MacDonald, D., Hammou, N., Lehne, E., Wu, J., Zuo, J.Y., Dong, C., Mullins, O., 2012, Downhole fluid analysis and asphaltene nanoscience coupled with VIT for risk reduction in black oil production, SPE 159857
- [23] Durand, C., Cerepi, A., Brosse, E., 2000, Effect of pore-lining chlorite on petrophysical properties of low-resistivity sandstone reservoir, SPE 63070
- [24] Saadi, F., Wolf, K.H., Kruijsdijk, C., 2017, Characterization of Fontainebleau Sandstone: Quartz overgrowth and its impact on pore-throat framework, Vol 8, Journal of Petroleum and Environmental Biotechnology
- [25] Glorioso, J.C., Aguirre, O., Piotti, G., Mengual, J.F., 2003, Deriving capillary pressure and water saturation from NMR transversal relaxation times, SPE 81057
- [26] Ramakrishnan, T.S., Wasan, D.T., 1994, The relative permeability function for two-phase flow in porous media: Effect of capillary number, SPE 12693
- [27] Brooks, R.H., Corey, A.T., 1964, Hydraulic properties of porous media, Colorado State University, Hydraulic paper 3
- [28] Darcy, H., 1856, Les fontaines publiques de la ville de Dijon. Paris, Dalmont
- [29] MathWorks, help document and community
- [30] Norwegian Petroleum Directorate (NPD), <http://factpages.npd.no/factpages/Default.aspx?culture=en>

APPENDICES

Appendix-A: Conferences representation



Digital Image Analysis of Thin Sections for Petrophysical Properties

M.H. Baig², A. Neramoen^{1,2,3}, P.H. Nadeau¹, P.Ø. Andersen^{1,2}, I. Austvoll⁴

¹The National IOR Centre of Norway
²Department of Energy Resources, University of Stavanger
³International Research Institute of Stavanger
⁴Department of Electrical Engineering and Computer Science, IDE, University of Stavanger

Introduction

Economic feasibility of any field development largely depends upon its reservoir storage and flow capacity. Porosity, saturation and permeability are important parameters to determine the type and volume of hydrocarbons in place and to estimate recoverable reserves.

Porosity, saturation and permeability of the reservoir can be determined with reasonable certainty through interpretation of petrophysical logs or through analysis of physical core samples.

To improve some of the inaccuracies and limitations, 'digital image analysis' on core or on drill cuttings 'thin sections' can be a useful technique in estimating reservoir properties. It can provide porosity, pore size distribution, flow path tortuosity (permeability), irreducible water saturation and mineralogy of the samples. The results of Digital Image Processing can be compared against Core and Logs data to understand formation heterogeneity and methods limitations.

Objectives

- Use NPD database resource to develop new better tools for petrophysical evaluation of porous rocks.
- Match logs observations (0.5 m scale) to core observations (0.025 m scale) to thin sections scale 3×10^{-5} m.
- Improve and develop image analysis capabilities at UIS.
- Analyze uncertainties and limitations.

Method

- Thin sections (30 micron thickness) of rock sample attached from core samples acquired from NCS were studied (Fig. 1ab). The pore space can be observed at microscopic scale via the blue colored glue. Samples were digitized using Canon 9000F Mark-II scanner with a resolution 22 um/pixel.
- Samples of 7218/6-1 well in Barents Sea from the NPD database were analyzed.
- Both sandstone reservoir and carbonate formations are studied.
- Via previous projects at UIS have developed scripts using Matlab image processing tool box to differentiate pore space from matrix using a threshold technique of the Red component of the image (RGB scale).
- Micro pores (smaller than pixel size) and macro pores were identified.
- Limitation so far has been the threshold technique in which manual adjustment are required (Fig. 1c) until rock/pore boundaries are visually satisfied.
- The method worked satisfactorily for pores larger than 22 um, but became increasingly subjective for smaller pores in which an adjustment factor for micro pores was required to remove sub-resolution matrix effect.

Figure 1: Thin section image analysis (RGB) for porosity (a) thin section sample (b) cropped image at 800x800 pixels (c) thresholds to capture micro and macro pores (d) zoomed image to quality control if pores (blue dye) is captured correctly where red boundary represents macro pores and green boundary is used for micro pores (Bereket et al., 2017)

- From Fig. 1d it can be visualized that 'bluishness' of the dye varies across the captured pores. There is still some blue shade left encircled in black that was not captured with the threshold technique.

K-means clustering

Improvement of the threshold technique is to use the **automated K-means clustering** where the aim has been to remove subjectivity associated with the selection of threshold values. So far it seems that three clusters are sufficient to extract the pores from the matrix enabling the blue color to be segmented into light blue (micro-pores) and dark blue (macro) (see Fig 2ab). An adjustment factor is still required to remove matrix effect from the sub-resolution micro pores.

Figure 2: K-means clustering image analysis (Lab) for porosity determination (a) blue cluster (b) micro (green boundary) and macro (red boundary) captured pores (c) red component pixels intensity marked by clustering for comparison with figure 1a (d) zoomed image to quality control if pores (blue dye) is captured correctly.

- In Fig 2d the macro pore (dark blue) and micro (light blue) pores are distinguished better than the threshold technique. Further on, *human interference* is not required to adjust thresholds.
- Another application of clustering can be to guide threshold values which from figure 2c can be 120 and 190 for micro and macro pores respectively as compared to 190 and 210 used in figure 1c thresholding technique.

$$\Phi_{tot} = A\phi_{micro} + \phi_{macro}$$

where adjustment factor **A** for sub-resolution micro pores used in Bereket et al. 2017 thesis was 0.4 and with clustering method was found out to be 0.8.

Results

- 26 thin section samples were analyzed for porosity with K-means clustering technique. Fig. 3 below display selected samples covering the range from low to high porosity sandstone samples, carbonate samples, fractured porosity and homogeneous & heterogeneous samples.

	Carbonate samples					Sandstone samples		Fracture porosity
1. Cropped Thin Section Image	(1.1)	(1.2)	(1.3)	(1.4)	(1.5)	(1.6)	(1.7)	
2. Captured Thin Section Image with micro & macro pores	(2.1)	(2.2)	(2.3)	(2.4)	(2.5)	(2.6)	(2.7)	
3. Blue color cluster for micro & macro pores	(3.1)	(3.2)	(3.3)	(3.4)	(3.5)	(3.6)	(3.7)	
4. Zoomed image of captured pores	(4.1)	(4.2)	(4.3)	(4.4)	(4.5)	(4.6)	(4.7)	

Figure 3: K-means clustering image analysis results where 3 clusters and Euclidean distance approach is used to capture blue dye associated with porosity (1) represents the original cropped image, (2) represents the captured porosity where green and red boundaries are associated with micro & macro pores respectively, (3) Blue color cluster for micro & macro pores is plotted on R-component of RGB scale to QC thresholding technique and (4) presents zoomed image to QC captured porosity (2.7) is shown in Lab scale to better visualize captured open fracture porosity. (4.3) where porosity inside micro-organisms is captured.

- Porosity from the thin section image analysis was compared to RCAL helium porosity (Fig. 4). In Fig. 4a the Bereket et al method is used, while the automatic K-means is shown in Fig. 4b. A one-to-one match would correspond to the dots to follow the dashed line. As can be seen, this only partly the case, although the vertical error bar reflects the standard deviation of the Helium porosity.
- Pore surface area, perimeter length, specific surface area, eccentricity and orientation is also computed. Fig. 5 display pore size distribution to be used to develop permeability estimates matched with core data.

Figure 4: (a) compares the results of thin section porosity with thresholding technique (4a) and with K-means clustering (4b). It can be observed that a tighter correlation between image and RCAL helium porosity is achieved with clustering technique and it also removed the subjectivity of manual selection of thresholds.

Figure 5: pore size distribution (um²) currently analyzed for three samples. It will be used to develop permeability model and to compare with core perm.

Further work

- Compile pore size distribution results for all samples to develop permeability model: Carman-Kozeny and Timur-Coates permeability models will be studied. Compare with core data.
- Calculate irreducible water saturation (Swirr) from micro pores. Compare with core experiments.
- This section porosity uncertainty analysis. 800x800 pixels region was used to crop thin section samples. It was observed for heterogeneous samples like (1.5) in figure 3 that a different cropping region (e.g. 200x200) will give a different porosity answer.
- The methodology has not been tested on pure carbonate (or chalk) reservoirs where it is expected that significant amount of porosity can be associated with sub-resolution micro pores.

Conclusion

- K-means clustering is demonstrated as a powerful technique for thin section porosity analysis. The methodology has shown a good correlation between image and RCAL helium porosity for the analyzed samples in a dominantly sandstone reservoir.
- Clustering can be used to suggest thresholds for micro and macro pores which will partially remove subjectivity of manually selecting threshold values.
- Image analysis can be used to quantify porosity associated with open fractures.
- This section analysis is limited to its pixels resolution of 22 microns, it becomes challenging to analyze porosity of sub-resolution micro pores (e.g. chalk reservoirs) and an adjustment factor is required to remove the matrix effect from the captured micro pores. It may not pose a problem for high resolution images from back scatter electron density.
- The resolution and depths of cored samples, thin sections and logs are different and such differences shall be taken into account while comparing the results from these data sources. It can address heterogeneity of reservoir rock.

References

- [1] I.Z. Bereket, A. Neramoen, P.H. Nadeau, 2017. Digital Image Analysis for Petrophysical Characterization, UIS Masters Thesis
- [2] T.W. Fens, 2000. Petrophysical Properties from small rock samples using Image Analysis Technique
- [3] V. Varlamov, I. Yakimchuk, A. Denisov et al, 2016. Integrated Study of Thin Sections, Optical Petrography and Electron Microscopy, SPE 182071
- [4] Mathworks documentation for K-means clustering

Contact information

Mirza Hassan Baig (Mh.baig@stud.uis.no)
 Anders Neramoen (anders.neramoen@uis.no)
 Paul Henry Nadeau (paul.h.nadeau@uis.no)
 Pål Østebø Andersen (pal.andersen@uis.no)
 Ivar Austvoll (ivar.austvoll@uis.no)

Petrographic Properties Evaluation by Digital Image Analysis of Thin Sections

M.H. Baig², A. Nerøen^{1,2,3}, P.H. Nadeau¹, P.Ø. Andersen^{1,2}, I. Austvoll⁴

¹The National IOR Centre of Norway
²Department of Energy Resources, University of Stavanger
³International Research Institute of Stavanger
⁴Department of Electrical Engineering and Computer Science, IDE, University of Stavanger

Introduction

Economic feasibility of any field development largely depends upon its reservoir storage and flow capacity. Porosity, saturation and permeability are important parameters to determine hydrocarbon volume in place and recoverable reserves. Porosity, saturation and permeability of the reservoir can be determined with reasonable certainty through interpretation of petrophysical logs or through analysis of physical core samples. To improve some of the inaccuracies and limitations, 'digital image analysis' on core or on drill cuttings 'thin sections' can be a useful technique in estimating reservoir properties. It can provide porosity, pore size distribution, flow path tortuosity (permeability), irreducible water saturation and mineralogy of the samples. The results of digital image analysis can be compared against core and logs data to understand formation heterogeneity and methods limitations.

Objectives

- Use NPD database resource to further develop tools for petrophysical evaluation of porous rocks.
- Match petrophysical logs observations (1 m scale) to core observations (0.1 m scale) to thin sections scale 0.001 m.
- Improve and develop digital image analysis capabilities at UIIS.
- Analyze methods uncertainties and limitations.

Method

- **Optical microscopy:** Carbonate and Sandstone thin section samples (30 micron thickness) for the well 7218/6-1 in Barents sea were studied (Fig. 1ab). At this thickness, porosity can be quantified at microscopic scale via blue epoxy.
- Samples were digitized using Canon 9000F Mark-II scanner with a resolution of approx. 22 um/pixel. Pore size < 22 um (sub-resolution) was defined as 'micro pores' and pores with clear visible blue epoxy as 'macro pores'.
- **Threshold method:** Previously, projects at UIIS have developed scripts using Matlab image processing toolbox to differentiate pore space from matrix by using threshold technique on Red component of the image (RGB scale).
- Limitation so far had been the threshold technique in which manual adjustments were required (Fig. 1c) until matrix/pore boundaries were visually satisfied.
- The method worked satisfactorily for pores larger than 22 um, but became increasingly subjective to capture micro pores in which an adjustment factor of 0.4 was required to remove sub-resolution matrix effect.
- From Fig. 1d, it can be visualized that 'bushiness' of the epoxy varies across the captured pores. There was still some blue shade left encircled in black that was not captured with the threshold technique.

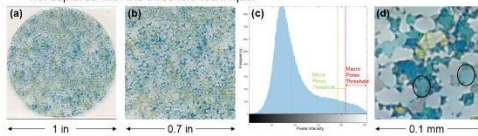


Figure 1: Threshold based thin section image analysis (RGB scale) for porosity (a) thin section sample (b) cropped image at 800x800 pixels (c) manual thresholds to capture micro and macro pores (d) zoomed image to quality control if pores (blue epoxy) were captured correctly, where red boundary represents macro pores and green boundary is used for micro pores (Berek et al., 2017)

- **K-means clustering:** Lab scale image segmentation and its clustering is introduced with the aim to remove subjectivity associated with the selection of threshold values. Limited by optical microscopy resolution, three clusters were observed sufficient to extract pores from matrix. Extracted blue epoxy was further segmented into light blue (micro pores) and dark blue (macro). Fig. 2ab. An adjustment factor (of 0.8) was still required to remove matrix effect from the sub-resolution micro pores.

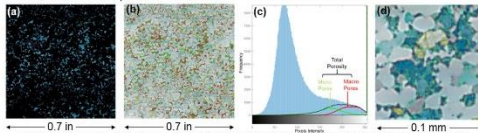


Figure 2: K-means clustering image analysis (Lab) for porosity determination (a) blue cluster (b) micro (green boundary) and macro (red boundary) captured pores (c) red component pixels intensity marked by clustering for comparison with Fig. 1a (d) zoomed image to quality control if pores (blue epoxy) is captured correctly.

- In Fig. 2d, macro pore (dark blue) and micro (light blue) pores were distinguished better than the threshold technique. Furthermore, captured pixel distribution on Fig. 2c can be used to guide threshold values.

- **Porosity:**
$$\phi_{total} = A * \phi_{micro} + \phi_{macro}$$
 (where, A is adjustment factor to remove matrix effect from sub-resolution micro pores)
- **Permeability:**
$$K_{Timur-Coates} = a * 10000 * (\phi_{total})^b + (\phi_{macro} / \phi_{micro})^c$$
 (where, a=1-4, b=4, c=2 and micro porosity is corrected for its adjustment factor)
- $$K_{Kozeny-Carman} = (\phi_{total})^2 / (C_0 * S^2)$$
 (where, x=3, y=2.34, C₀=5 Kozeny-Carman constant and S is specific surface area)

Results

- 26 thin section samples were analyzed with K-means clustering technique. Fig. 3 below display selected carbonate, sandstone and fractured shale samples.

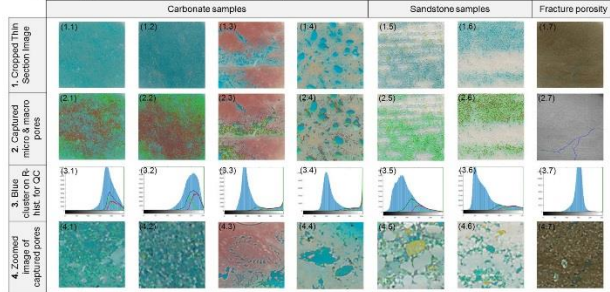


Figure 3: K-means clustering image analysis results where 3 clusters and Euclidean distance approach is used to capture blue epoxy associated with porosity (1) represents the original cropped image, (2) captured porosity where green and red boundaries are associated with micro & macro pores respectively, (3) Blue color cluster for micro & macro pores is plotted on R-component of RGB scale to QC and predict threshold technique and (4) presents zoomed image to QC captured porosity.

- Porosity from the thin section image analysis was compared to RCAL helium porosity (Fig. 4). The porosity results of automated clustering and from its predicted thresholds were comparable with Berek et al manual threshold method. However, subjectivity in picking threshold values was removed.

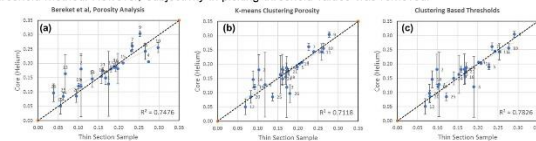


Figure 4: (a) results of Berek et al manual threshold method (b) auto K-means clustering porosity (c) porosity analysis using threshold values as predicted by K-means, an adjustment factor of 0.3 was used for its micro pores.

- Image derived absolute permeability was compared against core plugs air permeability (Fig. 5). An acceptable match between image and core permeabilities was achieved in Figs. 5b & 5c except for the samples 16, 17, 24, 25 & 26.

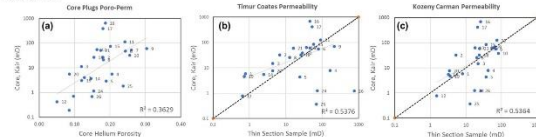


Figure 5: (a) core plugs poro-perm data (b) Timur-Coates permeability using porosity data from clustering method of Fig. 4b (c) Kozeny-Carman permeability derivation by using porosity from clustering method of Fig. 4b

Conclusion

- K-means clustering and threshold prediction is demonstrated as an automated and alternate methodology to determine porosity from thin sections.
- Thin section analysis is limited to its pixels resolution of 22 microns, it becomes challenging to analyze porosity of sub-resolution micro pores (e.g. in chalk reservoirs) and a subjective adjustment factor is required to remove the matrix effect from the captured micro pores.
- The resolution and depths of cored samples, thin sections and logs are different and such differences shall be taken into account while comparing the results from these data sources. It can address heterogeneity of reservoir rock.

Further work

- Pore size distribution and irreducible water saturation (Swirr).
- Thin section porosity uncertainty analysis. 800x800 pixels region was used to crop thin section samples. It was observed for heterogeneous samples like (2.6) in Fig. 3 that a different cropping region (e.g. 200x200) will give a different porosity answer.
- The methodology has not been tested on chalk reservoirs where it is expected that significant amount of porosity is associated with sub-resolution micro pores. More tests on carbonate and sandstone reservoirs.

References

- [1] T.Z. Berek, A. Nerøen, P.H. Nadeau, 2017, Digital Image Analysis for Petrophysical Characterization, UIIS Masters Thesis.
- [2] TW. Fens, 2000, Petrophysical Properties from small rock samples using Image Analysis Technique.
- [3] I. Vartolomeev, I. Yakimchuk, A. Denisenko et al, 2016, Integrated Study of Thin Sections: Optical Petrography and Electron Microscopy, SPE 182071.
- [4] Mathworks documentation for K-means clustering.

Contact information

Mirza Hassan Baig (Mh.baig@stvd.uio.no)
 Anders Nerøen (anders.neroen@uis.no)
 Paul Henry Nadeau (paul.h.nadeau@uis.no)
 Pal Østebø Andersen (pal.andersen@uis.no)
 Ivar Austvoll (ivar.austvoll@uis.no)

Appendix-B: MatLab scripts

Main script

```
% mainScript.m
% Objective: To call all functions from one single script

%%
clc
clear all          % clear workspace
close all

%% Read the image & crop
[FileName,PathName] = uigetfile({'*.jpg'; '*.tif';}, 'Select the image');

if FileName ==0
    return;
end
ImageData = imread(strcat(PathName,FileName));
[X, Y, ~] = size(ImageData);
if (X > Y)
    ImageData = imrotate(ImageData,90);
end
figure, imshow(ImageData);
h = imrect(gca,[900, 200, 799, 799]);
position = wait(h);
Im = imcrop(ImageData, position);

figure(1),
imshow(Im)
title('Cropped image from original')

%% select the required function
% Select 7 (Exit) after running a function so you can see its results in
workspace
i = 1; % To keep the while loop true
while(i)
    fprintf('-----\n')
    disp('Select the function and press enter')
    disp('1. Slide Color Test')
    disp('2. Thin Section Test')
    disp('3. Thin Section Test Rc')
    disp('4. Fourier Threshold')
    disp('5. Thin Section Test Rc_Auto')
    disp('6. Image K-means Clustering')
    disp('7. Exit')
    fprintf('Select the function and press enter :');
    select = input('');
    switch (select)
        case 1
            disp('Calling slide Color Test function');
            [Lint,aint,bint,R,G,B] = SlideColorTest(Im,1);

        case 2
            disp('Calling Thin Section Test function');
```

```

[BW,bintc,thr] = ThinSectionTest(Im,1);
disp('Image Analysis function');
fprintf('Enter Minimum Area : ');
minArea = input('');
R = ImAnalysis(BW, minArea);

case 3
disp('Calling Thin Section Test Rc function');
[BW,Rc,thr,M1,N1] = ThinSectionTestRc(Im,1);
disp('Image Analysis function');
fprintf('Enter Minimum Area : ');
minArea = input('');
R = ImAnalysis(BW, minArea);

case 4
disp('Calling Fourier Threshold');
[finalThX,finalThY] = fourierThreshold(Im,1);

case 5
disp('Calling Thin Section Test Rc Auto function');

[BW_macro,BW_micro,BW,thr_macro,thr_total,PHIT,PHI_Micro,PHI_Micro_UnCal,PHI_Macro,PHIT_UnCal] = ThinSectionTestRc_Auto(Im,1);
disp('Image Analysis function');
fprintf('Enter Minimum Area : ');
minArea = input('');
R = ImAnalysis(BW, minArea);

case 6
disp('Calling Image K-means Clustering');
[PHI_Macro, PHI_Micro, PHIT_UnCal, PHIT, BW] =
ImClusters_Kmean(Im,1);
disp('Image Analysis function');
fprintf('Enter Minimum Area : ');
minArea = input('');
R = ImAnalysis(BW, minArea);

case 7
i = 0; % To end the while loop (false)
disp('The program ends');
otherwise
disp('Please enter a valid number');
end

if (select == 7)
break;
else
S = input('Do you want to do another test, Y/N [Y]:','s');
if (S == 'N') || (S == 'n')
i = 0;
disp('The program ends');
end
end
end
end

```

Slide color test

```
function [Lint,aint,bint,R,G,B] = SlideColorTest(Im,figno)
% Objective: To observe sensitivity of blue epoxy on RGB and Lab scale
% Slide Color Test
Ilab = rgb2lab(Im);
[M1,N1,~] = size(Im);
L = reshape(Ilab(:,:,1),M1,N1);
a = reshape(Ilab(:,:,2),M1,N1);
b = reshape(Ilab(:,:,3),M1,N1);
%
R = reshape(Im(:,:,1),M1,N1);
G = reshape(Im(:,:,2),M1,N1);
B = reshape(Im(:,:,3),M1,N1);
% Invert red component image such that blue areas are white
Rc = imcomplement(R);
% Enhance blue component image by histogram equalization
Lg = mat2gray(L);
ag = mat2gray(a);
bg = mat2gray(b);
%
Lint = im2uint8(Lg);
aint = im2uint8(ag);
bint = im2uint8(bg);
figure(figno), clf, imshow(Im), title('Color Image');
figure(figno+1), clf
subplot(4,2,1), imshow(R), title('Red component');
subplot(4,2,2), imhist(R), title('Red histogram');
subplot(4,2,3), imshow(Rc), title('Inverted R');
subplot(4,2,4), imhist(Rc), title('Red inverted histogram');
subplot(4,2,5), imshow(G), title('Green component');
subplot(4,2,6), imhist(G), title('Green histogram');
subplot(4,2,7), imshow(B), title('Blue component');
subplot(4,2,8), imhist(B), title('Blue histogram');
%
figure(figno+2), clf
subplot(3,2,1), imshow(Lint), title('Luminance');
subplot(3,2,2), imhist(Lint), title('L histogram');
subplot(3,2,3), imshow(aint), title('a color component');
subplot(3,2,4), imhist(aint), title('a histogram');
subplot(3,2,5), imshow(bint), title('b color component');
subplot(3,2,6), imhist(bint), title('b histogram');
```

Thin section test Rc

```
function [BW,Rc,thr,M1,N1] = ThinSectionTestRc(Im,figno)
% Objective: Uses manual threshold method [Zerabruk 2017] on inverted R
% component
% Detailed explanation goes here
[M1,N1,~] = size(Im);
R = reshape(Im(:,:,1),M1,N1);
Rc = imcomplement(R);
figure(figno), clf, imhist(Rc), title('Rc histogram');
figure(figno+1), clf, imshow(Rc)
%str1a = ['M = ' strM ' and N = ' strN];
str1 = 'Find and chose a threshold';
disp(str1);
%disp(str1b); pause;
str2 = 'Give a value for the threshold (0 - 255) : ';
disp(str2);
thr = input(' = ');
BW = imbinarize(Rc,thr/255);
figure(figno+2), clf, imshow(BW);
mask = uint8(~BW);
Imt(:,:,1) = Im(:,:,1).*mask;
Imt(:,:,2) = Im(:,:,2).*mask;
Imt(:,:,3) = Im(:,:,3).*mask;
figure(figno+3), clf, imshow(Imt);
;
%
[B,~] = bwboundaries(BW,'noholes');
figure(figno+3), clf, imshow(Im)
hold on
for k = 1:length(B)
boundary = B{k};
plot(boundary(:,2), boundary(:,1), 'r', 'LineWidth', 1)
end
hold off
end
```

Fourier threshold

```
function [dZ1,dZ2] = fourierThreshold(Im,figno);
% Objective: Purpose of the script is to suggest Micro and Macro threshold
% values based on Fourier fit to intensity histogram of inverted red
% component. This technique did not work well, as for some samples it fails
% to suggest threshold values and analyst has to interpret inflexion points
% by themselves

[M1,N1,~] = size(Im);
R = reshape(Im(:,:,1),M1,N1);
Rc = imcomplement(R);
figure(figno), clf, imhist(Rc);
hold on
[Freq,Int] = imhist(Rc);
%plot(Int,Freq);
%hold on

% defining the range to fit the curve
[maxFreq, indexInt] = max(Freq);
IntVal = Int(indexInt);
Freq_Filt = Freq((IntVal+10):(252));
Int_Filt = Int((IntVal+10):(252));

% sine curve fit solution
S = fit(Int_Filt,Freq_Filt,'fourier3');
Z = S(Int_Filt); % finding values of Freq w.r.t Int based on
sine curve fit
plot(Int_Filt,Z, 'r', 'LineWidth', 2, 'DisplayName', 'Fourier Fit');
legend ('show')
legend ('boxoff')
hold off

% taking first and second derivatives to evaluate threshold values for
% Micro and Macro pores
dZ1 = diff(Z);%./diff(Int_Filt);
figure(figno+1),
dZ2 = diff(dZ1);%./diff(Int_Filt(2:end));

plot(Int_Filt(3:end), dZ2, 'r', 'DisplayName', 'Fourier Fit 2nd Derivative');
legend ('Location', 'North')
%title ('2nd Derivative')

% finding rate of change
j=1;
for i = 1 : length(dZ2)-2

    x = dZ2(i);
    y = dZ2(i + 1);
    z = dZ2(i + 2);

    if (x > y && y > z)
    elseif (x < y && y < z)
    else
        changingIndex(j,1) = i + 1;
```

```

        j=j+1;
    end
end

% if no rate of change found in curve than j should be 1 and no threshold
% found
if (j==1)
    h = msgbox('No Threshold Detected');
    return;
end
thresholdsX = Int_Filt(changingIndex) + 2;
thresholdsY = dZ2(changingIndex);
[val, ~] = max(dZ2);

ind = find(thresholdsY > val / 2); % finding any change less than 50 percent
of maxima
thresholdsX(ind)=[];
thresholdsY(ind)=[];
if (isempty(thresholdsY))
    h = msgbox('No Threshold Detected');
    return;
end
% if more than two thresholds take the first and last peak
% finding length of thresholds
if (length(thresholdsX)>2)
    finalThX(1,1) = thresholdsX(1,1);
    finalThY(1,1) = thresholdsY(1,1);
    finalThX(1,2) = thresholdsX(end,1);
    finalThY(1,2) = thresholdsY(end,1);
else
    finalThX = thresholdsX;
    finalThY = thresholdsY;
end

hold on, plot(finalThX, finalThY, 'r *', 'MarkerSize',12, 'DisplayName',
'Threshold values' );
legend ('Location', 'North')
legend ('boxoff')
hold off

end

```


Thin section test Rc auto

```
function
[BW_macro,BW_micro,BW,thr_macro,thr_total,PHIT,PHI_Micro,PHI_Micro_UnCal,PHI_Macro,PHIT_UnCal] = ThinSectionTestRc_Auto(Im,figno)
% Objective: Use auto threshold values either from Fourier Threshold script
% or based on K-means clustering suggested threshold
% For K-means clustering suggested threshold analyst has to read threshold
% values by themselves from intensity histogram plot of micro and macro pores
% on inverted red component plot
% Micro porosity and PHIT answer is using tapering function to exclude
% matrix effect from micro pores
%
% Detailed explanation goes here
[M1,N1,~] = size(Im);
R = reshape(Im(:,:,1),M1,N1);
Rc = imcomplement(R);
figure(figno), clf, imhist(Rc), title('Rc histogram');

% finding thresholds to exclude matrix
str_macro = 'Give a value for the Macro Pores threshold (0 - 255):';
disp(str_macro);
thr_macro = input(' = ');
BW_macro = imbinarize(Rc,thr_macro/255);
str_total = 'Give a value for All Pores threshold (0 - Macro Pores
threshold):';
disp(str_total);
thr_total = input(' = ');
BW = imbinarize(Rc,thr_total/255);
BW_micro = BW - BW_macro;

% Uncalibrated total porosity, micro pores has matrix effect in it
PHIT_UnCal = sum(BW(:))/(M1*N1);
% Macro pore porosity
PHI_Macro = sum(BW_macro(:))/(M1*N1);

PHI_Micro_UnCal = PHIT_UnCal - PHI_Macro;

% marking boundaries for the captured Micro and Macro pores
[B_micro] = bwboundaries(BW_micro);
[B_macro] = bwboundaries(BW_macro);
figure(figno+1), imshow(Im), title('Micro-Macro Map');
hold on
for k = 1:length(B_micro)
    boundary = B_micro{k};
    plot(boundary(:,2),boundary(:,1),'g','LineWidth',1)
end
hold on
for k = 1:length(B_macro)
    boundary = B_macro{k};
    plot(boundary(:,2),boundary(:,1),'r','LineWidth',1)
end
hold off

% Linear normalization function for Micro pores porosity
```

```

Rc_double = double(Rc);

% Value of n need to be defined by the analyst, tapering function
n = 1.5;
for ii = 1:N1
    for jj = 1:M1
        if BW_micro(ii,jj) == 1
            BW_micro_norm(ii,jj) = ((Rc_double(ii,jj)-thr_total)/(thr_macro-
thr_total))^n;
        else
            end
        end
    end
end
PHI_Micro = sum(BW_micro_norm(:))/(M1*N1);

% Total porosity
PHIT = PHI_Micro + PHI_Macro;

```

ImClusters K-mean

```
function [PHI_Macro, PHI_Micro, PHIT_UnCal, PHIT,
BW]=ImClusters_Kmean(Im,figno);
% Objective: No user input, script is using 3 clusters
% Output PHIT is using adjustment factor of 0.8 to remove matrix effect
% from Micro pores

%Example from Matlab helpfile, color-based segmentation using K-means
clustering
%Step: Convert Image from RGB Color Space to L*a*b* Color Space
%The L*a*b* space consists of a luminosity layer 'L*',
%chromaticity-layer 'a*' indicating where color falls along the red-green
axis,
%and chromaticity-layer 'b*' indicating where the color falls along the blue-
yellow axis.
%All of the color information is in the 'a*' and 'b*' layers.
cform = makecform('srgb2lab');
Ilab = applycform(Im,cform);

%Step: Classify the Colors in 'a*b*' Space Using K-Means Clustering
%Since the color information exists in the 'a*b*' space, the objects are
pixels
%with 'a*' and 'b*' values. Use kmeans to cluster the objects into three
clusters
%using the Euclidean distance metric.
ab = double(Ilab(:,:,2:3));
[M1,N1,~] = size(Im);
ab = reshape(ab,M1*N1,2);

% nColors control number of clusters
nColors = 3;
%repeat the clustering 3 times to avoid local minima
[cluster_idx, cluster_center] =
kmeans(ab,nColors,'distance','sqEuclidean','Replicates',3);

%Step: Label Every Pixel in the Image Using the Results from KMEANS
%For every object in the input, kmeans returns an index corresponding to a
cluster.
%Label every pixel in the image with its cluster_index.
pixel_labels = reshape(cluster_idx,M1,N1);

%Step: Create Images that Segment the Image by Color
%using pixel labels the objects can be separated by color, resulting in
%three images
segmented_images = cell(1,nColors);
rgb_label = repmat(pixel_labels,[1 1 3]);
for k = 1:nColors
    color = Im;
    color(rgb_label~=k) = 0;
    segmented_images{k} = color;
end

figure, clf
subplot(2,3,1), imshow(Im), title('Original cropped image');
```

```

subplot(2,3,2), imshow(pixel_labels,[]), title('Image labeled by cluster
index');
subplot(2,3,4), imshow(segmented_images{1}), title('Objects in cluster 1');
subplot(2,3,5), imshow(segmented_images{2}), title('Objects in cluster 2');
subplot(2,3,6), imshow(segmented_images{3}), title('Objects in cluster 3');

%Step: Segment Macro and Micro in separate images
%we have an assumption that bluishness of the color determines our
%confidence on captured pores. Hence, we can separate more blue (Macro)
high
%confidence pores from less blue (Micro) low confidence pores
%dark blue from light blue can be separated using the 'L*' layer in the
%L*a*b* color space.
mean_cluster_value = mean(cluster_center,2);
[tmp,idx] = sort(mean_cluster_value);
blue_cluster_num = idx(1);
L = Ilab(:,:,1);
blue_idx = find(pixel_labels == blue_cluster_num);
L_blue=L(blue_idx);
Is_blue = imbinarize(L_blue);

Macro_labels = repmat(uint8(0),[M1, N1]);
Macro_labels(blue_idx(Is_blue==false)) = 1;
Macro_pores = repmat(Macro_labels,[1 1 3]);
Macro_blue = Im;
Macro_blue(Macro_pores~=1) = 0;
BW_macro = imbinarize(reshape(Macro_blue(:,:,3),M1,N1));

Micro_labels = repmat(uint8(0),[M1,N1]);
Micro_labels(blue_idx(Is_blue==true)) = 1;
Micro_pores = repmat(Micro_labels,[1 1 3]);
Micro_blue = Im;
Micro_blue(Micro_pores~=1) = 0;
BW_micro = imbinarize(reshape(Micro_blue(:,:,3),M1,N1));

MicMac_labels = repmat(uint8(0),[M1, N1]);
MicMac_labels(blue_idx) = 1;
MicMac_pores = repmat(MicMac_labels,[1 1 3]);
MicMac_blue = Im;
MicMac_blue(MicMac_pores~=1) = 0;
BW = imbinarize(reshape(MicMac_blue(:,:,3),M1,N1));

figure, clf
subplot(1,2,1), imshow(Micro_blue), title('Light Blue');
subplot(1,2,2), imshow(Macro_blue), title('Dark Blue');

% marking boundaries for the captured Micro and Macro pores
[B_micro] = bwboundaries(BW_micro);
[B_macro] = bwboundaries(BW_macro);
figure, imshow(Im), title('Micro-Macro Map');
hold on
for k = 1:length(B_micro)
    boundary = B_micro{k};
    plot (boundary(:,2),boundary(:,1), 'g', 'LineWidth',1)

```

```

end
hold on
for k = 1:length(B_macro)
    boundary = B_macro{k};
    plot (boundary(:,2),boundary(:,1), 'r', 'LineWidth',1)
end
hold off

Rc_Im = imcomplement(reshape(Im(:,:,1),M1,N1));
figure, imshow(Rc_Im);
hold on
for k = 1:length(B_micro)
    boundary = B_micro{k};
    plot (boundary(:,2),boundary(:,1), 'g', 'LineWidth',1)
end
hold on
for k = 1:length(B_macro)
    boundary = B_macro{k};
    plot (boundary(:,2),boundary(:,1), 'b', 'LineWidth',1)
end
hold off

Rc_Macro = imcomplement(reshape(Macro_blue(:,:,1),M1,N1));
Rc_Micro = imcomplement(reshape(Micro_blue(:,:,1),M1,N1));
Rc_MicMac = imcomplement(reshape(MicMac_blue(:,:,1),M1,N1));
[Freq_Macro,Int_Macro] = imhist(Rc_Macro);
[Freq_Micro,Int_Micro] = imhist(Rc_Micro);
[Freq_MicMac,Int_MicMac] = imhist(Rc_MicMac);

figure, imhist(Rc_Im);
hold on
plot (Int_Macro(1:end-1),Freq_Macro(1:end-1), 'r', 'LineWidth', 2);
plot (Int_Micro(1:end-1),Freq_Micro(1:end-1), 'g', 'LineWidth', 2);
plot (Int_MicMac(1:end-1),Freq_MicMac(1:end-1), 'k', 'LineWidth', 1);
hold off

PHI_Micro = sum(BW_micro(:))/(M1*N1);
PHI_Macro = sum(BW_macro(:))/(M1*N1);

% PHIT_UnCal has matrix effect in it from micro pores
PHIT_UnCal = sum(BW(:))/(M1*N1);

% Define adjustment factor (Adj) to take out matrix effect from micro pores
Adj = 0.8;
PHIT = 0.8*PHI_Micro + PHI_Macro;

end

```






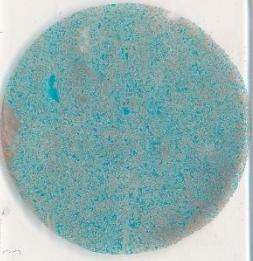
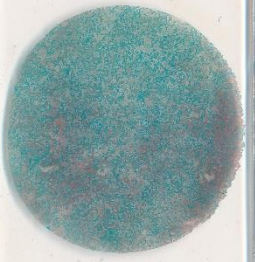
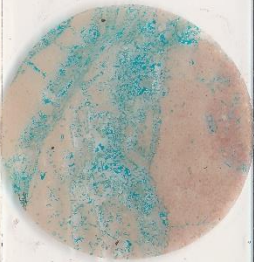




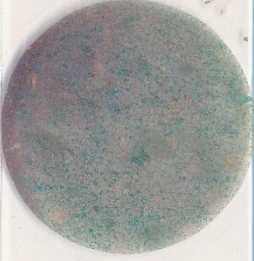



ImAnalysis














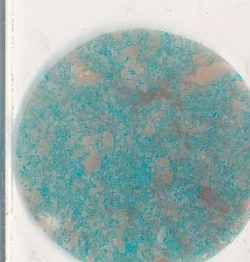


```
function R = ImAnalysis(BW,Amin)
% Objective: Morphological properties of captured pores
% R = ImAnalysis(Imroi,thr,Amin) finds a binary image of
% Imroi : intensity image region
% thr : threshold
% and finds the properties of the regions in the complementary binary image
% Only regions with area larger than
% Amin : minimum area
% are included in the results. The results are written to a data structure
% R
% R.BW is the binary image used
% R.P is the property matrix of size [K,8] where
% K is the number of regions
% 8 is the number of properties
% BW = im2bw(Imroi,thr); % ROI threshold
R.BW = BW;
%
% Properties found
sA = 'Area';
sC = 'Centroid';
sL1 = 'MajorAxisLength';
sL2 = 'MinorAxisLength';
sE = 'Eccentricity';
sO = 'Orientation';
sP = 'Perimeter';
%
s = regionprops (BW, sA, sL1, sL2, sC, sP, sO, sE);
%
% Preparing the output property matrix
K = size(s,1); % Number of regions found
Prop = zeros(K,8);
for k = 1:K
    A = s(k).Area;
    C = s(k).Centroid;
    x = C(1); y = C(2);
    L1 = s(k).MajorAxisLength;
    L2 = s(k).MinorAxisLength;
    P = s(k).Perimeter;
    O = s(k).Orientation;
    E = s(k).Eccentricity;
    prow = [A x y L1 L2 P E O];
    Prop(k,:) = prow;
end
% Area
A = Prop(:,1); % Area vector
[~,I] = sort(A); % Sorting according to area size
I = flipud(I); % Largest first
Props = Prop(I,:);
I = Props(:,1) > Amin; % Finds rows with area larger than Amin
Props = Props(I,:); % Removes rows with smaller areas
%
R.P = Props;
R.Numobj = K;
```

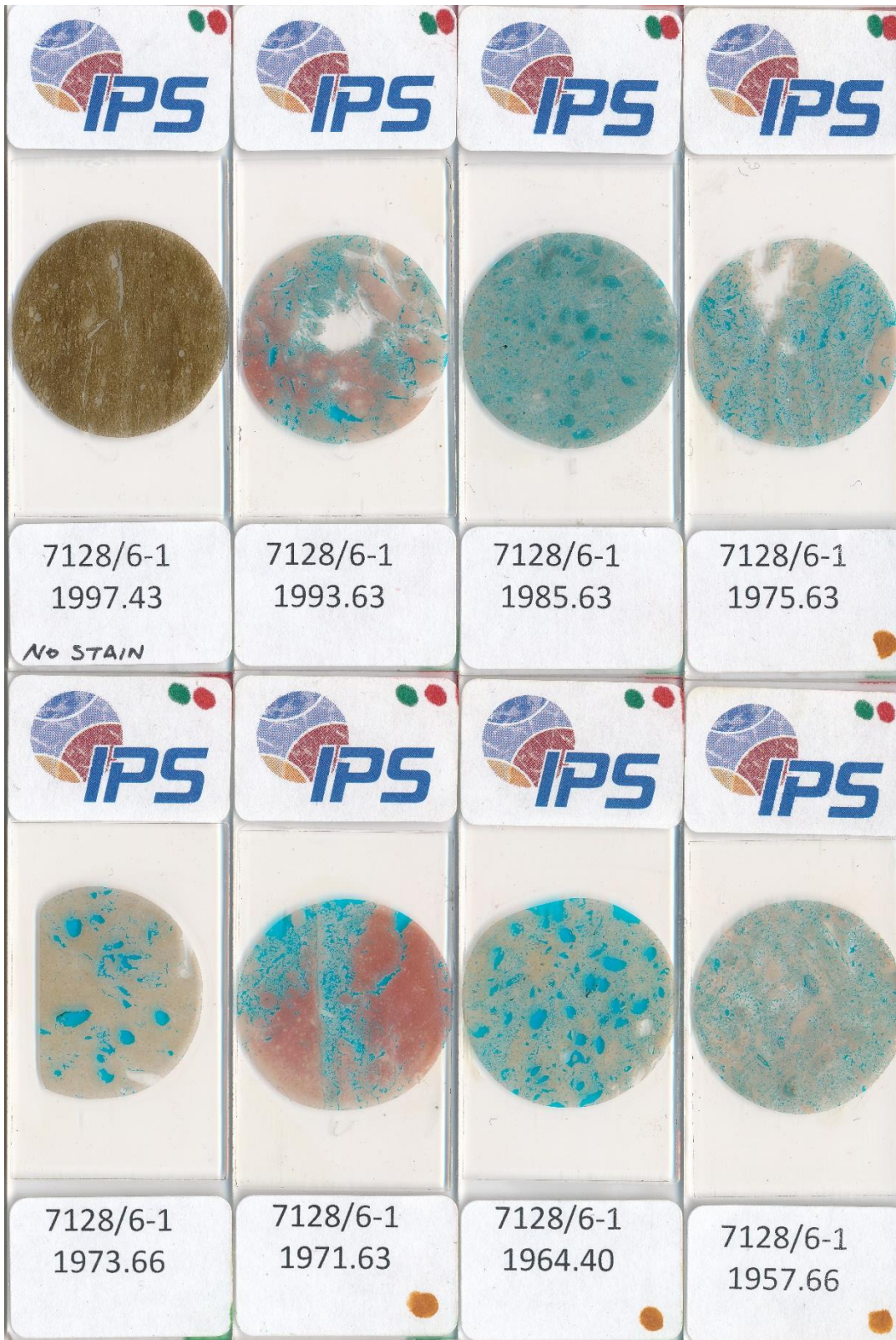
Appendix-C: Optical microscopy scans of thin section samples






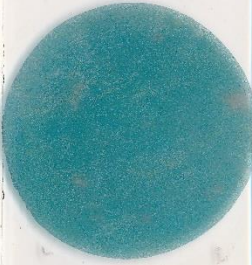







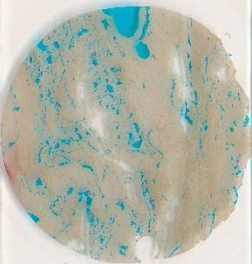

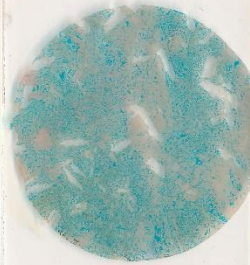
All samples scans for the well 7128/6-1 are included here, but only 26 samples were used in the current study.










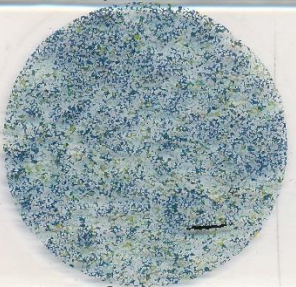


			
			
7128/6-1 1896.70	7128/6-1 1891.90	7128/6-1 1883.41	7128/6-1 1877.48
			
			
7128/6-1 1868.51	7128/6-1 1866.52 NOT STAINED	7128/6-1 1845.75	7128/6-1 1836.03

			
			
7128/6-1 1952.04	7128/6-1 1947.94	7128/6-1 1945.28	7128/6-1 1930.44
			
			
7128/6-1 1916.15	7128/6-1 1913.49	7128/6-1 1904.75	7128/6-1 1902.72
			

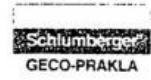


			
			
7128/6-1 2049.78 NO STAIN	7128/6-1 2046.03	7128/6-1 2044.52	7128/6-1 2025.12
			
			
7128/6-1 2019.03	7128/6-1 2015.03	7128/6-1 2006.47	7128/6-1 2000.70

		
		
7128/6-1 2222.60	7128/6-1 2128.82	7128/6-1 2109.34
		
		
7128/6-1 2097.95	7128/6-1 2077.29	7128/6-1 2073.92

		<p>7128/6-1 2225.58</p>
		<p>7128/6-1 2232.84 NO STAIN</p>
		<p>7128/6-1 2540.60</p>
		<p>7128/6-1 2243.39</p>
		<p>7128/6-1 2247.40 NO STAIN</p>

Appendix-D: Core analysis report (7128/6-1 well)



CONOCO NORWAY INC.
CONVENTIONAL CORE ANALYSIS

WELL: 7128/6-1

D-21

DATE: FEBRUARY 1992

7128/6-1 D-21
— CONOCO NORWAY INC. —
— CENTRAL FILES —
— LIBRARY —

Company CONOCO

Well 7128/6-1

Field 7128/6

Core no. 1

CONVENTIONAL CORE ANALYSIS

Depth M	Permeability (mD)								Porosity (%)		Pore		Grain	
	Horizontal 1/Prr				Vertical 1/Prr				Ruid He	sum.	saturation (%)	density	RKB	Plug MD (g/cm)
1629.00														
1 1629.00	npp									14.3				2.65
2 1629.25	npp									npp				npp
3 1629.50	1.69	0.449	2.13	1.33	1.02	0.343	1.45	0.796	16.8				2.62	
4 1629.70	4.81	0.449	5.81	4.00	0.124	0.343	0.183	0.092	4.8	17.4	10.3	52.8	2.60	
5 1630.00	nmp				0.193	0.343	0.284	0.146	20.8				2.62	
6 1630.25	npp									npp			npp	
7 1630.60	npp									npp	16.8	17.7	72.0	npp
8 1630.75	2.80	0.449	3.50	2.23	0.489	0.343	0.706	0.376	16.7				2.60	
9 1631.00	12.0	0.452	13.8	10.5	4.03	0.464	4.89	3.28	19.4				2.61	
10 1631.25	nmp				1.41	0.463	1.76	1.10	20.7				2.61	
11 1631.60	nmp				0.485	0.342	0.700	0.373	21.2	19.9	6.8	80.5	2.64	
12 1631.75	npp								24.4				2.63	
13 1632.00	nmp				3.58	0.451	4.39	2.90	19.6				2.62	
14 1632.40	npp								npp				npp	
15 1632.60	npp								npp	17.5	12.6	78.8	npp	

Company : CONOCO
 Well : 7128/6-1
 Field : 7128/6
 Core no. : 1

CONVENTIONAL CORE ANALYSIS

Plug no.	Depth (m) RKB MD	Permeability (mD)								Porosity (%)		Pore saturation (%)		Grain density (g/cm ³)
		Horizontal				Vertical				He	Fluid sum.	S _o	S _w	
		K _g	1/P _m	K _a	K _{el}	K _g	1/P _m	K _a	K _{el}					
	1629.00													
1	1629.00	npp								14.3				2.65
2	1629.25	npp								npp				npp
3	1629.50	1.69	0.449	2.13	1.33	1.02	0.343	1.45	0.796	16.8				2.62
4	1629.70	4.81	0.449	5.81	4.00	0.124	0.343	0.183	0.092	4.8	17.4	10.3	52.8	2.60
5	1630.00	nmp				0.193	0.343	0.284	0.146	20.8				2.62
6	1630.25	npp								npp				npp
7	1630.60	npp								npp	16.8	17.7	72.0	npp
8	1630.75	2.80	0.449	3.50	2.23	0.489	0.343	0.706	0.376	16.7				2.60
9	1631.00	12.0	0.452	13.8	10.5	4.03	0.464	4.89	3.28	19.4				2.61
10	1631.25	nmp				1.41	0.463	1.76	1.10	20.7				2.61
11	1631.60	nmp				0.485	0.342	0.700	0.373	21.2	19.9	6.8	80.5	2.64
12	1631.75	npp								24.4				2.63
13	1632.00	nmp				3.58	0.451	4.39	2.90	19.6				2.62
14	1632.40	npp								npp				npp
15	1632.60	npp								npp	17.5	12.6	78.8	npp
16	1632.80	npp								npp				npp
17	1633.00	2.70	0.449	3.38	2.15	0.512	0.342	0.738	0.394	21.7				2.62
18	1633.25	nmp				0.656	0.343	0.942	0.508	23.7				2.60
19	1633.60	npp								npp	20.9	8.2	64.8	npp
20	1633.75	npp								npp				npp
21	1634.00	2.02	0.449	2.54	1.60	29.4	0.479	32.4	26.6	20.4				2.57
22	1634.25	npp								20.0				2.63
23	1634.60	npp								20.4	22.5	7.9	71.0	2.62
24	1634.75	npp								19.2				2.61
25	1635.05	1.35	0.448	1.71	1.06	2.04	0.344	2.86	1.62	10.2				2.56
26	1635.25	npp								28.7				2.63
27	1635.60	0.117	0.344	0.173	0.087	0.166	0.343	0.245	0.125	0.7	2.7	45.0	45.0	2.56
28	1635.75	3.32	0.447	4.11	2.69	0.738	0.343	1.06	0.572	24.3				2.65
29	1636.00	1.81	0.447	2.28	1.43	<0.04		<0.04	<0.02	1.6				2.52
30	1636.25	<0.04		<0.04	<0.02	<0.04		<0.04	<0.02	12.5				2.59

Company : CONOCO Well : 7128/6-1 Field : 7128/6 Core no. : 1	CONVENTIONAL CORE ANALYSIS
---	-----------------------------------

Plug no.	Depth (m) RKB MD	Permeability (mD)								Porosity (%)		Pore saturation (%)		Grain density (g/cm ³)
		Horizontal				Vertical				He	Fluid sum.	S _o	S _w	
		K _g	1/P _m	K _a	K _{el}	K _g	1/P _m	K _a	K _{el}					
31	1636.60	npp								17.6	17.3	3.4	83.9	2.63
32	1636.75	npp								14.3				2.64
33	1637.00	npp								8.0				2.55
34	1637.20	0.801	0.343	1.14	0.622	0.321	0.343	0.468	0.245	19.6				2.61
35	1637.50	29.0	0.486	32.0	26.3	3.29	0.451	4.06	2.65	14.3	17.2	4.6	69.3	2.60
36	1637.75	npp								npp				npp
37	1638.00	npp								21.8				2.60
38	1638.25	1.71	0.346	2.40	1.35	6.96	0.452	8.22	5.91	19.9				2.58
39	1638.60	4.13	0.455	5.03	3.39	0.931	0.451	1.18	0.725	27.4	24.3	4.0	61.5	2.62
40	1638.75	npp								14.5				2.71
41	1639.00	npp								npp				npp
42	1639.25	18.6	0.467	21.0	16.6	73.0	0.497	78.2	67.9	22.8				2.63
43	1639.50	npp								5.6				2.52
44	1639.76	npp								npp	22.3	3.4	78.6	npp
45	1640.00	npp								24.4				2.60
46	1640.25	0.866	0.345	1.23	0.673	1.20	0.343	1.70	0.940	22.5				2.61
47	1640.50	npp								npp				npp
48	1640.70	npp								npp	18.4	4.2	79.1	npp
49	1641.00	nmp					1.59	0.448	2.01	1.25	19.6			2.59
50	1641.25	npp								npp				npp
51	1641.50	16.0	0.462	18.2	14.2	nmp				18.9	21.3	3.9	77.4	2.60
52	1641.75	npp								0.9				2.56
	1641.83													

Plug no.	Depth (m) RKB MD	Permeability (mD)								Porosity (%)		Pore saturation (%)		Grain density (g/cm ³)
		Horizontal				Vertical				He	Fluid sum.	S _o	S _w	
		K _g	1/P _m	K _a	K _{el}	K _g	1/P _m	K _a	K _{el}					
	1643.00													
53	1643.05	<0.04		<0.04	<0.02	0.139	0.342	0.205	0.104	1.7				2.55
54	1643.30	1.22	0.344	1.73	0.959	0.366	0.342	0.532	0.280	15.4	12.0	5.8	83.9	2.60
55	1643.50					0.231	0.411	0.312	0.175					
56	1643.70	nmp				0.861	0.411	1.13	0.669	19.5				2.60
57	1644.00	12.9	0.457	14.7	11.3	nmp				4.4				2.52
58	1644.25	8.05	0.455	9.43	6.90					17.1				2.60
59	1644.50													
60	1644.75	1.96	0.453	2.45	1.55					21.8				2.59
	1644.86													
	1645.00													
61	1645.30	<0.04		<0.04	<0.02	6.25	0.414	7.52	5.35	1.7	16.3	2.1	58.4	2.53
	1646.60													

Plug no.	Depth (m) RKB MD	Permeability (mD)								Porosity (%)		Pore saturation (%)		Grain density (g/cm ³)
		Horizontal				Vertical				He	Fluid sum.	S _o	S _w	
		K _g	1/P _m	K _a	K _{el}	K _g	1/P _m	K _a	K _{el}					
62	1701.10													
62	1701.40	<0.04		<0.04	<0.02	0.042	0.341	0.064	0.031	5.4	10.0	4.2	78.3	2.71
63	1701.55	0.108	0.341	0.161	0.081	<0.04		<0.04	<0.02	12.2				2.69
64	1701.80	0.092	0.341	0.137	0.068	0.082	0.341	0.123	0.061	8.3				2.66
65	1702.05	<0.04		<0.04	<0.02	0.180	0.341	0.266	0.136	2.5				2.60
66	1702.30	<0.04		<0.04	<0.02	<0.04		<0.04	<0.02	4.5				2.60
67	1702.55	0.048	0.341	0.073	0.035	<0.04		<0.04	<0.02	8.9	10.0	6.2	53.8	2.66
68	1702.80	<0.04		<0.04	<0.02	nvpp				0.9				2.68
69	1703.05	<0.04		<0.04	<0.02	<0.04		<0.04	<0.02	0.232				2.58
70	1703.30	<0.04		<0.04	<0.02	<0.04		<0.04	<0.02	10.1	12.6	4.7	73.7	2.65
71	1703.55	nhpp				<0.04		<0.04	<0.02	npp				npp
72	1703.80	nhpp				0.121	0.341	0.180	0.090	npp				npp
73	1704.05	<0.04		<0.04	<0.02	<0.04		<0.04	<0.02	4.2				2.62
74	1704.30	<0.04		<0.04	<0.02	<0.04		<0.04	<0.02	8.0	7.5	7.0	53.9	2.64
75	1704.55	<0.04		<0.04	<0.02	nvpp				6.9				2.61
76	1704.80	<0.04		<0.04	<0.02	<0.04		<0.04	<0.02	5.5				2.65
77	1705.05	<0.04		<0.04	<0.02	nmp				6.7				2.65
78	1705.30	nmp				<0.04		<0.04	<0.02	6.5	9.3	6.7	76.5	2.66
79	1705.55	<0.04		<0.04	<0.02	<0.04		<0.04	<0.02	7.6				2.63
80	1705.80	<0.04		<0.04	<0.02	<0.04		<0.04	<0.02	7.6				2.64
81	1706.05	nmp				nmp				8.5				2.65
82	1706.30	<0.04		<0.04	<0.02	<0.04		<0.04	<0.02	6.7	7.5	14.3	71.5	2.65
83	1706.55	<0.04		<0.04	<0.02	nvpp				7.3				2.64
84	1706.88	nmp				<0.04		<0.04	<0.02	6.4				2.66
85	1707.05	nmp				nvpp				7.2	10.9	9.6	57.6	2.64
86	1707.30	<0.04		<0.04	<0.02	<0.04		<0.04	<0.02	7.6				2.64
87	1707.55	<0.04		<0.04	<0.02	<0.04		<0.04	<0.02	5.9				2.65
88	1707.80	0.051	0.340	0.077	0.037	nvpp				10.9				2.64
89	1708.05	nmp				<0.04		<0.04	<0.02	13.9	11.4	12.3	71.8	2.65
90	1708.30	0.038	0.341	0.058	0.028	nvpp				9.0				2.60
91	1708.55	<0.04		<0.04	<0.02	<0.04		<0.04	<0.02	11.4				2.62
92	1708.80	nhpp				nvpp				npp				npp
93	1709.05	nmp				nvpp				9.1	8.6	8.8	77.2	2.66
94	1709.30	<0.04		<0.04	<0.02	<0.04		<0.04	<0.02	7.9				2.66
95	1709.55	nmp				nvpp				9.5				2.66
96	1709.80	<0.04		<0.04	<0.02	<0.04		<0.04	<0.02	6.6	10.1	6.1	65.2	2.62
97	1710.05	nhpp				nvpp				npp				npp
98	1710.30	<0.04		<0.04	<0.02	<0.04		<0.04	<0.02	8.4				2.65
	1710.30													

Plug no.	Depth (m) RKB MD	Permeability (mD)								Porosity (%)		Pore saturation (%)		Grain density (g/cm ³)	
		Horizontal				Vertical				He	Fluid sum.	S _o	S _w		
		K _g	1/P _m	K _a	K _{el}	K _g	1/P _m	K _a	K _{el}						
99	1710.30														
99	1710.35	nmp				<0.04		<0.04	<0.02	7.6					2.70
100	1710.50	<0.04		<0.04	<0.02	<0.04		nhpp	nhpp	7.7	6.6	8.7	87.0		2.64
101	1710.75	<0.04		<0.04	<0.02	<0.04		<0.04	<0.02	7.8					2.63
102	1711.00	nmp				<0.04		<0.04	<0.02	7.9					2.67
103	1711.25	nmp				<0.04		<0.04	<0.02	7.1					2.72
104	1711.50	<0.04		<0.04	<0.02	<0.04		<0.04	<0.02	7.7	6.1	7.1	92.9		2.63
105	1711.75	<0.04		<0.04	<0.02	<0.04		<0.04	<0.02	7.1					2.62
106	1712.00	nmp				<0.04		<0.04	<0.02	7.6					2.67
107	1712.25	<0.04		<0.04	<0.02	<0.04		<0.04	<0.02	1.9					2.62
108	1712.50	<0.04		<0.04	<0.02	<0.04		nhpp	nhpp	6.1	7.1	5.9	89.1		2.67
109	1712.75	<0.04		<0.04	<0.02	<0.04		<0.04	<0.02	9.3					2.66
110	1713.00	<0.04		<0.04	<0.02	<0.04		<0.04	<0.02	9.7					2.61
111	1713.25	nmp				0.034	0.342	0.052	0.025	9.1					2.66
112	1713.50	nmp				<0.04		<0.04	<0.02	6.3	9.0	7.2	88.5		2.67
113	1713.75	<0.04		<0.04	<0.02	<0.04		<0.04	<0.02	11.5					2.63
114	1714.00	<0.04		<0.04	<0.02	<0.04		<0.04	<0.02	10.6					2.63
115	1714.25	<0.04		<0.04	<0.02	<0.04		<0.04	<0.02	10.2					2.62
116	1714.50	<0.04		<0.04	<0.02	<0.04		<0.04	<0.02	10.9	10.1	6.0	90.4		2.61
117	1714.75	<0.04		<0.04	<0.02	<0.04		<0.04	<0.02	10.9					2.61
118	1715.00	<0.04		<0.04	<0.02	0.078	0.342	0.117	0.058	7.0					2.63
119	1715.25	nmp				<0.04		<0.04	<0.02	3.3					2.63
120	1715.50	<0.04		<0.04	<0.02	<0.04		<0.04	<0.02	6.0	6.9	6.3	81.5		2.70
121	1715.75	<0.04		<0.04	<0.02	<0.04		<0.04	<0.02	2.0					2.70
122	1716.00	<0.04		<0.04	<0.02	<0.04		nhpp	nhpp	1.7					2.70
123	1716.25	<0.04		<0.04	<0.02	nmp				2.9					2.58
124	1716.55	nhpp				<0.04		<0.04	<0.02	npp	8.2	8.5	85.4		npp
125	1716.75	nhpp				<0.04		nhpp	nhpp	npp					npp
126	1717.00	<0.04		<0.04	<0.02	<0.04		nhpp	nhpp	0.5					2.58
127	1717.25	<0.04		<0.04	<0.02	<0.04		nhpp	nhpp	7.9					2.65
128	1717.50	nmp				<0.04		<0.04	<0.02	8.3	9.5	4.3	81.5		2.62

Plug no.	Depth (m) RKB MD	Permeability (mD)								Porosity (%)		Pore saturation (%)		Grain density (g/cm ³)
		Horizontal				Vertical				He	Fluid sum.	S _o	S _w	
		K _g	1/P _m	K _a	K _{el}	K _g	1/P _m	K _a	K _{el}					
129	1717.75	<0.04		<0.04	<0.02	<0.04		<0.04	<0.02	2.6				2.68
130	1718.00	nhpp				<0.04		nhpp	nhpp	npp				npp
131	1718.25	<0.04		<0.04	<0.02	<0.04		<0.04	<0.02	3.9				2.64
132	1718.50	<0.04		<0.04	<0.02	<0.04		<0.04	<0.02	6.8	9.0	6.9	61.9	2.69
133	1718.75	<0.04		<0.04	<0.02	<0.04		nhpp	nhpp	9.1				2.66
134	1719.00	nmp				<0.04		<0.04	<0.02	6.0				2.62
135	1719.25	<0.04		<0.04	<0.02	<0.04		nhpp	nhpp	7.4				2.61
136	1719.50	<0.04		<0.04	<0.02	<0.04		<0.04	<0.02	10.0	7.1	6.0	86.3	2.62
137	1719.75	<0.04		<0.04	<0.02	<0.04		<0.04	<0.02	9.7				2.63
138	1720.00	<0.04		<0.04	<0.02	<0.04		<0.04	<0.02	1.6				2.67
139	1720.25	<0.04		<0.04	<0.02	<0.04		nhpp	nhpp	9.0				2.68
140	1720.50	<0.04		<0.04	<0.02	<0.04		<0.04	<0.02	9.1	10.3	6.0	84.3	2.62
141	1720.75	<0.04		<0.04	<0.02	<0.04		<0.04	<0.02	12.5				2.68
142	1721.05	0.028	0.342	0.043	0.021	<0.04		<0.04	<0.02	8.1				2.67
143	1721.25	<0.04		<0.04	<0.02	<0.04		<0.04	<0.02	7.7				2.63
144	1721.50	nmp				<0.04		<0.04	<0.02	8.8	6.7	9.6	79.6	2.66
145	1721.75	<0.04		<0.04	<0.02	<0.04		<0.04	<0.02	6.4				2.68
146	1722.00	<0.04		<0.04	<0.02	<0.04		<0.04	<0.02	7.1				2.68
147	1722.25	<0.04		<0.04	<0.02	<0.04		<0.04	<0.02	6.5				2.66
148	1722.50	<0.04		<0.04	<0.02	<0.04		<0.04	<0.02	7.8	7.9	5.3	84.1	2.67
149	1722.75	<0.04		<0.04	<0.02	<0.04		<0.04	<0.02	6.8				2.68
150	1723.00	<0.04		<0.04	<0.02	<0.04		<0.04	<0.02	9.5				2.62
151	1723.25	<0.04		<0.04	<0.02	<0.04		nhpp	nhpp	7.1				2.67
152	1723.50	<0.04		<0.04	<0.02	<0.04		<0.04	<0.02	8.1	11.3	5.4	67.2	2.64
153	1723.75	<0.04		<0.04	<0.02	<0.04		<0.04	<0.02	4.1				2.68
154	1724.00	<0.04		<0.04	<0.02	<0.04		<0.04	<0.02	7.5				2.62
155	1724.25	nmp				<0.04		<0.04	<0.02	9.4				2.62
156	1724.45	<0.04		<0.04	<0.02	<0.04		<0.04	<0.02	8.3	9.8	6.4	65.9	2.65
157	1724.75	<0.04		<0.04	<0.02	<0.04		<0.04	<0.02	5.7				2.68
158	1725.00	<0.04		<0.04	<0.02	<0.04		<0.04	<0.02	6.6				2.67
159	1725.25	0.039	0.342	0.059	0.029	<0.04		<0.04	<0.02	6.3				2.68
160	1725.50	nmp				<0.04		<0.04	<0.02	7.0	7.2	8.9	74.2	2.66
161	1725.75	<0.04		<0.04	<0.02	<0.04		<0.04	<0.02	7.6				2.66
162	1726.00	<0.04		<0.04	<0.02	<0.04		<0.04	<0.02	6.0				2.68
163	1726.25	<0.04		<0.04	<0.02	<0.04		<0.04	<0.02	8.2				2.63
164	1726.50	<0.04		<0.04	<0.02	<0.04		<0.04	<0.02	8.8	9.4	8.9	70.9	2.68
165	1726.75	nmp				<0.04		<0.04	<0.02	9.2				2.70
166	1727.00	<0.04		<0.04	<0.02	<0.04		<0.04	<0.02	9.4				2.67
167	1727.25	<0.04		<0.04	<0.02	<0.04		<0.04	<0.02	5.4				2.68
168	1727.50	<0.04		<0.04	<0.02	<0.04		<0.04	<0.02	7.8	7.8	5.4	89.0	2.67
169	1727.75	nmp				<0.04		<0.04	<0.02	9.5				2.68
170	1728.00	nmp				<0.04		<0.04	<0.02	8.2				2.68
	1728.10													

Plug no.	Depth (m) RKB MD	Permeability (mD)								Porosity (%)		Pore saturation (%)		Grain density (g/cm ³)
		Horizontal				Vertical				He	Fluid sum.	S _o	S _w	
		K _g	1/P _m	K _a	K _{el}	K _g	1/P _m	K _a	K _{el}					
171	1728.20	nmp				<0.04		<0.04	<0.02	9.3				2.69
172	1728.25	0.042	0.342	0.063	0.031	<0.04		<0.04	<0.02	7.8	8.0	5.3	82.4	2.69
173	1728.50	<0.04		<0.04	<0.02	<0.04		<0.04	<0.02	7.4				2.68
174	1728.75	<0.04		<0.04	<0.02	<0.04		<0.04	<0.02	2.1				2.70
175	1729.00	<0.04		<0.04	<0.02	<0.04		<0.04	<0.02	5.7				2.65
176	1729.25	<0.04		<0.04	<0.02	<0.04		<0.04	<0.02	6.9	6.0	10.5	80.4	2.67
177	1729.50	<0.04		<0.04	<0.02	<0.04		<0.04	<0.02	7.4				2.68
178	1729.75	nmp				<0.04		<0.04	<0.02	8.9				2.67
179	1730.00	<0.04		<0.04	<0.02	<0.04		<0.04	<0.02	6.6				2.63
180	1730.25	nmp				<0.04		<0.04	<0.02	8.0	8.3	7.8	77.6	2.68
181	1730.50	<0.04		<0.04	<0.02	<0.04		<0.04	<0.02	5.6				2.69
182	1730.75	<0.04		<0.04	<0.02	<0.04		<0.04	<0.02	5.7				2.66
183	1731.00	<0.04		<0.04	<0.02	<0.04		<0.04	<0.02	6.0				2.65
184	1731.25	<0.04		<0.04	<0.02	<0.04		<0.04	<0.02	8.0	8.1	17.9	63.9	2.66
185	1731.50	<0.04		<0.04	<0.02	<0.04		<0.04	<0.02	6.3				2.66
186	1731.75	<0.04		<0.04	<0.02	<0.04		<0.04	<0.02	5.6				2.65
187	1732.00	<0.04		<0.04	<0.02	<0.04		<0.04	<0.02	5.6				2.67
188	1732.25	<0.04		<0.04	<0.02	<0.04		<0.04	<0.02	6.6	9.6	6.4	55.7	2.65
189	1732.50	<0.04		<0.04	<0.02	<0.04		<0.04	<0.02	6.9				2.64
190	1732.75	nmp				<0.04		<0.04	<0.02	6.2				2.68
191	1733.00	<0.04		<0.04	<0.02	<0.04		<0.04	<0.02	5.9				2.69
192	1733.25	<0.04		<0.04	<0.02	<0.04		<0.04	<0.02	7.5	14.6	4.2	43.1	2.67
193	1733.50	<0.04		<0.04	<0.02	<0.04		<0.04	<0.02	6.7				2.67
194	1733.75	nmp				<0.04		<0.04	<0.02	6.2				2.67
195	1734.00	<0.04		<0.04	<0.02	<0.04		<0.04	<0.02	5.3				2.67
196	1734.25	nmp				<0.04		<0.04	<0.02	6.5	12.2	3.4	44.5	2.67
197	1734.50	<0.04		<0.04	<0.02	<0.04		<0.04	<0.02	6.7				2.68
198	1734.75	<0.04		<0.04	<0.02	<0.04		<0.04	<0.02	6.9				2.68
199	1735.00	<0.04		<0.04	<0.02	<0.04		<0.04	<0.02	5.7				2.67
200	1735.25	<0.04		<0.04	<0.02	<0.04		<0.04	<0.02	6.1	6.3	6.7	53.7	2.67
	1735.50	<0.04		<0.04	<0.02	<0.04		<0.04	<0.02					

Plug no.	Depth (m) RKB MD	Permeability (mD)								Porosity (%)		Pore saturation (%)		Grain density (g/cm ³)
		Horizontal				Vertical				He	Fluid sum.	S _o	S _w	
		K _g	1/P _m	K _a	K _{el}	K _g	1/P _m	K _a	K _{el}					
201	1735.75	<0.04		<0.04	<0.02	<0.04		<0.04	<0.02	6.8				2.66
202	1736.00	<0.04		<0.04	<0.02	<0.04		<0.04	<0.02	6.0				2.65
203	1736.25	<0.04		<0.04	<0.02	<0.04		<0.04	<0.02	6.8				2.65
204	1736.50	<0.04		<0.04	<0.02	<0.04		<0.04	<0.02	6.4	9.1	4.5	72.6	2.66
205	1736.75	nmp				<0.04		<0.04	<0.02	6.9				2.67
206	1737.00	<0.04		<0.04	<0.02	<0.04		<0.04	<0.02	6.6				2.65
207	1737.20	<0.04		<0.04	<0.02	<0.04		<0.04	<0.02	6.6				2.66
208	1737.50	<0.04		<0.04	<0.02	<0.04		<0.04	<0.02	6.3	9.8	6.4	55.6	2.67
209	1737.75	<0.04		<0.04	<0.02	<0.04		<0.04	<0.02	7.1				2.66
210	1738.00	<0.04		<0.04	<0.02	<0.04		<0.04	<0.02	7.6				2.66
211	1738.25	<0.04		<0.04	<0.02	<0.04		<0.04	<0.02	6.5				2.65
212	1738.50	<0.04		<0.04	<0.02	<0.04		<0.04	<0.02	7.5	7.8	10.7	69.5	2.65
213	1738.75	<0.04		<0.04	<0.02	<0.04		<0.04	<0.02	7.2				2.66
214	1739.00	nmp				<0.04		<0.04	<0.02	5.8				2.65
215	1739.25	<0.04		<0.04	<0.02	<0.04		<0.04	<0.02	6.1				2.67
216	1739.50	<0.04		<0.04	<0.02	<0.04		<0.04	<0.02	7.5	7.8	7.6	63.4	2.66
217	1739.75	<0.04		<0.04	<0.02	<0.04		<0.04	<0.02	6.1				2.66
218	1740.00	<0.04		<0.04	<0.02	<0.04		<0.04	<0.02	5.4				2.67
219	1740.25	<0.04		<0.04	<0.02	<0.04		<0.04	<0.02	5.4				2.65
220	1740.50	<0.04		<0.04	<0.02	<0.04		<0.04	<0.02	5.0	15.1	6.1	35.0	2.66
221	1740.75	nmp				<0.04		<0.04	<0.02	7.6				2.67
222	1741.00	<0.04		<0.04	<0.02	<0.04		<0.04	<0.02	6.7				2.69
223	1741.25	<0.04		<0.04	<0.02	<0.04		<0.04	<0.02	6.8				2.68
224	1741.50	<0.04		<0.04	<0.02	<0.04		<0.04	<0.02	6.5	5.7	15.2	75.9	2.68
225	1741.75	<0.04		<0.04	<0.02	<0.04		<0.04	<0.02	6.8				2.67
226	1742.00	<0.04		<0.04	<0.02	<0.04		<0.04	<0.02	5.0				2.69
227	1742.25	<0.04		<0.04	<0.02	<0.04		<0.04	<0.02	7.6				2.67
228	1742.50	<0.04		<0.04	<0.02	<0.04		<0.04	<0.02	5.1	4.3	14.9	74.6	2.69
229	1742.75	<0.04		<0.04	<0.02	<0.04		<0.04	<0.02	6.8				2.67
230	1743.00	<0.04		<0.04	<0.02	<0.04		<0.04	<0.02	6.9				2.68
231	1743.25	<0.04		<0.04	<0.02	<0.04		<0.04	<0.02	4.5				2.69
232	1743.50	<0.04		<0.04	<0.02	<0.04		<0.04	<0.02	6.1	5.5	7.8	85.5	2.67
233	1743.75	<0.04		<0.04	<0.02	<0.04		<0.04	<0.02	5.5				2.67
234	1744.00	<0.04		<0.04	<0.02	<0.04		<0.04	<0.02	5.6				2.66
235	1744.25	<0.04		<0.04	<0.02	<0.04		<0.04	<0.02	4.5				2.64
236	1744.50	<0.04		<0.04	<0.02	<0.04		<0.04	<0.02	6.1	6.8	15.6	81.3	2.67
237	1744.75	<0.04		<0.04	<0.02	<0.04		<0.04	<0.02	5.8				2.67
	1745.00													

Plug no.	Depth (m) RKB MD	Permeability (mD)								Porosity (%)		Pore saturation (%)		Grain density (g/cm ³)
		Horizontal				Vertical				He	Fluid sum.	S _o	S _w	
		K _g	1/P _m	K _a	K _{el}	K _g	1/P _m	K _a	K _{el}					
238	1745.00					<0.04		<0.04	<0.02	4.6				2.63
239	1745.25	nmp				<0.04		<0.04	<0.02	5.3				2.66
240	1745.50	0.033	0.341	0.051	0.024	<0.04		<0.04	<0.02	3.3	3.0	14.8	81.3	2.74
241	1745.75	<0.04		<0.04	<0.02	<0.04		<0.04	<0.02	2.3				2.71
242	1745.75	0.077	0.341	0.116	0.057	<0.04		<0.04	<0.02	2.3				2.71
242	1746.00	<0.04		<0.04	<0.02	<0.04		<0.04	<0.02	2.6				2.71
243	1746.25	<0.04		<0.04	<0.02	<0.04		<0.04	<0.02	1.0				2.70
244	1746.50	<0.04		<0.04	<0.02	<0.04		<0.04	<0.02	2.9	4.8	9.3	55.8	2.70
245	1746.75	<0.04		<0.04	<0.02	<0.04		<0.04	<0.02	3.6				2.70
246	1747.00	<0.04		<0.04	<0.02	<0.04		<0.04	<0.02	3.0				2.71
247	1747.25	<0.04		<0.04	<0.02	<0.04		<0.04	<0.02	3.3				2.70
248	1747.50	<0.04		<0.04	<0.02	<0.04		<0.04	<0.02	3.3	3.8	11.6	52.2	2.71
249	1747.75	<0.04		<0.04	<0.02	<0.04		<0.04	<0.02	3.5				2.70
250	1748.00	6.07	0.419	7.31	5.18	0.707	0.342	1.01	0.548	3.6				2.70
251	1748.25	<0.04		<0.04	<0.02	<0.04		<0.04	<0.02	3.5				2.70
252	1748.50	<0.04		<0.04	<0.02	<0.04		<0.04	<0.02	2.1	2.1	0.0	42.5	2.69
253	1748.75	0.038	0.340	0.058	0.028	<0.04		<0.04	<0.02	1.6				2.70
254	1749.00	<0.04		<0.04	<0.02	<0.04		<0.04	<0.02	1.1				2.69
255	1749.25	<0.04		<0.04	<0.02	<0.04		<0.04	<0.02	8.4				2.65
256	1749.50	<0.04		<0.04	<0.02	<0.04		<0.04	<0.02	4.0	2.3	0.0	35.2	2.69
257	1749.75	<0.04		<0.04	<0.02	<0.04		<0.04	<0.02	2.6				2.70
258	1750.00	<0.04		<0.04	<0.02	<0.04		<0.04	<0.02	1.7				2.69
259	1750.25	<0.04		<0.04	<0.02	<0.04		<0.04	<0.02	3.5				2.70
260	1750.50	<0.04		<0.04	<0.02	<0.04		<0.04	<0.02	3.4	4.4	0.0	49.8	2.69
261	1750.75	<0.04		<0.04	<0.02	<0.04		<0.04	<0.02	3.5				2.70
262	1751.00	0.458	0.340	0.664	0.351	<0.04		<0.04	<0.02	3.4				2.68
263	1751.25	<0.04		<0.04	<0.02	5.44	0.452	6.52	4.55	2.7				2.70
264	1751.50	<0.04		<0.04	<0.02	<0.04		<0.04	<0.02	0.9	5.4	0.0	16.6	2.70
265	1751.75	<0.04		<0.04	<0.02	<0.04		<0.04	<0.02	3.9				2.63
266	1752.00	<0.04		<0.04	<0.02	<0.04		<0.04	<0.02	2.4				2.70
267	1752.25	<0.04		<0.04	<0.02	<0.04		<0.04	<0.02	2.6				2.70
268	1752.50	<0.04		<0.04	<0.02	<0.04		<0.04	<0.02	3.0	5.4	0.0	40.3	2.68
269	1752.75	<0.04		<0.04	<0.02	<0.04		<0.04	<0.02	3.0				2.69
270	1753.00	<0.04		<0.04	<0.02	nvpp				6.8				2.66
271	1753.25	<0.04		<0.04	<0.02	<0.04		<0.04	<0.02	2.9				2.71
272	1753.50	<0.04		<0.04	<0.02	<0.04		<0.04	<0.02	3.4	2.9	0.0	53.1	2.70
273	1753.75	<0.04		<0.04	<0.02	<0.04		<0.04	<0.02	3.1				2.70
274	1754.00	<0.04		<0.04	<0.02	<0.04		<0.04	<0.02	2.0				2.70
275	1754.25	<0.04		<0.04	<0.02	<0.04		<0.04	<0.02	1.9				2.70
276	1754.50	<0.04		<0.04	<0.02	<0.04		<0.04	<0.02	2.6	4.5	0.0	62.8	2.71
277	1754.75	<0.04		<0.04	<0.02	<0.04		<0.04	<0.02	1.9				2.70
	1755.00													

Plug no.	Depth (m) RKB MD	Permeability (mD)								Porosity (%)		Pore saturation (%)		Grain density (g/cm ³)
		Horizontal				Vertical				He	Fluid sum.	S _o	S _w	
		K _g	1/P _m	K _a	K _{el}	K _g	1/P _m	K _a	K _{el}					
	1891.60													
824	1892.00	6.51	0.423	7.80	5.57	7.17	0.452	8.46	6.11	20.6				2.71
825	1892.25	3.42	0.437	4.23	2.78	1.35	0.450	1.70	1.06	19.6				2.71
826	1892.50	112	0.505	118	105	172	0.505	181	163	22.0	20.3	0.0	64.4	2.71
827	1892.75	9.80	0.476	11.3	8.43	101	0.502	107	94.7	10.1				2.77
828	1893.00	199	0.506	209	190	151	0.504	159	143	25.3				2.71
829	1893.25	65.3	0.502	70.0	60.5	20.5	0.481	22.8	18.2	24.3				2.71
830	1893.50	4.60	0.461	5.55	3.79	0.865	0.374	1.19	0.673	21.9	22.4	0.0	61.2	2.70
831	1893.75	0.715	0.343	1.02	0.554	0.425	0.374	0.591	0.326	17.3				2.71
832	1894.00	0.469	0.344	0.676	0.360	0.349	0.342	0.508	0.267	15.6				2.72
833	1894.25	6.25	0.423	7.50	5.33	18.0	0.483	20.2	16.0	19.4				2.71
834	1894.50	91.8	0.500	97.7	85.9	19.5	0.494	21.8	17.3	23.0	22.1	0.0	55.2	2.71
835	1894.75	0.633	0.345	0.907	0.489	0.352	0.343	0.511	0.269	11.4				2.73
836	1895.00	0.037	0.344	0.056	0.027	<0.04		<0.04	<0.02	7.3				2.74
837	1895.25	0.151	0.344	0.223	0.114	0.183	0.343	0.269	0.138	9.59				2.75
838	1895.50	0.127	0.344	0.189	0.095	0.037	0.343	0.056	0.027	9.0	12.3	0.0	65.5	2.75
839	1895.75	0.282	0.344	0.410	0.214	0.228	0.343	0.334	0.173	17.0				2.80
840	1896.00	0.125	0.344	0.185	0.093	0.313	0.343	0.456	0.239	10.3				2.78
841	1896.25	1.54	0.345	2.16	1.21	0.961	0.343	1.37	0.749	15.3				2.76
842	1896.50	3.07	0.437	3.83	2.48	0.902	0.343	1.28	0.702	18.3	21.5	0.0	68.9	2.71
843	1896.75	3.94	0.438	4.84	3.25	2.00	0.416	2.58	1.58	19.6				2.72
844	1897.00	4.06	0.438	4.98	3.35	7.09	0.450	8.37	6.04	16.7				2.71
845	1897.25	46.9	0.498	50.8	43.1	130	0.505	137	122	22.7				2.72
846	1897.50	29.2	0.492	32.1	26.3	11.1	0.477	12.8	9.65	21.4	24.8	0.0	57.1	2.77
847	1897.75	1.01	0.395	1.34	0.785	0.879	0.396	1.18	0.683	15.4				2.78
848	1898.00	5.08	0.398	6.22	4.32	3.04	0.397	3.86	2.50	22.0				2.72
849	1898.25	89.8	0.503	95.6	84.0	31.4	0.489	34.5	28.5	26.6				2.72
850	1898.50	2.88	0.423	3.63	2.33	2.08	0.417	2.69	1.65	19.5	19.2	0.0	69.1	2.76
851	1898.75	3.03	0.423	3.81	2.46	1.93	0.417	2.50	1.53	19.6				2.76
852	1899.00	3.86	0.423	4.77	3.19	1.18	0.417	1.54	0.924	20.1				2.76
853	1899.25	3.67	0.423	4.55	3.02	2.82	0.418	3.56	2.28	19.0	19.1	0.0	67.9	2.76
862	1901.50	83.0	0.497	88.5	77.5	14.4	0.491	16.2	12.6	24.9	23.8	0.0	68.1	2.71
863	1901.75	18.5	0.471	20.8	16.5	nmp				23.4				2.73
864	1902.00	48.8	0.491	52.8	44.9	15.3	0.491	17.2	13.4	24.9				2.71
865	1902.25	32.9	0.485	36.1	29.9	40.5	0.501	44.0	37.0	20.0				2.77
866	1902.50	25.4	0.480	28.2	22.9	25.7	0.498	28.4	23.1	24.2	22.8	0.0	63.6	2.74
867	1902.75	77.1	0.497	82.5	71.9	81.3	0.505	86.8	75.8	24.6				2.71
868	1903.00	30.5	0.483	33.5	27.6	42.8	0.502	46.4	39.1	23.6				2.73
869	1903.25	22.9	0.477	25.4	20.5	37.2	0.501	40.5	33.8	21.8				2.85
870	1903.50	49.8	0.492	53.9	45.9	42.6	0.503	46.2	38.9	24.8	22.0	0.0	67.5	2.75
871	1903.75	26.2	0.480	29.0	23.7	8.62	0.479	9.99	7.36	23.3				2.77
872	1904.00	51.8	0.492	56.0	47.8	39.8	0.500	43.3	36.3	25.8				2.75
873	1904.25	62.4	0.495	67.1	57.8	85.0	0.502	90.6	79.4	25.7				2.73
874	1904.50	110	0.500	117	104	44.9	0.502	48.7	41.2	27.5	26.6	0.0	69.1	2.73
875	1904.75	65.3	0.495	70.2	60.6	63.5	0.504	68.2	58.8	27.0				2.75
876	1905.00	47.4	0.491	51.3	43.5	24.2	0.496	26.7	21.7	25.2				2.76

Plug no.	Depth (m) RKB MD	Permeability (mD)								Porosity (%)		Pore saturation (%)		Grain density (g/cm ³)
		Horizontal				Vertical				He	Fluid sum.	S _o	S _w	
		K _g	1/P _m	K _a	K _{el}	K _g	1/P _m	K _a	K _{el}					
885	1907.25	5.30	0.448	6.37	4.43	7.36	0.472	8.61	6.23	18.6				2.83
886	1907.50	9.15	0.450	10.7	7.92	0.146	0.369	0.209	0.110	21.1	22.2	0.0	73.1	2.83
887	1907.75	1.07	0.343	1.51	0.832	15.8	0.481	17.8	13.9	9.9				2.86
888	1908.00	15.7	0.470	17.8	13.9	3.75	0.403	4.69	3.12	17.5				2.85
889	1908.25	21.1	0.478	23.6	18.9	14.1	0.484	15.9	12.3	18.1				2.85
890	1908.50	4.46	0.420	5.46	3.73	4.61	0.447	5.59	3.82	16.2	18.8	0.0	69.0	2.92
891	1908.75	4.11	0.393	5.11	3.45	8.44	0.448	9.89	7.27	12.0				2.80
892	1909.00	49.8	0.498	53.9	45.8	12.6	0.494	14.3	10.9	19.6				2.84
893	1909.25	91.5	0.502	97.3	85.6	41.5	0.505	45.0	37.9	22.5				2.85
894	1909.50	20.7	0.489	23.1	18.5	0.776	0.408	1.03	0.602	14.4	21.5	0.0	61.6	2.85
895	1909.75	0.139	0.343	0.205	0.104	0.425	0.408	0.569	0.326	17.2				2.83
896	1910.00	7.89	0.459	9.25	6.75	4.14	0.452	5.03	3.39	22.0				2.74
897	1910.25	4.31	0.454	5.23	3.54	2.39	0.452	2.98	1.89	11.7				2.82
898	1910.50	23.9	0.482	26.5	21.4	17.7	0.484	19.8	15.7	22.2	19.9	0.0	66.0	2.85
899	1910.75	9.38	0.454	10.9	8.11	0.464	0.342	0.671	0.357	15.2				2.85
900	1911.00	22.6	0.481	25.2	20.3	5.79	0.451	6.91	4.86	16.0				2.86
901	1911.25	0.303	0.416	0.404	0.231	0.044	0.343	0.066	0.032	2.8				2.79
902	1911.50	1.94	0.416	2.51	1.53	0.032	0.343	0.048	0.023	16.3	16.6	0.0	56.5	2.86
903	1911.75	4.45	0.417	5.47	3.73	5.10	0.462	6.11	4.23	15.3				2.85
904	1912.00	5.36	0.418	6.50	4.54	0.090	0.342	0.135	0.067	18.7				2.84
905	1912.25	<0.04		<0.04	<0.02	<0.04		<0.04	<0.02	6.2				2.81
906	1912.50	0.029	0.342	0.045	0.021	0.039	0.342	0.059	0.029	9.2	6.6	0.0	81.3	2.80
907	1912.75	0.315	0.343	0.459	0.240	0.036	0.342	0.055	0.027	13.5				2.81
908	1913.00	0.411	0.343	0.595	0.315	0.141	0.342	0.209	0.106	12.2				2.72
909	1913.25	1.50	0.343	2.12	1.18	3.85	0.429	4.75	3.18	14.4				2.86
910	1913.50	44.8	0.492	48.6	41.1	31.8	0.492	34.9	28.9	21.9	14.0	0.0	78.5	2.85
911	1913.75	8.52	0.455	9.96	7.33	20.0	0.484	22.3	17.8	19.0				2.85
912	1914.00	0.764	0.343	1.09	0.593	6.57	0.453	7.78	5.56	10.0				2.77
913	1914.25	0.415	0.343	0.601	0.318	0.172	0.368	0.245	0.130	8.4				2.80
914	1914.50	0.420	0.343	0.609	0.322	0.050	0.368	0.073	0.037	6.0	14.9	0.0	53.5	2.86
915	1914.75	10.4	0.465	12.0	9.04	9.07	0.480	10.5	7.77	15.7				2.85

916	1915.00	9.53	0.459	11.1	8.24	10.2	0.481	11.7	8.77	14.6				2.86
917	1915.25	0.054	0.343	0.081	0.040	<0.04		<0.04	<0.02	6.7				2.88
918	1915.50	1.49	0.344	2.10	1.17	9.78	0.472	11.3	8.43	11.2	18.5	0.0	50.9	2.84
919	1915.75	28.2	0.487	31.1	25.5	14.9	0.482	16.9	13.1	29.9				2.83
920	1916.00	78.8	0.499	84.2	73.5	33.7	0.495	36.8	30.6	29.7				2.91
921	1916.25	48.9	0.495	52.9	45.0	51.1	0.500	55.2	47.1	31.1				2.84
922	1916.50	53.4	0.500	57.6	49.2	45.4	0.500	49.1	41.6	31.3	29.9	0.0	78.5	2.84
923	1916.75	3.25	0.433	4.05	2.64	0.131	0.359	0.190	0.098	17.0				2.82
924	1917.00	nmp				0.513	0.359	0.724	0.395	10.7				2.86
925	1917.25	14.7	0.482	16.6	12.9	18.4	0.499	20.5	16.2	22.7				2.82
926	1917.50	8.90	0.472	10.3	7.63	7.99	0.488	9.27	6.77	27.0	32.0	0.0	75.5	2.79
927	1917.75	16.8	0.485	18.9	14.9	0.737	0.404	0.981	0.571	28.9				2.83
928	1918.00	nmp				2.10	0.449	2.64	1.66	24.1				2.83
929	1918.25	11.6	0.477	13.2	10.0	14.3	0.497	16.2	12.5	17.5				2.80
930	1918.50	0.381	0.340	0.554	0.291	0.073	0.344	0.110	0.054	12.1	9.7	0.0	57.6	2.89

Plug no.	Depth (m) RKB MD	Permeability (mD)								Porosity (%)		Pore saturation (%)		Grain density (g/cm ³)	
		Horizontal				Vertical				He	Fluid sum.	S _o	S _w		
		K _g	1/P _m	K _a	K _{el}	K _g	1/P _m	K _a	K _{el}						
972	1928.96														2.97
973	1929.00	22.4	0.476	24.9	20.0	17.4	0.491	19.5	15.4	20.3					npp
974	1929.25	nhpp				nvpp				npp					npp
975	1929.50	nhpp				nvpp				npp					npp
975	1929.75	19.7	0.473	22.0	17.5	22.2	0.495	24.7	19.9	25.9	23.2	0.0	71.9		2.83
976	1930.00	27.0	0.481	29.9	24.4	26.9	0.496	29.7	24.2	23.7					2.85
977	1930.25	30.2	0.483	33.2	27.4	24.5	0.495	27.1	21.9	24.3					2.83
978	1930.50	39.3	0.488	42.9	36.0	36.4	0.499	39.7	33.1	26.8	25.6	0.0	73.8		2.85
979	1930.75	13.0	0.460	14.9	11.4	20.4	0.493	22.7	18.1	22.7					2.84
980	1931.00	<0.04		<0.04	<0.02	<0.04		<0.04	<0.02	1.8					2.85
981	1931.25	<0.04		<0.04	<0.02	<0.04		<0.04	<0.02	2.0					2.86
982	1931.50	3.28	0.433	4.08	2.66	0.966	0.341	1.38	0.753	16.3	2.5	0.0	47.6		2.81
983	1931.75	0.144	0.342	0.213	0.108	<0.04		<0.04	<0.02	7.2					2.79
984	1932.00	1.72	0.342	2.42	1.36	<0.04		<0.04	<0.02	8.7					2.81
985	1932.25	0.867	0.342	1.24	0.674	0.101	0.341	0.151	0.075	11.8					2.80
986	1932.50	1.57	0.342	2.22	1.24	1.45	0.457	1.82	1.14	11.3	13.4	0.0	58.0		2.80
987	1932.75	0.425	0.342	0.616	0.326	0.461	0.457	0.589	0.354	8.3					2.81
988	1933.00	0.159	0.342	0.235	0.120	<0.04		<0.04	<0.02	5.6					2.86
989	1933.25	<0.04		<0.04	<0.02	1.15	0.342	1.63	0.896	3.5					2.88
990	1933.50	1.64	0.431	2.10	1.29	0.834	0.341	1.19	0.648	9.0	8.0	0.0	44.4		2.86
991	1933.75	<0.04		<0.04	<0.02	<0.04		<0.04	<0.02	0.7					2.95
992	1934.00	<0.04		<0.04	<0.02	<0.04		<0.04	<0.02	3.7					2.91
993	1934.25	<0.04		<0.04	<0.02	<0.04		<0.04	<0.02	0.3					2.95
994	1934.50	<0.04		<0.04	<0.02	<0.04		<0.04	<0.02	0.8	2.7	0.0	72.5		2.95
995	1934.75	0.105	0.343	0.156	0.078	0.033	0.341	0.051	0.024	6.2					2.87
996	1935.00	2.34	0.434	2.98	1.86	0.835	0.341	1.20	0.649	11.0					2.85
997	1935.25	0.492	0.433	0.641	0.378	0.074	0.340	0.111	0.055	8.2					2.86
998	1935.50	0.031	0.343	0.047	0.023	<0.04		<0.04	<0.02	4.8	5.7	0.0	43.5		2.87
999	1935.75	0.989	0.343	1.41	0.772	0.456	0.341	0.660	0.350	7.1					2.87
1000	1936.00	0.447	0.343	0.647	0.343	0.441	0.341	0.639	0.338	8.4					2.85
1001	1936.25	nmp				0.139	0.341	0.207	0.104	9.5					2.91

1033	1944.25	357	0.504	370	343	120	0.503	127	113	24.7					2.84
1034	1944.50	1.62	0.343	2.29	1.28	3.84	0.420	4.76	3.18	14.3	12.9	0.0	47.6		2.85
1035	1944.75	9.53	0.451	11.1	8.25	1.85	0.431	2.36	1.46	12.4					2.85
1036	1945.00	52.8	0.493	57.0	48.6	52.3	0.497	56.4	48.1	18.4					2.85
1037	1945.25	137	0.501	145	130	76.4	0.500	81.7	71.2	26.3					2.84
1038	1945.50	98.6	0.499	105	92.4	82.4	0.501	87.9	76.9	22.2	10.7	0.0	60.5		2.86
1039	1945.75	nmp				22.8	0.486	25.3	20.4	16.0					2.86
1040	1946.00	17.7	0.472	19.9	15.7	19.5	0.466	21.9	17.4	14.8					2.86
1041	1946.25	11.4	0.458	13.2	9.99	2.71	0.414	3.45	2.19	12.7	11.8	0.0	63.1		2.86
1042	1946.50	2.29	0.343	3.20	1.82	0.951	0.394	1.27	0.741	8.8					2.88
1043	1946.75	2.85	0.370	3.68	2.36	1.05	0.413	1.38	0.819	7.9					2.86
1044	1947.00	nhpp				nvpp				npp					npp
1045	1947.25	11.5	0.452	13.3	10.1	0.594	0.414	0.786	0.459	7.5					2.89
1046	1947.50	0.685	0.448	0.876	0.530	0.047	0.352	0.071	0.035	5.9	5.3	0.0	46.9		2.86
1047	1947.75	0.028	0.341	0.043	0.021	0.053	0.352	0.079	0.039	3.1					2.88
1048	1948.00	1.05	0.342	1.49	0.820	<0.04		<0.04	<0.02	7.0					2.82

Plug no.	Depth (m) RKB MD	Permeability (mD)								Porosity (%)		Pore saturation (%)		Grain density (g/cm ³)
		Horizontal				Vertical				He	Fluid sum.	S _o	S _w	
		K _g	1/P _m	K _a	K _{el}	K _g	1/P _m	K _a	K _{el}					
1064	1952.00	95.7	0.501	102	89.7	0.150	0.383	0.210	0.112	21.1				2.79
1065	1952.25	20.7	0.479	23.1	18.4	48.0	0.491	52.0	44.1	11.6				2.81
1066	1952.50	2.02	0.388	2.69	1.60	0.614	0.383	0.839	0.474	8.9	10.7	0.0	50.8	2.87
1067	1952.75	2.53	0.417	3.23	2.03	0.337	0.383	0.465	0.257	8.9				2.85
1068	1953.00	0.876	0.416	1.15	0.681	0.077	0.383	0.109	0.057	4.5				2.87
1069	1953.25	0.181	0.342	0.268	0.137	0.085	0.383	0.121	0.063	15.8				2.79
1070	1953.50	nmp				<0.04		<0.04	<0.02	15.2	15.7	0.0	78.8	2.77
1071	1953.75	0.043	0.341	0.065	0.031	<0.04		<0.04	<0.02	10.4				2.74
1072	1954.00	<0.04		<0.04	<0.02	<0.04		<0.04	<0.02	7.6				2.83
1073	1954.25	<0.04		<0.04	<0.02	<0.04		<0.04	<0.02	8.54				2.78
1074	1954.50	0.090	0.341	0.134	0.067	<0.04		<0.04	<0.02	10.0	9.8	0.0	88.6	2.78
1075	1954.75	0.046	0.341	0.070	0.034	<0.04		<0.04	<0.02	4.6				2.72
1076	1955.00	<0.04		<0.04	<0.02	<0.04		<0.04	<0.02	2.7				2.73
1077	1955.25	<0.04		<0.04	<0.02	<0.04		<0.04	<0.02	4.0				2.74
1078	1955.50	<0.04		<0.04	<0.02	<0.04		<0.04	<0.02	4.3	3.3	0.0	80.2	2.71
1079	1955.75	<0.04		<0.04	<0.02	<0.04		<0.04	<0.02	2.2				2.71
1080	1956.00	<0.04		<0.04	<0.02	<0.04		<0.04	<0.02	1.6				2.71
1081	1956.25	<0.04		<0.04	<0.02	<0.04		<0.04	<0.02	2.0				2.71
1082	1956.50	<0.04		<0.04	<0.02	<0.04		<0.04	<0.02	0.9	1.5	0.0	91.2	2.71
1083	1956.75	<0.04		<0.04	<0.02	nvpp				1.0				2.71
1084	1957.00	<0.04		<0.04	<0.02	<0.04		<0.04	<0.02	2.7				2.71
1085	1957.25	0.116	0.342	0.172	0.086	<0.04		<0.04	<0.02	6.3				2.71
1086	1957.50	2.27	0.343	3.16	1.80	0.394	0.340	0.573	0.302	12.5	14.4	0.0	57.2	2.71
1087	1957.75	6.44	0.422	7.71	5.50	19.2	0.487	21.4	17.0	16.7				2.71
1088	1958.00	16.4	0.489	18.4	14.4	22.1	0.489	24.5	19.7	21.5				2.71
1110	1963.50	17.7	0.485	19.8	15.7	23.1	0.494	25.6	20.7	18.6	19.9	0.5	63.7	
1111	1963.75	5.90	0.463	7.01	4.94	1.34	0.420	1.74	1.05	9.4				
1112	1964.00	9.94	0.465	11.5	8.60	4.68	0.421	5.72	3.92	14.7				
1113	1964.25	127	0.501	135	120	77.5	0.500	82.8	72.2	20.0				
1114	1964.50	31.2	0.486	34.3	28.3	40.1	0.493	43.7	36.7	20.3	15.1	0.8	77.5	
1115	1964.75	644	0.506	663	624	4.71	0.412	5.78	3.97	24.1				
1132	1971.00	16.5	0.462	18.6	14.6	nvpp				15.7				
1133	1971.25	16.5	0.461	18.7	14.7	nvpp				13.5				
1134	1971.50	1090	0.507	1120	1060	nvpp				19.9	19.1	0.0	59.5	
1135	1971.75	234	0.503	244	223	nvpp				17.6				
1136	1972.00	551	0.506	569	533	nvpp				18.1				
1150	1975.50	305	0.506	317	292	nvpp				18.8	19.9	0.0	52.6	2.74
1151	1975.75	493	0.506	509	476	nvpp				17.3				2.72
1152	1976.00	26.2	0.489	28.9	23.6	9.07	0.454	10.6	7.83	12.2				2.76

Plug no.	Depth (m) RKB MD	Permeability (mD)								Porosity (%)		Pore saturation (%)		Grain density (g/cm ³)
		Horizontal				Vertical				He	Fluid sum.	S _o	S _w	
		K _g	1/P _m	K _a	K _{el}	K _g	1/P _m	K _a	K _{el}					
1243	1998.75	<0.04		<0.04	<0.02	<0.04		<0.04	<0.02	4.1				2.78
1244	1999.00	<0.04		<0.04	<0.02	<0.04		<0.04	<0.02	8.5				2.80
1245	1999.25	<0.04		<0.04	<0.02	<0.04		<0.04	<0.02	10.1				2.81
1246	1999.50	<0.04		<0.04	<0.02	<0.04		<0.04	<0.02	5.6	8.7	0.0	63.6	2.81
1247	1999.75	0.044	0.343	0.067	0.033	0.045	0.342	0.068	0.033	1.9				2.70
1248	2000.00	2.08	0.344	2.90	1.64	0.406	0.342	0.589	0.311	9.6				2.85
1249	2000.25	8.53	0.445	9.99	7.36	7.67	0.471	8.96	6.52	16.3				2.78
1250	2000.50	44.5	0.491	48.3	40.8	25.7	0.496	28.3	23.0	17.2	17.8	0.0	66.7	2.76
1251	2000.75	13.8	0.463	15.7	12.1	18.8	0.491	21.0	16.6	13.7				2.75
1252	2001.00	6.66	0.435	7.93	5.68	0.403	0.398	0.546	0.309	9.6				2.81
1253	2001.25	1.67	0.344	2.35	1.32	2.82	0.398	3.60	2.31	12.0				2.85
1269	2005.50	1.74	0.418	2.25	1.37	2.83	0.425	3.57	2.28	10.7	8.8	0.0	42.9	2.85
1270	2005.75	1.38	0.417	1.79	1.08	0.237	0.393	0.326	0.180	8.2				2.85
1271	2006.00	0.189	0.342	0.278	0.142	0.116	0.393	0.161	0.087	9.1				2.81
1272	2006.25	4.14	0.441	5.06	3.41	3.23	0.441	4.01	2.61	12.7				2.87
1273	2006.50	3.32	0.441	4.11	2.69	1.66	0.441	2.10	1.31	11.4	13.4	0.0	52.3	2.87
1274	2006.75	<0.04		<0.04	<0.02	<0.04		<0.04	<0.02	5.7				2.75
1275	2007.00	0.848	0.342	1.21	0.659	1.58	0.386	2.11	1.24	15.3				2.76
1306	2014.75	0.537	0.396	0.726	0.414	nvpp				9.0				2.83
1307	2015.00	11.2	0.456	12.9	9.77	nvpp				10.1				2.83
1308	2015.25	1.68	0.342	2.36	1.32	nvpp				7.0				2.85
1309	2015.50	0.489	0.342	0.707	0.376	nvpp				7.3	7.5	0.0	29.3	2.86
1310	2015.75	<0.04		<0.04	<0.02	nmp				6.0				2.81
1311	2016.00	nmp				<0.04		<0.04	<0.02	2.0				2.79
1312	2016.25	7.58	0.429	8.98	6.53	nvpp				14.4				2.75
1313	2016.50	37.4	0.484	40.9	34.2	nvpp				15.3	13.6	0.0	46.5	2.78
1314	2016.75	26.0	0.488	28.7	23.4	nvpp				15.4				2.80
1315	2017.00	39.5	0.499	43.0	36.0	13.5	0.485	15.3	11.8	20.2				2.80
1316	2017.25	43.5	0.495	47.2	39.8	nvpp				15.9				2.84
1317	2017.50	12.8	0.485	14.6	11.2	15.1	0.481	17.1	13.3	15.0	16.8	0.0	34.7	2.82
1318	2017.75	29.3	0.489	32.2	26.5	nvpp				19.7				2.78
1319	2018.00	49.0	0.496	53.0	45.0	nvpp				16.8				2.84
1320	2018.25	6.65	0.423	7.95	5.69	nvpp				9.2				2.84
1321	2018.50	10.8	0.480	12.4	9.31	<0.04		<0.04	<0.02	10.5	6.3	0.0	25.1	2.84
1322	2018.75	<0.04		<0.04	<0.02	nvpp				2.6				2.77
1323	2019.00	58.7	0.499	63.1	54.2	nvpp				18.1				2.82
1324	2019.25	51.0	0.499	55.1	46.9	nvpp				16.7				2.81
1325	2019.50	97.8	0.504	104	91.6	12.8	0.478	14.6	11.2	20.8	18.3	0.0	56.2	2.79
1418	2044.00	<0.04		<0.04	<0.02	0.516	0.340	0.747	0.397	6.5				2.77
1419	2044.25	2.13	0.447	2.68	1.69	0.536	0.412	0.711	0.413	18.6				2.80
1420	2044.50	2.76	0.447	3.45	2.20	1.54	0.412	2.01	1.21	21.8	19.7	0.0	72.8	2.81
1421	2044.75	0.094	0.342	0.140	0.070	0.121	0.412	0.164	0.090	9.0				2.81
1422	2045.00	1.69	0.422	2.18	1.33	2.75	0.413	3.50	2.23	20.2				2.82
1423	2045.25	2.61	0.422	3.32	2.09	3.66	0.414	4.56	3.03	19.7				2.81
1424	2045.50	1.16	0.422	1.50	0.906	1.67	0.412	2.17	1.31	18.9	17.4	0.0	85.9	2.78
1425	2045.75	0.754	0.343	1.08	0.585	1.15	0.412	1.51	0.900	14.3				2.81
1426	2046.00	1.96	0.343	2.75	1.55	1.67	0.412	2.18	1.32	23.2				2.81
1427	2046.25	2.65	0.457	3.31	2.09	0.919	0.412	1.21	0.716	24.3				2.82
1428	2046.50	0.394	0.342	0.571	0.301	0.507	0.412	0.673	0.390	10.1	3.0	0.0	30.0	2.84
1429	2046.75	0.814	0.342	1.16	0.632	0.303	0.412	0.406	0.231	23.4				2.81
1430	2047.00	0.512	0.342	0.739	0.394	0.293	0.412	0.392	0.223	23.0				2.81

Plug no.	Depth (m) RKB MD	Permeability (mD)								Porosity (%)		Pore saturation (%)		Grain density (g/cm ³)
		Horizontal				Vertical				He	Fluid sum.	S _o	S _w	
		K _g	1/P _m	K _a	K _{el}	K _g	1/P _m	K _a	K _{el}					
1650	2102.25	<0.04		<0.04	<0.02	<0.04		<0.04	<0.02	0.5				2.71
1651	2102.50	<0.04		<0.04	<0.02	<0.04		<0.04	<0.02	1.8	1.9	0.0	71.4	2.76
1652	2102.75	<0.04		<0.04	<0.02	<0.04		<0.04	<0.02	1.8				2.76
1653	2103.00	0.160	0.348	0.234	0.120	<0.04		<0.04	<0.02	0.8				2.71
1654	2103.25	0.162	0.348	0.238	0.122	<0.04		<0.04	<0.02	2.2				2.75
1655	2103.50	0.038	0.348	0.057	0.028	<0.04		<0.04	<0.02	2.8	3.9	0.0	44.6	2.76
1656	2103.75	0.049	0.348	0.073	0.036	0.042	0.342	0.064	0.031	4.1				2.74
1657	2104.00	<0.04		<0.04	<0.02	<0.04		<0.04	<0.02	5.6				2.75
1658	2104.25	0.174	0.349	0.255	0.131	0.179	0.342	0.265	0.135	14.8				2.77
1659	2104.50	0.129	0.349	0.189	0.096	0.133	0.342	0.197	0.100	11.7	12.4	0.0	65.1	2.76
1660	2104.75	0.141	0.343	0.208	0.106	0.121	0.342	0.180	0.091	11.5				2.76
1661	2105.00	0.307	0.343	0.447	0.234	0.106	0.342	0.157	0.079	15.3				2.75
1662	2105.25	<0.04		<0.04	<0.02	<0.04		<0.04	<0.02	6.3				2.69
1663	2105.50	0.032	0.343	0.049	0.023	<0.04		<0.04	<0.02	5.4	9.4	0.0	54.9	2.69
1664	2105.75	<0.04		<0.04	<0.02	<0.04		<0.04	<0.02	7.2				2.70
1665	2106.00	<0.04		<0.04	<0.02	<0.04		<0.04	<0.02	2.2				2.70
1666	2106.25	0.181	0.344	0.265	0.136	0.153	0.353	0.223	0.115	12.7				2.72
1667	2106.50	0.316	0.344	0.459	0.241	0.173	0.353	0.251	0.130	15.1	18.4	0.0	59.5	2.73
1668	2106.75	1.19	0.345	1.68	0.932	0.451	0.354	0.643	0.346	19.0				2.75
1669	2107.00	0.582	0.344	0.835	0.449	0.379	0.354	0.542	0.290	16.4				2.71
1670	2107.25	0.417	0.345	0.602	0.320	0.343	0.353	0.491	0.262	16.5				2.72
1671	2107.50	0.346	0.344	0.502	0.265	0.336	0.353	0.481	0.256	15.2	15.7	0.0	70.5	2.71
1672	2107.75	0.213	0.344	0.313	0.161	0.327	0.338	0.479	0.249	13.9				2.71
1673	2108.00	0.585	0.345	0.839	0.451	0.369	0.353	0.529	0.282	17.0				2.72
1674	2108.25	1.17	0.345	1.65	0.913	0.665	0.353	0.940	0.514	18.4				2.72
1675	2108.50	1.24	0.345	1.75	0.974	0.528	0.337	0.767	0.407	16.9	16.9	0.0	57.7	2.75
1676	2108.75	1.33	0.345	1.87	1.04	0.394	0.337	0.575	0.302	12.3				2.72
1677	2109.00	0.610	0.345	0.873	0.471	0.103	0.337	0.154	0.077	9.6				2.72
1678	2109.25	1.02	0.345	1.44	0.793	0.219	0.338	0.324	0.166	16.5				2.73
1679	2109.50	0.728	0.345	1.04	0.564	0.118	0.338	0.177	0.088	13.3	9.5	0.0	71.9	2.74
1680	2109.75	1.13	0.346	1.60	0.887	0.213	0.338	0.314	0.161	16.1				2.74
1753	2128.00	0.119	0.345	0.176	0.089	0.182	0.342	0.268	0.137	8.3				2.70
1754	2128.25	0.493	0.345	0.710	0.379	0.351	0.342	0.510	0.268	10.2				2.67
1755	2128.50	0.869	0.345	1.24	0.676	1.22	0.343	1.73	0.957	9.7	10.1	0.0	57.6	2.66
1756	2128.75	0.321	0.345	0.466	0.245	0.247	0.342	0.362	0.187	9.5				2.67
1757	2129.00	0.183	0.345	0.269	0.138	0.135	0.342	0.200	0.101	7.5				2.69
1758	2129.25	0.133	0.345	0.196	0.100	0.072	0.342	0.107	0.053	7.5				2.70
1759	2129.50	<0.04		<0.04	<0.02	<0.04		<0.04	<0.02	5.3	6.6	0.0	64.4	2.72
1760	2129.75	0.078	0.345	0.117	0.058	0.064	0.342	0.096	0.047	8.4				2.70
1761	2130.00	0.287	0.345	0.417	0.218	nmp				8.2				2.66
1849	2242.00	nhpp				nvpp				nhpp				nhpp
1850	2242.25	nhpp				nvpp				nhpp				nhpp
1851	2242.50	nhpp				nvpp				nhpp	6.7	22.1	41.0	nhpp
1852	2242.75	nhpp				nvpp				nhpp				nhpp
1853	2243.00	1.51	0.374	2.05	1.19	1.49	0.374	2.02	1.17	11.9				2.71
1854	2243.25	0.274	0.373	0.385	0.208	nmp				7.5				2.73
1855	2243.50	0.080	0.372	0.115	0.059	0.049	0.342	0.073	0.036	2.9	9.0	0.0	55.7	2.81
1856	2243.75	nmp				0.192	0.342	0.282	0.145	5.5				3.35
1857	2244.00	1.57	0.374	2.12	1.23	0.740	0.343	1.06	0.574	10.6				2.68